POLITECNICO DI TORINO

Corso di Laurea Magistrale in Ingegneria Aerospaziale

Tesi di Laurea Magistrale

Effects of arrhythmias on the arterial fluid dynamics

Relatore
Ing. Stefania Scarsoglio

Caterina Gallo

Correlatore:
Prof. Luca Ridolfi

Aprile 2017

A mio fratello...

Contents

Introduction

Hemodynamics or dynamics of blood flow is one of the possible areas of fluid mechanics research. In the attempt to make a contribution to both physiology and medicine, it has gained a lot of popularity in the last few decades. In fact, on the one hand, it is essential to know more about the physical phenomena behind the normal functioning of our cardiovascular system. On the other hand, researchers are interested in studying the effects of particular pathologies on circular system, giving a contribution to some medical treatments in this field. To these purposes, a great variety of mathematical models have been developed, in order to describe more or less accurately the hemodynamics of the human cardiovascular system. Some of these are based on lumped submodels only, others, instead, known as multiscale models, combine the classical mass and momentum balance equations, representing the largest vessels, with a series of different lumped submodels, describing elements such as the micro-circulation groups and the valves.

In this work, we aim at achieving two objectives. Firstly, we want to analyse the role played by the heartbeat period on the response of both the heart and the systemic arteries, under steady and transitory conditions. Secondly, we are interested in analysing what happens in case of atrial fibrillation, one of the most common form of arrhythmias [2], [9]. In particular, we do not take into account the variations in the mean heartbeat frequency in case of atrial fibrillation and focus on the consequences of the arrhythmical distribution of the beat periods, during this specific arrhythmia, on the systemic circulation response. Note that, to date, the effect of atrial fibrillation on our large-to-medium arteries is not completely understood [32], [44], with literature data indicating contrasting trends for the pressures. Indeed, oscillometric instruments, used for invasive measures, do not succeed to catch up with the high heart beat frequency typical in atrial fibrillation and are not beneficial to provide useful results. Moreover, atrial fibrillation usually combines with other pathologies, so, it is not easy to detect its net role by the available medical data. All these limitations can be overcome

by our numerical approach, giving new insights into the behaviour of the arterial tree during this special type of arrhythmia.

We adopt a multi-scale mathematical model of the arterial system, solved numerically through a Rouge-Kutta Discontinuous-Galerkin scheme. It has the great advantage to provide, beat by beat, the complete pressure and flow time-series at each arterial site. This means that, not only we can observe the pressure and flow variations due to the heartbeat period alteration, but we can also inquire into problems such as the wave propagation and reflection along the arterial tree, impossible to explain when using pure lumped models.

The thesis is organised as follows.

Chapter 1 gives a general description about the structure of the human cardiovascular system and depicts briefly how it works under physiological conditions. Here, one can also find a basic explanation of the concepts of arrhythmia and atrial fibrillation.

In Chapter 2, we introduce some useful elements of the arterial hemodynamics to analyse, in the subsequent chapters, the behaviour of the large-to-medium arteries. We look at the pulse wave velocity and the phase velocity, the input impedance and the characteristic impedance, the technique usually adopted to decompose total pressure and flow waves in their forward and backward contributions and, finally, some parameters to estimate the entity of the wave reflections at the arterial junctions.

Chapter 3 presents the domain and the mathematical model used throughout this work, with a clear presentation of all the elements contributing to the global model. The numerical scheme necessary to solve the mathematical problem, instead, is briefly summarized.

Chapter 4 indicates the method of calibration to make the mathematical model reproduce acceptable results, for heart and systemic vessels, under physiological conditions. We also offer a complete view of the way heart and large-to-medium arteries behave for a perfectly standard beat, according to the model results. We see that what the adopted model provides is in good agreement with literature data, under standard conditions.

Chapter 5 reports the way systemic circulation acts for a constant sequence of heartbeats shorter or longer than the standard one, as numerical solutions of the model. At this point, we can see how the fixed simulated heartbeat period contributes to the stroke work, the pressure and flow records, as well as the phase velocities and magnitudes of reflections, at different arterial points.

In Chapters 6 and 7, we identify, through the model, how transition phases evolve, in terms of pressure and flow, at different arterial sites, as passing

from one sequence of constant beats to one another and after introducing an irregular beat within a sequence of normal beats, respectively. In these chapters, we also inquire into the number of beats requested by the various sites to conclude the transition phase.
Chapter 8 shows the response of both the heart and the systemic arteries during an event of atrial fibrillation of about 2000 heartbeats, without varying the mean heartbeat frequency usually measured for a normal beat. At the beginning of the same chapter, we present the characteristics of a chain of fibrillated beat periods, as used for the simulation in this chapter.
In Chapter 9, we offer an interpretation of the results reported in Chapter 8 and present some literature data, collected during episodes of atrial fibrillation on real patients, as an instruments of validation of the numerical model when this particular arrhythmia is present.
Final remarks, regarding possible improvements and future developments for this work, are then discussed in the Conclusions section.

Chapter 1

Physiological and arrhythmic heart functioning

This chapter is separated into two distinctive sections. The first one concerns a minimal description of the human cardiovascular system, focusing on the normal heart functioning. The second part, instead, gives a general definition of arrhythmia and offers a more detailed depiction of atrial fibrillation, one of the most common form of arrhythmia.

1.1 Standard heart functioning within the cardiovascular system

Heart is nothing but a muscle. It acts as a pump to sustain the blood flow along the complex vascular tree of our body.

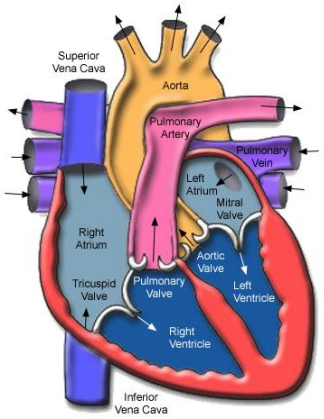

Figure 1.1: Schematic representation of the main elements constituting human heart.

From Figure 1.1, we can see that heart is made of two different and independent pumps: the left and the right heart. Each of these consists of a thin-walled atrium and a thick-walled ventricle, two contractile chambers communicating with each other through a proper valve: the atrioventricular valve or A-V valve. Right and left A-V valves are quite different in shape. The first one has three flaps and is known as tricuspid valve while the other is called mitral valve and has only two cusps. Left and right atria are separated through the interatrial septum (not visible in the image above) while left and right ventricles are divided by the interventricular septum. Each ventricle is then linked with a major distributing artery, preceded by another valve: the semilunar valve. Exit valves from ventricles have similar structures for left and right heart but we distinguish them as well. We have the aortic valve on the left and the pulmonary valve on the right. The shape of the four valves makes them close, when there is a backward pressure gradient forcing flow backward, and open, as a forward pressure gradient pushes blood in the forward direction.

Figure 1.2 depicts the structure of human circulation. Left ventricle is connected to the aortic opening from which oxygenated blood is distributed

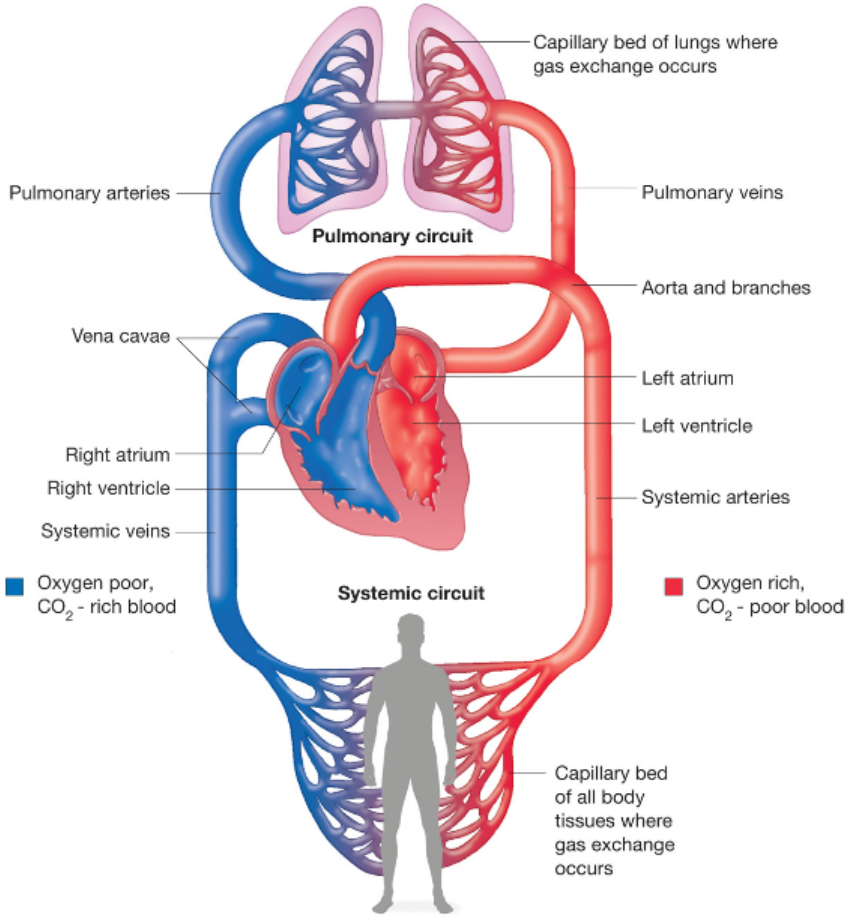

Figure 1.2: Schematic representation of human circulation.

to all the body organs. Aorta divides into numerous progressively smaller branches, until we reach the arterioles, followed by the capillaries. Through the walls of the capillaries, that are extremely thin vessels, it is possible an intense exchange of nutrients, waste products and hormones between tissue fluids and blood. Capillaries turn into the smallest group of veins, called venules. These develop into larger veins as returning to heart. Here, we have the superior vena cava and the inferior vena cava, directly connected to the right atrium. While the former collects the blood low in oxygen from superior regions of our body, the latter does the same thing for those areas below the diaphragm. From the right atrium, blood passes into the right

ventricle and then into the pulmonary artery. The pulmonary artery, in turns, branches off many times leading to the pulmonary capillaries around the pulmonary alveoli. In this part of our body, blood releases carbon dioxide and acquires oxygen. After blood is oxygenated again, it can leave the lungs through two pulmonary veins, finally merging into the left atrium and then into the left ventricle. At this point, the just presented cycle can repeat again.

We can identify two different circulations. Systemic circulation has to provide all the body organs with blood rich in oxygen, starting from the left ventricle, and gives back blood rich in carbon dioxide to the right atrium. By contrast, pulmonary circulation is responsible for carrying deoxygenated blood away from the right ventricle to the lungs and returning oxygen-rich blood back to the left atrium.

During each standard heartbeat, heart undergoes the classical cardiac cycle. It consists of periods of relaxation (diastole) and contraction (systole) for both atria and ventricles. These events are out of synchronization for atrium and ventricle of the same pump (left or right heart) but are synchronous for atria and ventricles of the two pumps. However, when defining diastole and systole periods, we usually refer to the ventricular activity rather than to the atrial one.

An efficient way to describe the main events of a standard cardiac cycle is the Wiggers diagram (Figure 1.3). Through a combination of six curves, it depicts the complete normal functioning of the left side of the heart during each beat. In particular, it indicates the expected changes in the left atrial pressure, the left ventricular pressure, the left ventricular volume and the pressure at the entrance to the aorta. Moreover, it gives the corresponding electrocardiogram and phonocardiogram. The first is the graphical representation of the electrical activity of the heart, recorded through an electrocardiograph from the surface of our body. Under physiological conditions, it is made of three main groups of waves. The P wave corresponds to the atrial depolarization, the QRS group of waves is the expression of the ventricular depolarization and the T wave represents the ventricular repolarization. Note that, in this context, the depolarization is the event preceding muscular contraction while the repolarization is before muscular relaxation. Concerning the phonocardiogram, it is a recording of the main cardiac sounds produced by the beating heart. The first and the second heart sounds are due to the closure of the A-V valves and the semilunar valves, respectively. In addition to these, a variety of other weaker sounds can be heard. An example is the third sound, corresponding to the diastolic phase of fast filling.

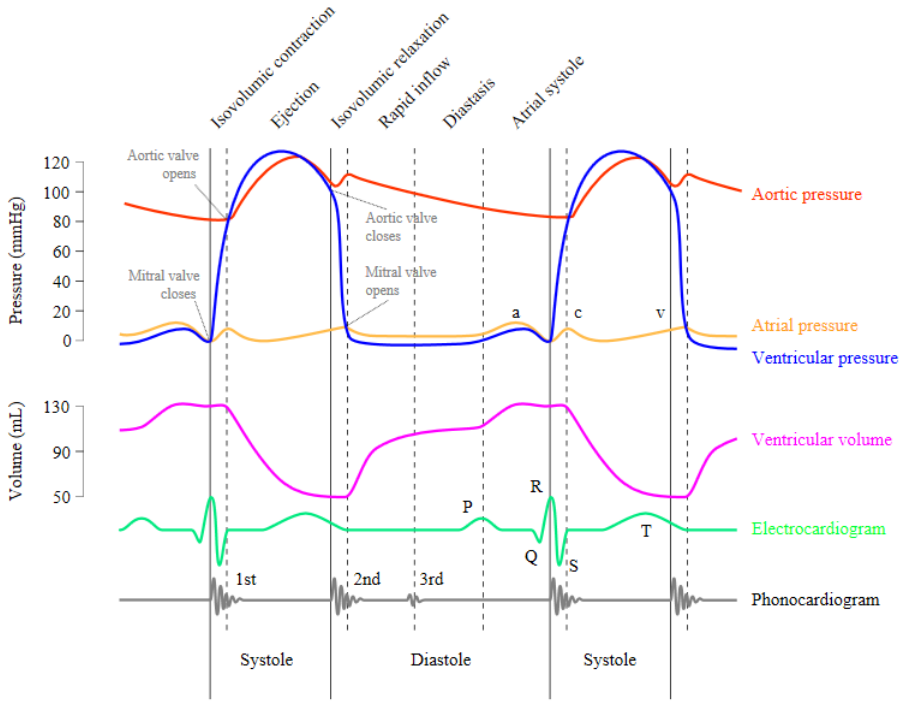

Figure 1.3: Wiggers diagram.

Looking at Figure 1.3, we infer what happens at the end of systole and beginning of diastole. Aortic valve has just closed and a phase of isovolumic relaxation starts. During this phase, ventricular volume remains constant, ventricular pressure sharply decreases while atrial pressure slightly grows. As atrial and ventricular pressures equal, with a certain tolerance, mitral valve opens and the ventricular filling begins. The period between mitral valve opening and closure can be divided into three different parts. The first one, that of rapid inflow, is characterised by a significant swell in ventricular volume as atrial and ventricular pressures practically do not vary. The second one, called diastasis, experiences a small additional increase in ventricular volume but nothing changes in pressures for atrium and ventricle. The last phase, responsible for a further growth in ventricular volume, corresponds to the atrial systole. As soon as atrial and ventricular pressures reach the same value again, mitral valve closes, diastole concludes and systole commences. Note that, during diastole, aortic pressure constantly reduces, just after an initial notch on its record, witness of the aortic valve

closure. Systole period can be seen as the sum of two moments: the isovolumic contraction and the ejection. The former makes constant ventricular volume whereas ventricular pressure rapidly rises and the aortic one continues diminishing. At the intersection between these two pressures, with a play of a few mmHg, aortic valve opens and ejection takes place. Now, while ventricular volume always drops, aortic and ventricular pressures follow a more complicated development. Indeed, they both rise towards their maximal values then come across and fall together. Aortic valve closes and systole ends, when aortic pressure overcomes the ventricular one. So, the cycle can begin again. Under standard conditions, a cardiac cycle takes, on average, around 0.8 s.

As a consequence of what we have just seen, pressure and flow records associated to different positions along the arterial tree are not constant in time. Fixed a site, they vary with time, deriving from the pumping action of the left ventricle. Really, at each point, the total pressure is the sum of three different contributions: the atmospheric pressure, the hydrostatic pressure and the pressure produced by the pumping activity of the heart. The last term is typically known as excess pressure and is the only responsible for making the blood flow along the blood vessels. The evolution of this excess pressure and its mean value, with the distance from the heart, are presented in the Figure 1.4. Important to say that, throughout this work, when talking about pressure, we always refer to the excess pressure, neglecting the other pressure elements contributing to the total real pressure at each point.

At this stage, I would like two face to other questions: what supplies the heart and what causes the rhythmic heart beat. About the first issue, we can take into account the following consideration. If one lived for 90 years with a constant cardiac frequency of 75 beats per minute, its heart would beat on the all around 3.5 billion of times. From this quick calculation, we immediately realise that heart is subjected to an enormous workload within all its life. For this reason, even more than other organs, the heart requires a great deal of oxygen and other nutrients to function properly. This need could not be satisfied by the blood inside the cardiac chambers, therefore, heart is equipped with its own vascular system: the coronary circulation. It starts from the aorta, which branches off into the left and the right coronary arteries, just after the left ventricle. The right coronary artery supplies blood to the right heart while the left one provides for the left side. These two arteries divide then into smaller vessels. Figure 1.5 gives more evidence of the previous description. One of the most striking aspect of the coronary circulation is the fact that, in its arterial vessels, the hematic flow reaches the maximal values during the ventricular relaxation rather than during the

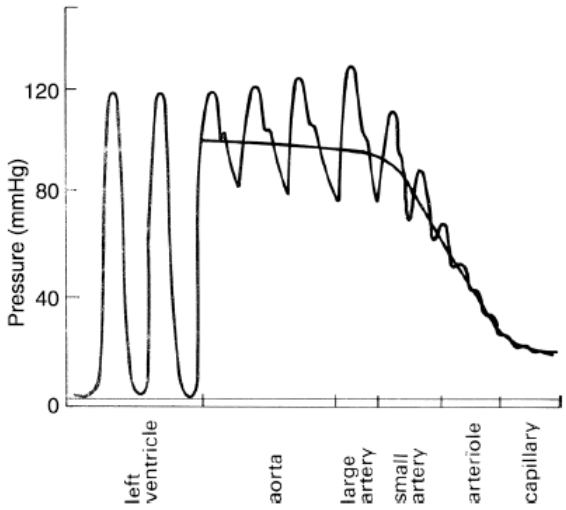

Figure 1.4: Evolution of the excess pressure and its mean value along the arterial tree [6].

ventricular contraction, as happens for all the other vessels. Clearly, next to the systemic circuit, the coronary circulation has its own venous circuit.

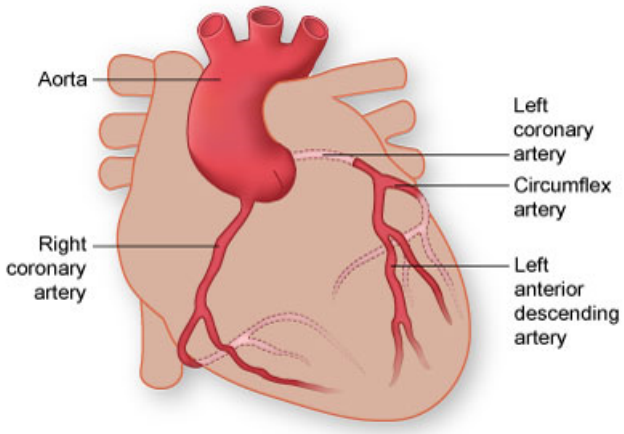

Figure 1.5: Representation of the main coronary arteries.

Concerning the mechanism responsible for the rhythmical functioning of the heart, we can start to say that our cardiac beat is defined myogenic.

This means that the signal leading to the beat derives from the heart itself rather than from the nervous system. So, human heart is provided with its own pacemaker, producing the initial rhythmical electrical impulse to the heart contraction, and its own conductive system, capable of communicating rapidly and effectively these impulses to the other heart regions. Figure 1.6 helps us identify the path followed by the prime electrical impulses generated in the heart.

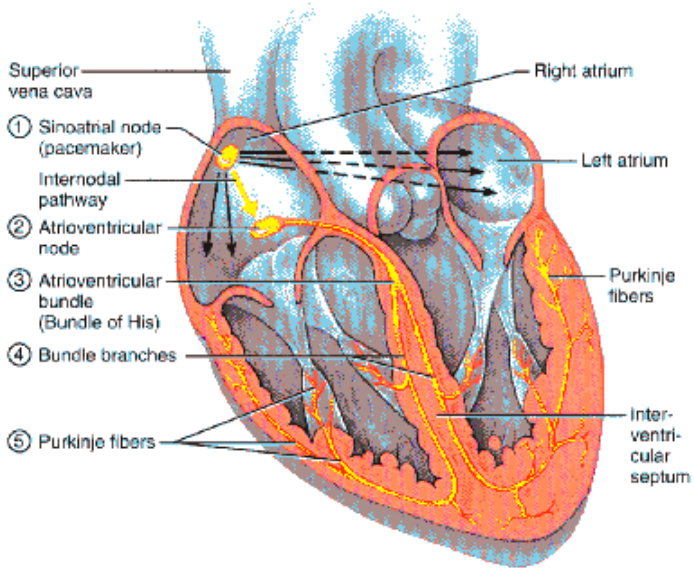

Figure 1.6: Representation of the conductive system of the heart.

For a standard heartbeat, the rhythmical electrical impulse starts in the sinoatrial node (point 1), also called sinus node. It is the natural human pacemaker: it leads to each beat and establishes the cardiac rhythm. It is located in the wall of the right atrium, just below the opening of the superior vena cava. The electrical signals can then spread into the atria, as indicated by the black arrows. Another essential element of the heart conductive system is the atrioventricular node or A-V node (point 2). It lies close to the A-V valve, at the inferior extremity of the interatrial septum. Note that every electrical signal has to pass through the A-V node before reaching the ventricles. As a consequence, the A-V node represents an electrical barrier inserted between atria and ventricles. It avoids that atria and ventricles contract simultaneously, that is essential to have our beat developed properly. The atrioventricular bundle or the bundle of His (point 3) is

the way followed by the electrical impulses as soon as the A-V node is left. It runs into the interventricular septum and branches into two parts: the left one and the right one. Finally, the Purkinje Fibres (point 5) distribute the electrical excitement to the ventricles. They create various network, more elaborated in the left ventricle than in the right one. Important to say that the electrical impulses, originated at the sinus node, not only travel along the conductive system but also can be transferred to all the cells of both the atria and ventricles. This is possible thanks to the special microscopical anatomy of the heart tissues.

The sinus node, the A-V node and the Purkinje Fibers are made of the so called cardiac pacemaker cells. These have the capability of self-excitation. It means that they can automatically discharge electrically at a regular pace. So, it is thanks to these cells that a spontaneous electrical impulse can be regularly generated within the heart, propagating quickly along the principal canals of the heart conductive system. At this point, it is licit to ask why the Purkinje Fibres and the A-V node leave the pacemaker role to the sinus node, even if they are constituted of cardiac pacemaker cells as well as the sinus node. This is because the discharge rate of the sinus node is decisively faster than the spontaneous rate of self-excitatory discharge of both the A-V node and the Purkinje Fibres. However, this is what happens in the case of normal heart functioning. Indeed, under anomalous conditions, the origin of the cardiac rhythm can shift from the sinus node to other regions, leading to specific forms of arrhythmias.

In order to propagate efficiently the electrical signals to the heart chambers, it is essential the role carried out by the cardiomyocytes. These are the cells constituting both atria and ventricles. They are linked each other through a special connection system, containing the so called gap junction. Thanks to it, each excited cardiomyocyte is able to stimulate electrically the neighbouring cardiomyocytes. As a consequence, when the electrical impulses reach the atria, they behave like a single cell. The same is true as the ventricles have to contract, therefore, when the electrical signals arrive at the Purkinje Fibres.

Note that both the cardiac pacemaker cells and the cardiomyocytes constitute the myocardium, the internal tissue of the heart wall, between the most external layer, epicardium, and the most internal one, endocardium.

Even if heart has its own pacemaker and conductive system, it receives both a sympathetic and parasympathetic innervation, which influence the cardiac rhythm and the heart contraction force. In particular, the sympathetic stimulation can accelerate the beat to 230 beats per minute while the parasympathetic stimulation is able to slow the beat rate to about 20 beats

per minute or stop the heart beating for a few seconds. These innervations are essential to make the heart adapt to our body's needs. For example, if we are doing physical exercise, our heart has to pump more blood to supply tissues with more oxygen.

1.2 Atrial fibrillation: a particular arrhythmia

Our heart can also exhibit an arrhythmic functioning. This is when the beat is altered in terms of frequency or rhythm. It means that the beat is too fast, too slow or has an irregular rhythm. Arrhythmias are electrical problems since are due to the fact that the generation/conduction of the electrical impulses within the heart are not developing as we would expect.

There are several classes of arrhythmias, each with its own specificity. However, the actual classification identifies three main categories of arrhythmias: the tachicardias, the bradycardias and the ectopic beats. Concerning tachicardias and ectopic beats, the main problem lies on the altered formation of the impulse leading to the beat. This means that the beat onset is not localised at the sinus node and arises sooner or later than the normal sinus rhythm would require. On the bradycardias, instead, the principal disorder is nearly always due to the conduction of the electrical signal rather than its creation.

The previous groups of arrhythmias can be more widely specified, defining a lot of different pathologies. We now concentrate only on one of these: the atrial fibrillation (AF). It is defined as a supraventricular arrhythmia and belongs to the area of tachicardias. In AF, the heart's electrical signals do not begin in the sinus node but in other parts of the atria and typically nearby the pulmonary veins. Moreover, the signals spread through the atria in a fast and irregular rhythm, with a maximal frequency of about 600 beats per minute. The immediate consequence of this is that the atria are not entirely depolarized for a small fraction of the beat duration, as happens in the case of standard beat. By contrast, they are activated continuously during the beat, with some regions polarized and others depolarized at each moment of the cardiac cycle. For this reason, in case of AF, we can talk about atrial paralysis: normal atrial contraction is no longer possible.

If the abnormal electrical impulses affecting the atria are adequately filtered at the A-V node, ventricular frequency will not reach extremely high values. Therefore, in absence of particular ventricular dysfunctions, ventricular filling is not compromised by AF and the heart can still pump enough blood to the lungs and the other organs. Indeed, as we have just seen

through the Wiggers diagram (Figure 1.3), the greatest portion of blood passes from the atria into the ventricles passively; atrial contraction has the only function to conclude the filling phase. However, if the ventricles have previous pathologies, the onset of AF will represent a serious threat: ventricles do not acquire sufficient blood to meet the body's needs. One of the most dangerous consequences of AF is that of stroke. The reduction in atrial contraction makes the hematic flow slow in the atria: the blood can pool in clots within the atria. These clots can cause embolization at any peripheral site of the systemic circulation. When it is involved the brain, we will have a stroke.

People affected by AF complain of different symptoms. The most common one is that of palpitations, mainly due to the irregularity of the beat rhythm. Other symptoms such as dystenia, asthenia and chest discomfort may be also present as a consequence of the abnormal atrial contraction.

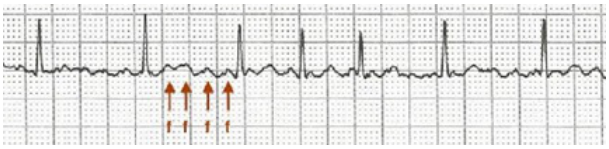

(a) f waves.

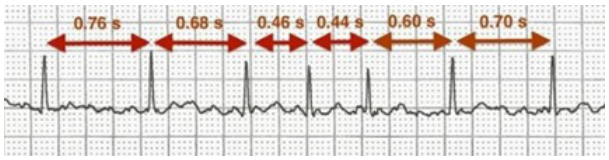

(b) Irregular RR intervals.

Figure 1.7: Electrocardiogram in case of atrial fibrillation.

AF can be recognized through a simple electrocardiogram. If one is affected by AF, its electrocardiogram will not show the P waves, expression of the standard atrial depolarisation. We can also recognise new waves, known as f waves, characteristics of the atrial behaviour during AF. These waves appear as irregular high frequency oscillations, altering the standard base line or isoelectric line. f waves constantly modify their shape, amplitude and frequency. The latter can range from 380 to 600 beats per minute. These aspects are visible in the Figure 1.7a. In AF, the time intervals between the ventricular complexes (groups of waves QRS), also indicated as RR intervals, are extremely variable. This is due the fact that many electrical impulses available in the atria are blocked in the A-V node, before passing through the ventricles. Irregular RR intervals are clearly shown in the Figure 1.7b.

Chapter 2

Elements of arterial hemodynamics

Before starting analysing what happens along the arterial tree during a normal or fibrillated heartbeat, we have to keep in mind this key point: pressure and flow signals, generated by the left ventricle contractions, travel down the aorta and its branches as waves. Since vessels are not perfectly rigid, pressure and flow waves propagate along the arterial tree with a finite speed. It is known as wave speed or pulse wave velocity and varies locally. Moreover, pressure and flow waves are progressively reflected during their propagation. This is especially because of the bifurcations and discontinuities of the vasculature.

We now consider some techniques used to calculate the wave speed at a general point. We also introduce the vessel input impedance, from which we can then derive the characteristic one. This enables us to decompose, under proper hypothesis, both the total pressure and flow waves, at each arterial site, into two different contributions: the forward one and the backward one. At this level, we can indicate how the magnitude of reflection may be evaluated at a generic vessel section. Finally, we will present a method to quantify the way in which the signals are reflected at the vessel junctions.

2.1 Speed velocity and phase velocity

The wave speed, c, is, by definition, the distance travelled by the wave over the time required to the passage. Clearly the wave transmission exists even though the blood flow is zero. Important to note that, at each site, c is relative to the local blood speed and not to the tube wall. So, locally, the sum of c and the mean blood velocity gives the effective wave speed. The effect of the blood velocity is typically neglected because it is usually much smaller than c.

It is possible to obtain c, at a generic vessel point, through different methods. We indicate some of them.

- METHOD 1. We can use

$$c = \frac{1}{\sqrt{\rho D}}. \tag{2.1}$$

For this, ρ is the blood density and D is the local vessel distensibility. Note that we use D to measure the stiffness of a vessel wall. Chosen a segment of a vessel of defined length, its distensibility is calculated as

$$D = \frac{1}{A}\frac{\triangle A}{\triangle p}, \tag{2.2}$$

where $\triangle A/A$ is the local fractional change in cross-sectional area and $\triangle p$ is a generic small change in the applied pressure. Eq. (2.1) is based on the conservation of mass and momentum principles. These are applied to an extremely simplified artery: an infinitely long distensible tube whose properties do not vary with length. Important to stress the fact that the (2.1) is obtained under two hypothesis: neglect of blood viscosity and linearity. The first one is usually acceptable when we refer to large vessels. The second one implies two types of linearity: the fluid dynamic linearity (the mean blood velocity is much smaller than c), and the elastic linearity (the disturbances of pressure pulse are small enough not to make vary significantly elastic wall properties such as distensibility). If we assume that vessel wall is similar to a thin and homogeneous membrane, we will have

$$D = \frac{1}{E_{inc}(h/d)}. \tag{2.3}$$

Here, E_{inc} is the incremental elastic modulus, h is the wall thickness and d is the lumen diameter, all of them at the chosen vessel site. So, Eq. (2.1) becomes

$$c = \sqrt{\frac{hE_{inc}}{d\rho}}. \tag{2.4}$$

It is the Moens-Korteweg equation. This can lead to some errors, when E_{inc} and h/d are not obtained by the distensibility measurements.

- METHOD 2. Alternatively, we can determine c, at a generic site, through the foot-to-foot method. In this case we have to know the total pressure signals at the entrance to the ascending aorta and at the chosen site. We calculate the distance between the two points, $\triangle x$, and the time it takes for the foot of the wave to go from the beginning of the aorta to the site of interest, $\triangle t$. The ratio between $\triangle x$ and $\triangle t$ is c. Figure 2.1 gives evidence of this technique.

- METHOD 3. The last method we see is similar to the previous one. But, now, we only work on the forward portion of the pressure signals, both at the beginning of the aorta and at the site of interest. When adopting this technique, we are expected to know how the pressure waves can be divided into their backward and forward components. This aspect will be discussed in section 2.3.

Note that, since pressure and flow waves travel at the same speed, when adopting the last two methods, we could use the flow waves too. However, we prefer work on pressure signals.

It is better to provide some clarifications about the previous techniques. Actually, at a general site, the definition of the wave speed could seem ambiguous. We imagine to evaluate c, locally, as the ratio between the distance travelled by the pressure wave, from the heart, to reach the chosen site and the time it takes for the same wave to make this transfer. Since the shape of the pressure signals varies during the beat, at the entrance to the aorta

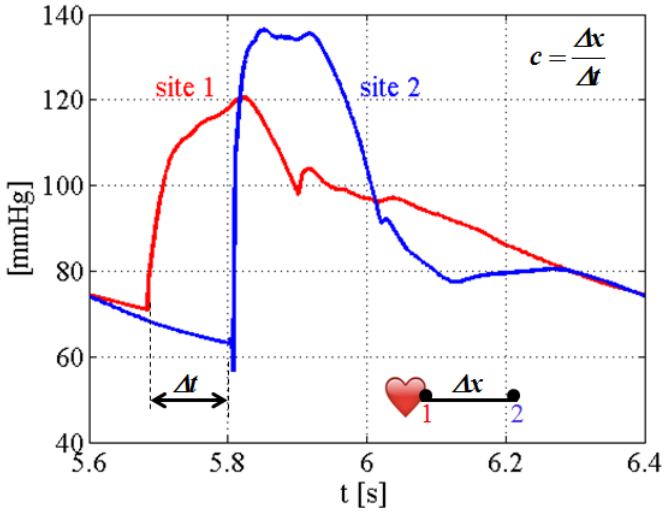

Figure 2.1: Representation of the foot-to-foot method.

as well as at the chosen site, c varies depending on the reference pressure values to calculate the time interval. To solve this problem, we always refer to the foot of the wave, leading to the second method presented above. Through it, we can break away from the effects of reflections, obtaining an average wave speed, known as phase velocity. The same result is clearly achievable through the third technique, previously introduced. According to this, we work only on the forward component of the waves. Therefore, the effects of reflections are necessarily neglected and the ambiguity of the result is overcome by referring to the foot of the forward waves. Note that, from now on, the symbol c is used to indicate local phase velocities and not ambiguous local wave speeds. As concern the Eq. (2.1) and the Eq. (2.4), it is said in the literature [50] that they do not consider the effects of reflections. For this reason, we can immediately think that, at a generic site, the value of c derived from the first method above is pretty much the same as the phase velocity obtained by the other two techniques. It is true when the distensibility required by the first method corresponds to the local foot of the pressure wave. This because D depends on the instant of the heartbeat simulated, i.e it depends on the frequency. For sake of clarity, we do an example. We want to determine the phase velocity at the entrance to the femoral artery. Adopting the first method, we choose a value of D relative

to a pressure of 100 mmHg, certainly higher than that associated to the foot of the pressure wave there. We obtain $c = 8.47$ m/s. However, adopting the second and the third method, we have a decisively smaller value of c. $\triangle x = 0.677$ m, so, with the second method, since $\triangle t = 0.122$ s, $c = 5.55$ m/s. For the last technique, $\triangle x$ as well as $\triangle t$ do not change and c is still 5.55 m/s, that is the correct value. It is demonstrated that, when D is not corresponding to the foot of the pressure wave, Eq. (2.1) and Eq. (2.4) certainly produce a measure of the wave speed, but it will not be equal to the local phase velocity given by the other two methods.

2.2 Input and characteristic impedance

To describe completely what happens at each site of the arterial system, we have to introduce the input impedance Z_{in}. It is a complex number, function of the frequency, that can be derived, fixed a site, from the total pressure and flow records, through the Fourier analysis. In particular, chosen a site, we have to apply Fourier analysis to the local pressure and flow signals, which can be broken down into a series of sine waves or harmonics. These have surely different amplitudes and frequencies and are out of phase with each other. The harmonics related to the pressure wave correspond to those of the flow wave. Therefore, for each pair of pressure and flow harmonics, we can derive the ratio of their amplitudes and the difference between their phase angles. The former is the modulus of Z_{in} while the latter is its phase angle, both at the chosen site and for the frequency of the selected pressure and flow harmonics. Figure 2.2 shows a possible evolution of the input impedance with the frequency.

The richness of this result is due to the fact that, knowing Z_{in} at a general point, we have an instrument to immediately correlate locally the pressure record with the flow one and vice versa. However, this result has some limitations. The most apparent is that it is not possible to apply Fourier analysis as the system is not linear. When we talk about linearity in this context, we are referring to the fluid dynamic linearity as well as the elastic linearity, briefly explained in section 2.1. If the hypothesis of linearity is not applicable, the different harmonics of a general wave will not be reciprocally independent and it will not be possible to deduce the behaviour of the total wave as combination of its constitutive sine waves: it will not be valid the superposition principle. Fortunately, as concern the application of Fourier analysis, the linearity hypothesis is well verified at the arterial conduits and for a physiological functioning [6].

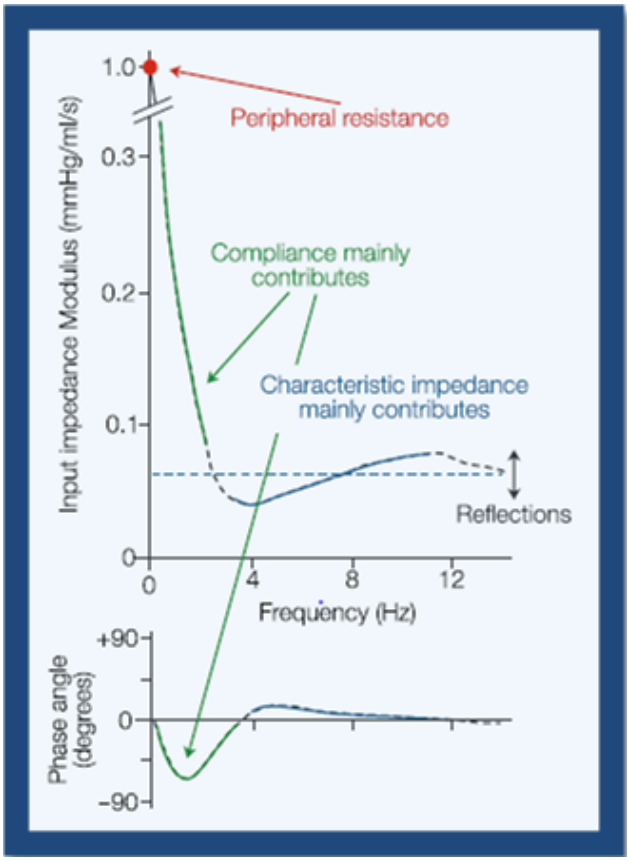

Figure 2.2: Example of evolution of the input impedance with frequency [50].

It is interesting to note that, at each site, Z_{in} can be substantially described through three different elements, also indicated in the Figure 2.2: the peripheral resistance and the input impedance, real numbers, and the compliance, complex number. These quantities are those adopted in a three Windkessel element [50].

The input impedance tends to the characteristic impedance as frequency is sufficiently high. This means that, if we refer to the initial time of a general heartbeat, the frequency function Z_{in}, at any arterial position, will be approximated with the value of the characteristic impedance there. Furthermore, if we neglect the effects of viscosity, as well as viscoelasticity, the local characteristic impedance will be evaluated as

$$Z_c = \frac{\rho c}{A}, \tag{2.5}$$

where A is the lumen area of the chosen site and c is the phase velocity at the same section. It is reasonable neglecting wall friction and viscoelasticity to calculate Z_c, as we work on conduit arteries [6], [50]. In light of the above, we can deduce that, during the first period of the heartbeat, the total pressure and flow waves are sync. We will see that it is never true during the other beat phases.

2.3 Forward and backward running waves

In general, chosen a point along an artery and given a total wave (pressure or flow wave), we can decompose it into two different parts: the backward running wave and the forward running wave. Clearly the sum of these has to return the complete local signal. The forward and backward running pressure and flow waves can be obtained by using both the total pressure and flow waves. We have

$$\begin{aligned} P_f = Z_c Q_f = \frac{P + Z_c Q}{2}, \\ P_b = -Z_c Q_b = \frac{P - Z_c Q}{2}, \end{aligned} \tag{2.6}$$

from the system

$$\begin{cases} P_f = Z_c Q_f, \\ P_b = -Z_c Q_b, \\ P = P_f + P_b, \\ Q = Q_f + Q_b. \end{cases} \tag{2.7}$$

Here, P and Q are the total pressure and flow waves, respectively. The subscript f stands for forward while the subscript b means backward. The minus sign in the equation $P_b = -Z_c Q_b$ is due to the fact that the backward flow is reflected inside out, compared to the backward pressure. Therefore,

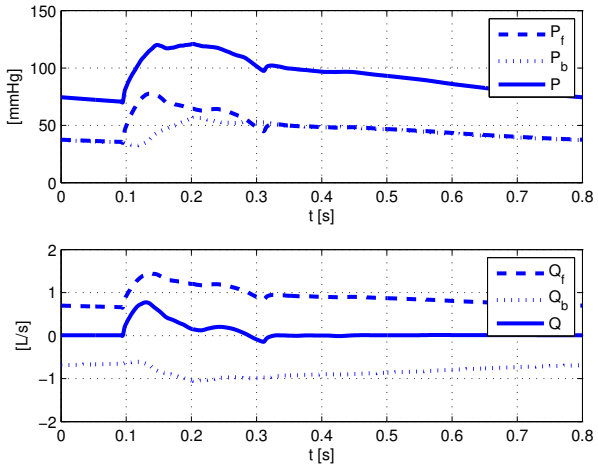

Figure 2.3: Decomposition of pressure and flow waves at the entrance to the ascending aorta.

while the forward running pressure and flow waves have the same shape, it is not true for the reflected pressure and flow waves. Evidence of this is given through the Figure 2.3.

When complete pressure and flow signals at a general site are different in shape, it means that the effects of reflections are not negligible. The magnitude of reflection can be quantified by the Reflection Magnitude, which is the ratio of the amplitudes of backward and forward waves: $RM = |P_b|/|P_f|$. Another important parameter to estimate the role of reflection is the Reflection Index, $RI = |P_b|/(|P_f| + |P_b|)$, ratio of the amplitude of the backward wave and the sum of the amplitudes of the forward and backward waves.

2.4 Reflection and transmission at a single junction

Where the vessel properties change, we have a site of partial reflection of the pressure and flow waves. Variations in the geometric and mechanical properties along the arterial tree are responsible for some reflection, but the most powerful sources of reflections are the arterial bifurcations.

It is useful to analyse what changes a wave experiments encountering a single junction. We consider a parent artery dividing into two daughter arteries, as shown in the Figure 2.4. The generic incident wave before the

junction is going to be reflected at the arterial discontinuity: we will have a reflected wave turning back through the parent artery and two transmitted waves travelling down the daughter vessels. As indicated in the Figure 2.4, the subscript 0 refers to the parent tube while the subscripts 1 and 2 are used for the daughter tubes. It is possible to calculate the characteristic impedances Z_c for the parent and the daughter arteries (Z_{c_0}, Z_{c_1} and Z_{c_2}, respectively) by the Eq. (2.5), under the assumption of large vessels. At the junction, we define the incident pressure and flow waves (P_i and Q_i, respectively), the reflected pressure and flow waves (P_r and Q_r, respectively) and the transmitted pressure and flow waves (P_{t_1}, P_{t_2} and Q_{t_1}, Q_{t_2}, respectively).

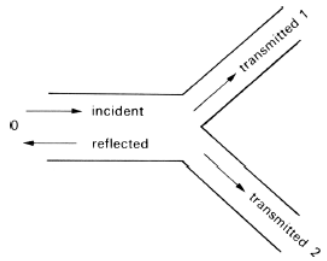

Figure 2.4: Sketch of an arterial bifurcation [6].

At the bifurcation, we have to fix the conservation of pressure (both the mean part and the oscillatory part) and mass. P_i, P_r, P_{t_1} and P_{t_2} can be related to the corresponding flow signals through the local characteristic impedances of the tubes. Note that the time course of the forward pressure waves is synchronous with the time course of the forward flow waves and the backward pressure waves vary with time in the same way as the backward flow waves, apart from a minus sign. According to the simplest wave theory, the forward or backward flow wave, at generic site x, Q_x, can be written as $Q_x = P_x/Z_{c_x}$, where P_x is the pressure wave in the same direction at x and Z_{c_x} represents the characteristic impedance at the chosen site x.

In consideration of the above, we can write the system

$$\begin{cases} P_i + P_r = P_{t_1} = P_{t_2} = P_t, \\ Q_i + Q_r = Q_{t_1} + Q_{t_2}, \\ P_i = Z_{c_0} Q_i, \\ P_r = -Z_{c_0} Q_r, \\ P_{t_1} = Z_{c_1} Q_{t_1}, \\ P_{t_2} = Z_{c_2} Q_{t_2}, \end{cases} \tag{2.8}$$

which leads to the ratios

$$\begin{aligned} \frac{P_r}{P_i} &= \frac{Z_{c_0}^{-1} - (Z_{c_1}^{-1} + Z_{c_2}^{-1})}{Z_{c_0}^{-1} + (Z_{c_1}^{-1} + Z_{c_2}^{-1})} = R, \\ \frac{P_t}{P_i} &= \frac{2Z_{c_0}^{-1}}{Z_{c_0}^{-1} + (Z_{c_1}^{-1} + Z_{c_2}^{-1})} = T. \end{aligned} \tag{2.9}$$

Here, the reciprocal of the characteristic impedances Z_c^{-1} are the admittances. The (2.9) tells us that the sum of the admittances of the vessels after bifurcation determines the conditions under which reflected and transmitted waves are created at the same arterial junction. It is also true even when the parent tube branches into three or more arteries.

Looking at the (2.9), it is clear that T is always positive. Therefore, the transmitted pressure wave is always in phase with the incident pressure wave before the bifurcation. Something different happens as concern R. When it is zero, waves are not reflected at the bifurcation, that is said to be one at which the characteristic impedances of the surrounded vessels are matched. This situation is quite improbable, so we have to look at the sign of R.

- for positive reflection ($R > 0$): the reflected pressure wave is in phase with the incident pressure wave, the reflected flow wave is out of phase with the incident flow wave and the transmitted pressure wave grows in amplitude.
- for negative reflection ($R < 0$): what we have just written for $R > 0$ has to be reversed.

We can also evaluate the amount of energy which transfers both in the reflected wave and in the transmitted waves [6]. The former is the reflection coefficient

$$R^2, \tag{2.10}$$

the latter, instead, is known as transmission coefficient

$$\frac{Z_{c_1}^{-1} + Z_{c_2}^{-1}}{Z_{c_0}^{-1}} T^2. \tag{2.11}$$

Since the energy must be conserved at the junction, the sum of the reflection and the transmission coefficients is always 1.

Chapter 3

Mathematical model

To obtain a better understanding of the effects of a fibrillated heartbeat on the cardiovascular system, different models have been developed [49]. Some of them extend the Windkessel approach to the whole circulation, described as a network of compliances, resistances and inductances. In this way, it is possible to gain an overall comprehension of the arrythmia impact on the global cardiovascular system.

In this work, by contrast, we adopt the multi-scale mathematical model by Guala [16], [19]. This approach consists of different coupled sub-models, each of which represents a specific sector of the circular system, with a suitable level of detail. In this way, we can study how irregular beats may affect the propagation of pressure and flow waves along the arterial tree.

Domain and mathematical model for this study are presented below.

3.1 Domain

A scheme of the domain is presented in the Figure 3.1. We have a network of 48 large vessels, 18 distal groups and 24 arterial bifurcations. Table 3.1 correlates vessels numbers to their names and some relevant properties [40].

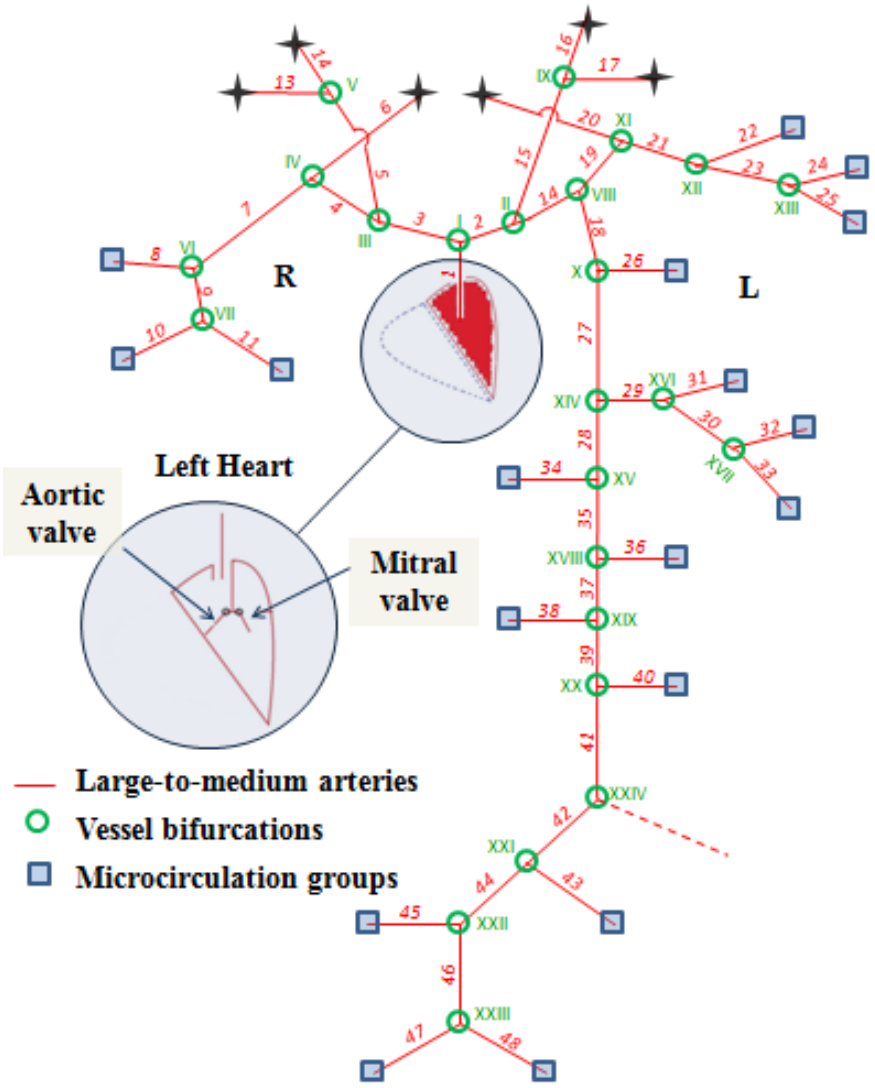

Figure 3.1: Representation of the arterial tree according to the model.

Table 3.1: Properties of the vessels of the arterial tree. (PLD) Proximal lumen diameter. (DLD) Distal lumen diameter [41].

Name	**Number**	**Length** [mm]	**PLD** [mm]	**DLD** [mm]	**Distensibility** [1/mmHg]
Ascending Aorta 1	1	5	29.4	29.3	5.46
Aortic Arch A	2	20	25.1	24.0	4.90
Brachiocephalic	3	34	20.2	18.0	4.22
Subclavian A	5/15	94/139	11.5/11.0	9.0/8.5	2.90/2.81
Common Carotid	4/19	34	11.5/11.0	9.0/8.5	2.90/2.81
Vertebral	6/20	149/148	3.7	2.8	1.46
Subclavian B	7/21	422	8.1	4.7	2.19
Radial	8/22	235	3.7/3.5	3.1/2.8	1.49/1.43
Ulnar A	9/23	67	3.7/4.3	3.4/4.3	1.53/1.72
Interosseous	10/24	79	2.1/1.8	1.8	1.08/1.03
Ulnar B	11/25	171	3.2/4.1	2.8/3.7	1.39/1.62
Internal Carotid	12/16	178	5.7/5.3	4.3/4.1	1.89/1.82
External Carotid 1	13/17	41	5.0/4.7	4.5/4.3	1.83/1.77
Aortic Arch B	14	39	21.4	20.8	4.48
Thoracic Aorta A	18	52	20.0	18.9	4.26
Intercostals	26	80	12.6	9.5	3.04
Thoracic Aorta B	27	104	16.5	12.9	3.60
Abdominal Aorta A	28	53	12.2	12.2	3.22
Celiac A	29	20	7.8	6.9	2.38
Celiac B	30	20	5.2	4.9	1.90
Hepatic	31	66	5.4	4.4	1.87
Gastric	32	71	3.2	3.0	1.42
Splenic	33	63	4.2	3.9	1.66
Superior Mesenteric	34	59	7.9	7.1	2.41
Abdominal Aorta B	35	20	11.5	11.3	3.09
Renal	36/38	32	5.2	5.2	1.93
Abdominal Aorta C	37	20	11.8	11.8	3.16
Abdominal Aorta D	39	106	11.6	11.0	3.07
Inferior Mesenteric	40	50	4.7	3.2	1.64
Abdominal Aorta E	41	20	10.8	10.4	2.96
Common Iliac	42	59	7.9	7.0	2.39
External Iliac	44	144	6.4	6.1	2.15
Inner Iliac	43	50	4.0	4.0	1.65
Femoral	46	443	5.2	3.8	1.77
Deep Femoral	45	126	4.0	3.7	1.61
Posterior Tibial	48	321	3.1	2.8	1.38
Anterior Tibial	47	343	2.6	2.3	1.24

The vessel geometry adopted in this study is that of a typical young health man. Cerebral circulation, venous return and coronary arteries are not considered. It is proved that the impact of cerebral circulation on the behaviour of the systemic one can be adequately described through proper Windkessel models, located where internal and external carotids, as well as vertebral arteries, should develop [41]. Surely, the absence of the coronary circulation is limiting, especially during the diastolic phase of the heartbeat, but it will be certainly possible to take into account its influence in future. Really, at the moment, we could implement the coronary circuit (whose corresponding model is ready), but here we neglect it for the sake of simplicity. Since venous return is neglected, heart is described as the combination of only two cavities: the left atrium and the left ventricle. They are connected through the mitral valve. Left ventricle and aorta, instead, are linked by the aortic valve. We account for both arms because the systemic circulation is not perfectly symmetric for them. On the contrary, we simulate only one leg, the right one, taking advantage of the symmetry. The groups of distal vessels are represented by using three element Windkessel models.

3.2 Sub-models

We now detail the equations used for modelling the different part of domain as well as at the hypothesis on which each sub-model is based.

3.2.1 Large arteries

The largest arteries of the systemic circulation represent the first sub-model. Here, the flow is assumed laminar [30]. This is true for most of time, having mean Reynolds numbers in the range 1000-100, between the beginning of aorta and the last medium vessels. Certainly, during ejection phase, high frequency disturbances are observed at the largest arteries, where peak Reynolds number fluctuates between 9000 and 2000. However, a previous analysis [37] demonstrated that similar disorders are not sufficient to make the flow turbulent. The geometry and the flow field of the vessels are supposed to be axisymmetric [34]. Arterial walls are taken longitudinally-tethered. This implies that the vessel motions are only radial and little [34]: the vessel length is never altered by any deformation and each cross sectional area is always perpendicular to the corresponding tube axis. The presence of suspended particles is neglected and the blood is treated as Newtonian, with constant density ρ and constant cinematic viscosity ν [34]. We fix $\rho = 1050$ kg/m^3 and $\nu = 3.8$ mm^2/s.

Under the previous hypothesis, we resolve the large and medium arteries through the one dimensional mass and momentum balance equations, integrated over the transversal section. These are:

$$\frac{\partial A}{\partial t} + \frac{\partial Q}{\partial x} = 0, \tag{3.1}$$

$$\frac{\partial Q}{\partial t} + \frac{\partial}{\partial x}\left(2\pi \int_0^R u^2 r\, dr\right) = -\frac{A}{\rho}\frac{\partial P}{\partial x} + Ag\sin\gamma + 2\pi\nu\left[r\frac{\partial u}{\partial r}\right]_{r=R}. \tag{3.2}$$

As concerns the symbols used, r is the radial coordinate, x is the position along the vessel axis, t is time, $A(x,t)$ is the arterial cross-sectional area, $P(x,t)$ is the radially-constant pressure, $R(x,t)$ is the arterial radius, $u(r,x,t)$ is the axial velocity profile, $Q(x,t) = 2\pi\int_0^R ur\, dr$ is the flow rate relative to the generic $A(x,t)$, g is the gravitational acceleration and $\gamma(x)$ is the angle between axial and horizontal directions. We remember that P, in this work, is the only excess pressure due to the contraction of the left ventricle (section 1.1).

Solving the problem given by the equations (3.1) and (3.2), at each site, implies the knowledge of the velocity profile there. It varies locally with time as concern both its mean value and its shape. This because of the pulsating activity of the left ventricle, which creates pulsating pressure and flow waveforms, variable with the distance from the heart.

While the central portion of the velocity profile is regulated by inertial forces, the regions closer to the wall are dominated by the effects of viscosity. However, according to Lighthill [31], the boundary layer thickness is significant only in the smallest vessels, where it results comparable with the vessel radius. Regarding large vessels, instead, the influence of viscosity is almost negligible and is only identified with the closest regions to the walls. Since we are working on large vessels, it is licit to assume a central flat profile, completed by a parabolic boundary layer of thickness $\delta(x,t)$. Hence, at each site, Guala [16] assumes the velocity profile

$$u(r,x,t) = \begin{cases} \overline{u}(x,t) & \text{if } 0 < r < R(x,t) - \delta(x,t), \\ \frac{R^2(x,t)-r^2}{2R(x,t)\delta(x,t)-\delta^2(x,t)}\overline{u}(x,t) & \text{if } r \geq R(x,t) - \delta(x,t). \end{cases} \tag{3.3}$$

Clearly, this is only a possible design of the velocity profile.

We can estimate the boundary layer thickness by using the Womersley number, α, non-dimensional parameter, seen as the ratio between the unsteady inertial forces and the viscous ones:

$$\alpha = \sqrt{\frac{\text{Volumic inertial transient forces}}{\text{Volumic viscous forces}}} = \sqrt{\frac{\rho\omega u}{\mu\frac{u}{R}\frac{1}{R}}} = R\sqrt{\frac{\omega}{\nu}}. \tag{3.4}$$

It comes from a dimensional analysis of the linearized Navier-Stokes equations, written for pipes in which an incompressible, laminar and periodic flow develops. For small α, the velocity profile approximates the Poiseuille one. By contrast, if α reaches high values (typically $\alpha > 10$), unsteady inertial forces will be more powerful than the viscous ones and the profile is predominantly flat. Note that ω is the dominant pulsation of the pressure wave going trough the pipe; in this problem it may be considered equal to the cardiac pulsation.

Imposing the Womersley number equal to one, we obtain the approximated value of the boundary layer thickness δ:

$$\alpha = 1 \Longleftrightarrow \delta = \sqrt{\frac{\nu}{\omega}}. \tag{3.5}$$

However, since in certain zones the arterial radius is littler than the value of δ estimated through the (3.5), it should be more correct to define δ as

$$\delta = min\left\{R(x,t), \sqrt{\frac{\nu}{\omega}}\right\}. \tag{3.6}$$

At each site, the velocity of the flat core can be expressed as a function of Q and R:

$$\overline{u}(x,t) = \frac{2Q(x,t)}{\pi\{[\delta(x,t)]^2 + 2R(x,t)[R(x,t) - \delta(x,t)]\}}. \tag{3.7}$$

If we adopt the Eq. (3.7), it will be possible to write in a more concise way both the convective and viscous terms of the (3.2). The former is

$$\frac{\partial}{\partial x}\left(2\pi\int_0^R u^2 r\,dr\right) = \frac{\partial}{\partial x}\left(\beta\frac{Q^2}{A}\right), \tag{3.8}$$

with β computed as

$$\beta(x,t) = \frac{4}{3}\frac{3A^2 - 4A^{3/2}\sqrt{\pi}\delta + 2A\pi\delta^2}{\left(2A - 2\sqrt{A}\sqrt{\pi}\delta + \pi\delta^2\right)^2}. \tag{3.9}$$

The viscous term of the momentum balance equation, instead, is rewritten as

$$2\pi\nu\left[r\frac{\partial u}{\partial r}\right]_{r=R} = \frac{8AQ\sqrt{\pi}\nu}{\delta(-4A^{3/2} + 6A\sqrt{\pi}\delta - 4\sqrt{A}\pi\delta^2 + \pi^{3/2}\delta^3)} = N_4. \tag{3.10}$$

Therefore, the (3.2) becomes

$$\frac{\partial Q}{\partial t} + \frac{\partial}{\partial x}\left(\beta\frac{Q^2}{A}\right) = -\frac{A}{\rho}\frac{\partial P}{\partial x} + Ag\sin\gamma + N_4. \tag{3.11}$$

One can see that the (3.11) contain three dependent variables: $P(x,t)$, $Q(x,t)$ and $A(x,t)$. As a matter of fact, it is requested another equation to solve the problem in each point and at each instant. We use a constitutive equation able to link $P(x,t)$ and $A(x,t)$. This relation tells us how much vessels are deformed radially by pressure changes. Since the arterial walls are proved to have a vessel-dependent anisotropic non-linear viscoelastic behaviour, a non-linear viscoelastic constitutive relation for $P(x,t)$ is adopted. It separates the elastic (P_e) and viscous (P_v) pressure components, as follows:

$$P(x,t) = P_e(x,t) + P_v(x,t). \tag{3.12}$$

Then, $P_e(x,t)$ is calculated as

$$\begin{aligned} &P_e(x,t) = \\ &= B_1(x,t) + B_2(x,t)A(x,t) + B_3(x,t)A^2(x,t) + B_4(x,t)A^3(x,t), \end{aligned} \tag{3.13}$$

while $P_v(x,t)$ is written like

$$P_v(x,t) = -B_5(x)\frac{1}{\sqrt{A(x,t)}}\frac{\partial Q(x,t)}{\partial x}. \tag{3.14}$$

The space-dependant coefficients B_i, for $i = 1 \div 5$, that embed information about the local mechanical properties of the arterial walls, are represented in the following block

$$\begin{aligned} B_1 &= -\frac{1}{{a_3}^3}({a_5}^3 + PWV^6\rho^3 + 3PWV^4\rho^2 a_5 + 3{a_5}^2 PWV^2\rho), \quad \left[\frac{\mathrm{N}}{\mathrm{m}^2}\right] \\ B_2 &= \frac{3\rho PWV^2}{A_0{a_3}^3}(\rho^2 PWV^4 + 2\rho a_5 PWV^2 + {a_5}^2), \quad \left[\frac{\mathrm{N}}{\mathrm{m}^4}\right] \\ B_3 &= -\frac{3\rho^2 PWV^4}{{A_0}^2{a_3}^3}(a_5 + \rho PVW^2), \quad \left[\frac{\mathrm{N}}{\mathrm{m}^6}\right] \\ B_4 &= \left(\frac{\rho PWV^2}{A_0 a_3}\right)^3, \quad \left[\frac{\mathrm{N}}{\mathrm{m}^8}\right] \\ B_5 &= \frac{kh_0}{2\sqrt{A_0}R_0}. \quad \left[\frac{\mathrm{m}}{\mathrm{s}}\right] \end{aligned} \tag{3.15}$$

The coefficients $a_3 = 1914\ \mathrm{N}^{2/3}/\mathrm{m}^{4/3}$ and $a_5 = -45.348\ \mathrm{N/m}^2$ are fixed. $R_0(x)$ and $A_0(x)$ are, respectively, the radius and the inner area of a generic vessel section, evaluated at the reference pressure $P_0 = 100$ mmHg [41]. $k(x)$ is the effective viscosity of the wall and $h_0(x)$ is the arterial wall thickness at the reference pressure. Finally, PWV is the pulse wave velocity, that we have expressed as a function of the diameter: $PWV(x,t) = a_2/d^{b_2}(x,t)$, with $a_2 = 13.3\ \mathrm{m}^{1.3}/\mathrm{s}$ and $b_2 = 0.3$.

Further information about the way in which the complete expression of $P(x,t)$ is derived are provided in the article [16].

Beyond the equations, the imposition of boundary conditions is necessary to solve the large vessels. Hence, the rigid impermeable wall condition ($[\mathbf{u} \bullet \hat{\mathbf{e}}_r]_{r=R} = 0$) and the no-slip condition ($[\mathbf{u} \wedge \hat{\mathbf{e}}_r]_{r=R} = 0$) are applied on the arterial walls.

3.2.2 Left ventricle

The left ventricle is modelled through the lumped model proposed by Sagawa [42]. According to this, the activity of the contracting myocardium is represented by using the time-varying elastance

$$E_{LV}(t) = \frac{P_{LV}(t)}{V_{LV}(t) - V_0}. \tag{3.16}$$

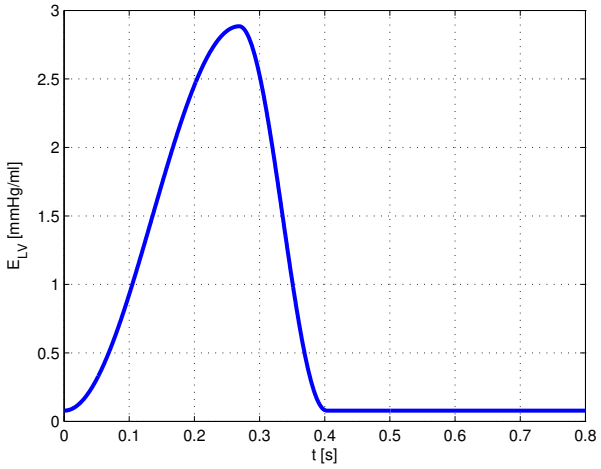

Figure 3.2: Elastance function for a cardiac cycle of period 0.8 s.

$E_{LV}(t)$ enables to link the ventricular pressure $P_{LV}(t)$ to the corresponding ventricular volume $V_{LV}(t)$, at each instant of any cardiac cycle of period RR. V_0, instead, is a corrective volume. The elastance function, defined as in [36], is

$$E_{LV}(t) = E_{LV,min} + \frac{E_{LV,max} - E_{LV,min}}{2} e_v(t), \tag{3.17}$$

where $E_{LV,min}$ and $E_{LV,max}$ are the minimum and maximum elastance values, respectively. The activation function $e_v(t)$ [44] is

$$e_v(t) = \begin{cases} 1 - \cos\left(\frac{t}{T_{me}}\pi\right) & \text{if } 0 \leq t < T_{me}, \\ 1 + \cos\left(\frac{t-T_{me}}{T_{ce}-T_{me}}\pi\right) & \text{if } T_{me} \leq t < T_{ce}, \\ 0 & \text{if } T_{ce} \leq t < RR. \end{cases} \tag{3.18}$$

For this, $T_{me} = 0.3\sqrt{RR}$ and $T_{ce} = 3/2T_{me}$ are the instants when elastance reaches its maximum and constant values, respectively.

The shape of the function $E_{LV}(t)$ for a cardiac cycle of period 0.8 s is shown in the Figure 3.2.

3.2.3 Cardiac valves

In this problem, we have to model two valves: the mitral one and the aortic one. The former is described as an ideal diode with a resistive component. The mitral flow is defined as

$$Q_{MI}(t) = \frac{P_{LA} - P_{LV}(t)}{R_{MI}}. \tag{3.19}$$

P_{LA} is the left-atrial pressure, which we set constant in time, as typically accepted [7]. The resistance R_{MI} turns from the value of 3 mmHg/L to infinite, as the pressure gradient becomes negative [41].

As concern the aortic valve, the pressure-flow relation is that of Blanco [4]:

$$\begin{aligned} &L\frac{dQin_{AscAor}}{dt} = \\ &= -RQin_{AscAor} - B|Qin_{AscAor}|Qin_{AscAor} + \Theta(P_{LV} - Pin_{AscAor}). \end{aligned} \tag{3.20}$$

In this equation, Pin_{AscAor} and Qin_{AscAor} are the pressure and flow at the entrance to the aorta, respectively, $L = 500$ Ns^2/m^5 is the inertance of the fluid, $B = 756 * 10^6$ Ns^2/m^8 is the turbulent flow separation coefficient, $R = 600$ Ns/m^5 is the viscous resistance and $\Theta(t)$ is a function of the aortic valve opening angle $\theta(t)$ and accounts for the non-ideal condition of the valve. $\Theta(t)$ is written as

$$\Theta(\theta) = \frac{(1 - \cos(\theta(t)))^4}{(1 - \cos(\theta_{max}))^4}. \tag{3.21}$$

$\theta(t)$ varies between a minimum opening angle $\theta_{min} = 0°$ and a maximum one $\theta_{max} = 75°$, depending on the forces applied. It is computed considering the pressure difference across the valve F_{pr}, the frictional effect of tissue resistance F_{fr}, the dynamic motion effect of the blood acting on the leaflets F_{bm} and the action of the vortex downstream of the valve F_{vo}. The equation

$$I_{ao}\frac{d^2\theta(t)}{dt^2} = F_{pr} - F_{fr} + F_{bm} - F_{vo}, \tag{3.22}$$

which is proposed by [28], summaries all these terms. I_{ao} is the momentum of inertia of the valve.

It is important to understand the physical meaning that hides behind the various terms in the previous equations. $L\frac{dQin_{AscAor}}{dt}$ represents the pressure difference required to produce an unitary acceleration of the volumetric flow. $B|Qin_{AscAor}|Qin_{AscAor}$ stands for the pressure loss caused by the flow separations. $RQin_{AscAor}$ is related to the pressure fall due to the viscous dissipation for an unitary volumetric flow. Now it is easy to comprehend the (3.20). This correlates the variation of blood flow to the responsible causes. While the terms $-RQin_{AscAor}$ and $-B|Qin_{AscAor}|Qin_{AscAor}$ provoke a reduction of flow, the pressure difference between the left ventricle and the beginning of the aorta creates a positive flow. This is then scaled according to the aortic valve opening angle. Moreover, the second member of the (3.20) brings on a bigger volumetric flow variation as the blood inertance is lower.

Looking at the (3.22), we find that the negative and dissipative terms (F_{fr} and F_{vo}) tend to reduce the aortic valve opening angle while the positive ones (F_{pr} and F_{bm}) determine a greater aortic valve opening. Finally, $\theta(t)$ is greater when the rotational inertia of the leaflets is littler.

3.2.4 Small arteries and micro-circulation

The last sub-model represents the distal arterial behaviour. When a large artery splits into vessels too small to be described through the model for large/medium arteries, it is terminated by a three element Windkessel model.

In this way, it is possible to take into account the effect of each distal circulation on the arterial response. The generic three Windkessel model is represented by using a first entering resistance R_1, which refers to the large vessel from which the distal group starts, followed by a parallel combination of a resistance R_2 and a capacitance C, both related to the micro-circulation group. At high frequencies, R_1 tends to the characteristic impedance of the large artery before the distal group while R_2 turns into the difference between the total resistance R_T and R_1. C always refers to the arterioles.

The distal model is written as

$$\frac{dQ}{dt} - \frac{1}{R_1}\frac{dP}{dt} = \frac{P - P_{ven}}{R_1 R_2 C} - \left(1 + \frac{R_1}{R_2}\right)\frac{Q}{R_1 C}. \tag{3.23}$$

Here, Q and P are the flow and the pressure for the generic distal circuit, respectively. $P_{ven} = 5$ mmHg is a constant pressure corresponding to the venous portion of the micro-circulation. Note that the capillary pressure is taken constant; this assumption is generally accepted [7].

3.3 Vessel bifurcations

At each bifurcation, it is necessary to impose two conditions: the conservation of the total pressure and mass. In reference to the Figure 2.4, the conservation of the total pressure is

$$\begin{cases} P_0(l_0,t) + \frac{1}{2}\rho\widehat{u}_0^2(l_0,t) = P_1(0,t) + \frac{1}{2}\rho\widehat{u}_1^2(0,t), \\ P_0(l_0,t) + \frac{1}{2}\rho\widehat{u}_0^2(l_0,t) = P_2(0,t) + \frac{1}{2}\rho\widehat{u}_2^2(0,t). \end{cases} \tag{3.24}$$

The conservation of the mass is written as

$$Q_0(l_0,t) = Q_1(0,t) + Q_2(0,t). \tag{3.25}$$

Note that l is the length of the considered vessel while $\widehat{u}$ stands for the local mean velocity.

3.4 Numerical method

The model, composed by the sub-models we have just presented, is solved using the Runge-Kutta Discontinuous-Galerkin method. In particular, space is discretized by a Discontinuous-Galerkin approach while time evolution is described by a second-order Runge-Kutta scheme. The numerical method, implemented in MATLAB, is better explained in [16], [19]. Simulations are carried out with a time step equal to 10^{-4} s and a mean element length of 2.5 cm.

Clearly the solution is not dependent on the initial conditions. We set everywhere an initial condition of constant pressure, 100 mmHg, and no flow. We assume that the convergence is reached when the maximal pressure difference between two consecutive cardiac cycles is less than 1%. Under this assumption, the numerical scheme converges after about seven heart cycles.

Chapter 4

Numerical results for a normal beat after calibration

Here, we describe the method followed to calibrate the mathematical model presented in the previous chapter. Moreover, we give the results provided by the same model, after calibration, for a normal beat. One will see that there is a good agreement between numerical simulations and fluid mechanics solutions.

4.1 Parameter calibration

The numerical scheme, implementing the adopted mathematical model, requires to be calibrated. This operation is led in order to assure a medium standard behaviour of the systemic circulation, for a young and health man, when the beat is normal, i.e $RR = 0.8$ s. Calibration is achieved by quantifying some parameters. We set V_0, P_{LA}, $E_{LV,min}$ and $E_{LV,max}$, already introduced in the previous chapter, as indicated in the Table below.

Table 4.1: Calibration parameters.

V_0	14 ml
P_{LA}	8.33 mmHg
$E_{LV,min}$	$7.86 * 10^{-2}$ mmHg/ml
$E_{LV,max}$	2.88 mmHg/ml

However, with these values, the model gives us pressures too high to be considered acceptable at all sites of domain. To solve this problem, we introduce a corrective factor, which multiplies the resistances of the distal vessels. In this way, the model is able to reproduce, for a normal beat, not only reliable pressures at each site of domain (Table 4.3) but also the expected values of those parameters describing heart performances (Table 4.2). Looking at Table 4.2, the subscripts *ed* and *es* stand for end diastole and end systole, respectively. SV represents the Stroke Volume, CO is the Cardiac Output and EF indicates the Ejection Fraction. Note that, to calculate CO, we have assumed 75 bpm. As concern Table 4.3, $Pdin$ and $Psin$ are the diastolic and systolic pressure, respectively, at the beginning of the vessel indicated as subscript.

Table 4.2: Parameters referred to the left ventricle for $RR = 0.8$ s.

$P_{LV,max}$ [mmHg]	$P_{LV,min}$ [mmHg]	$P_{LV,ed}$ [mmHg]	$P_{LV,es}$ [mmHg]	$V_{LV,max}$ [ml]	$V_{LV,min}$ [ml]	$V_{LV,ed}$ [ml]	$V_{LV,es}$ [ml]	SV [ml]	CO [L/min]	EF %
120.11	4.48	8.35	97.31	120.28	51.16	120.21	52.85	67.36	5.05	56.04

Table 4.3: Diastolic and systolic pressures at the entrance to different vessels for $RR = 0.8$ s.

$Pdin_{AscAor}$	71.01 mmHg
$Psin_{AscAor}$	120.54 mmHg
$Pdin_{AorArcA}$	69.89 mmHg
$Psin_{AorArcA}$	120.84 mmHg
$Pdin_{AorArcB}$	69.89 mmHg
$Psin_{AorArcB}$	120.84 mmHg
$Pdin_{ThoAorA}$	68.87 mmHg
$Psin_{ThoAorA}$	127.33 mmHg
$Pdin_{ThoAorB}$	67.72 mmHg
$Psin_{ThoAorB}$	133.80 mmHg
$Pdin_{AbdAorA}$	64.97 mmHg
$Psin_{AbdAorA}$	118.76 mmHg
$Pdin_{AbdAorB}$	63.42 mmHg
$Psin_{AbdAorB}$	120.72 mmHg
$Pdin_{AbdAorC}$	62.84 mmHg
$Psin_{AbdAorC}$	122.18 mmHg
$Pdin_{AbdAorD}$	62.01 mmHg
$Psin_{AbdAorD}$	124.27 mmHg
$Pdin_{AbdAorE}$	61.68 mmHg
$Psin_{AbdAorE}$	131.14 mmHg
$Pdin_{ComIli}$	61.05 mmHg
$Psin_{ComIli}$	132.40 mmHg
$Pdin_{ExtIli}$	57.54 mmHg
$Psin_{ExtIli}$	132.21 mmHg
$Pdin_{Fem}$	56.74 mmHg
$Psin_{Fem}$	136.39 mmHg
$Pdin_{lSubB}$	66.84 mmHg
$Psin_{lSubB}$	125.52 mmHg
$Pdin_{rSubB}$	66.84 mmHg
$Psin_{rSubB}$	124.03 mmHg
$Pdin_{lRad}$	57.85 mmHg
$Psin_{lRad}$	144.63 mmHg
$Pdin_{rRad}$	55.38 mmHg
$Psin_{rRad}$	156.34 mmHg

4.2 Detailed results for a standard beat

At this point, we can present, in rather more detail, some of the results provided by the model, after the calibration, setting a beat of period 0.8 s.

4.2.1 Pressures and flows for a standard beat

As concern pressures and flows, we are interested in what happens at different sections of the arterial tree. First, we focus on the left ventricle and the beginning of the aorta. After that, we move on to the first stretch of the ascending aorta, looking at the variations in pressure and flow records along the blood vessel. Finally, we study how pressures and flows tend to evolve as we get farther away from the heart.

Left heart and entrance to the ascending aorta

Table 4.4 shows the letters we have used to indicate some relevant instants of a general heartbeat in the Figures below.

Table 4.4: Reference points for describing cardiac cycle.

A	Mitral valve closes
B	Aortic valve opens
C	Peak of flow at the beginning of Ascending Aorta
D	Maximum pressure at the beginning of Ascending Aorta
E	Aortic valve closes
F	Mitral valve opens

Apart from the points C and D, which are clearly unambiguous, it is better to provide some clarifications about the way in which we identify the other characteristic moments of a generic heartbeat. Point A is located at the first instant of the beat, so it is relative to the simulated moment after the end of the previous beat. B is corresponding to the first intersection between P_{LV} and Pin_{AscAor}. Point E is placed where Pin_{AscAor} becomes slightly higher than P_{LV} (just before the dicrotic notch on the Pin_{AscAor} signal). Finally, F is assumed at the second in time intersection between P_{LV} and P_{LA}.

Figure 4.1 presents the P_{LV} and V_{LV} records from simulation. Looking at it, we can recognise the expected functioning of the left ventricle for a typical heartbeat [20]. But, remember that we assume a constant left atrial pressure. At initial time (A), when mitral valve closes, diastole ends

and systole starts, P_{LV} is slightly higher than P_{LA} and V_{LV} is almost up. The very first stage of the cardiac cycle (A-B) consists of an isovolumic contraction: V_{LV} is roughly constant while its pressure begins to rise. As P_{LV} crosses Pin_{AscAor} (B), aortic valve opens and blood is ejected from the left ventricle to the aorta. Opening up the aortic valve creates a reduction in V_{LV} and an increase in P_{LV}. It is not visible in the Figure 4.1, but, about halfway through the ejection (B-E), P_{LV} and Pin_{AscAor} trace across. This creates an adverse pressure gradient across the aortic valve, which is maintained as both pressures start to fall. This is in good agreement with what declared in the literature [6], [37]. When Pin_{AscAor} is sufficiently higher than P_{LV}, there is a notch, best known as dicrotic notch, on the Pin_{AscAor} record. It indicates the closure of the aortic valve (E). Now P_{LV} decreases very rapidly as the heart muscle relaxes. It should be noted that Pin_{AscAor} falls much more slowly than P_{LV} between E and the end of the beat. This discrepancy between the two pressures is easy to understand if we remember that the large central arteries, through their elasticity, act as a cushioning reservoir of high pressure during systole. Diastole begins with an isovolumic relaxation (E-F): V_{LV} is almost constant as P_{LV} reduces. As soon as P_{LV} gets to P_{LA}, mitral valve opens (F) and the left ventricle filling starts. Therefore, V_{LV} goes up until it is equal to the value corresponding to the end of diastole. In this period, P_{LV} first gets below (by around 4 mmHg) then slightly overcomes P_{LA}, when mitral valve closes again.

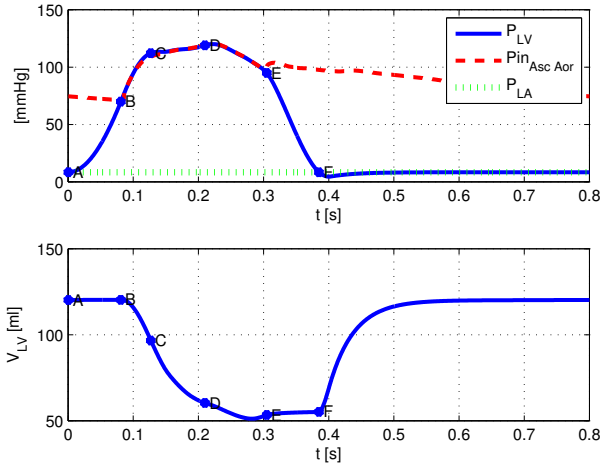

Figure 4.1: P_{LV} (top) and V_{LV} (bottom) for $RR = 0.8$ s.

This study shows that the mouth of the ascending aorta is the only place of the model in which the highest values of pressure for both a vessel and the left ventricle are sync. This is visible in the Figure 4.1.

Typically, the functioning of the left ventricle is also described through the famous PV loop. It links P_{LV} and V_{LV} during a complete heartbeat. Figure 4.2 shows the PV loop constructed through the results of the model. It is in good agreement with that usually reported in the literature [20]. Figure 4.2 makes clear the fact that, at the end of the systole (E), V_{LV} is somewhat higher than its minimum. This is due to the fact that the suck of flow at the beginning of the aorta, well stressed in the Figure 4.3, makes some blood go back to the left ventricle, leading to a small growth in V_{LV}.

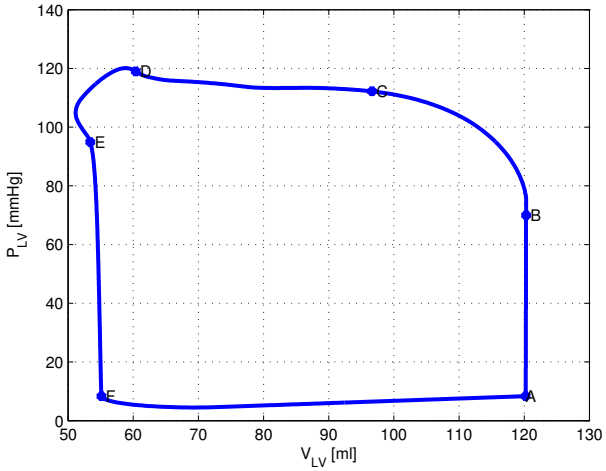

Figure 4.2: PV loop for $RR = 0.8$ s.

Figure 4.3 provides the pressure and flow signals at the entrance of the ascending aorta. They are completely consistent with the predicted ones [6], [37]. We note that Pin_{AscAor} declines mildly between the mitral valve closure and the aortic valve opening (A-B). In the same time framing, Qin_{AscAor} is zero value. Just when the aortic valve opens (B), pressure at the beginning of the aorta reaches its minimum ($Pdin_{AscAor}$= 71.01 mmHg). At B, both Pin_{AscAor} and Qin_{AscAor} start raising. One can also see that the greatest values for Pin_{AscAor} and Qin_{AscAor} are out of sync. As a matter of fact, while the spike of Qin_{AscAor} (C) comes 0.046 s after the aortic valve opening, the peak of Pin_{AscAor} ($Psin_{AscAor}$= 120.54 mmHg) appears 0.141 s later the instant corresponding to point A. This absence of synchrony is

confirmed from a fluid mechanics point of view [6], [37] and enable us to stress two important points.

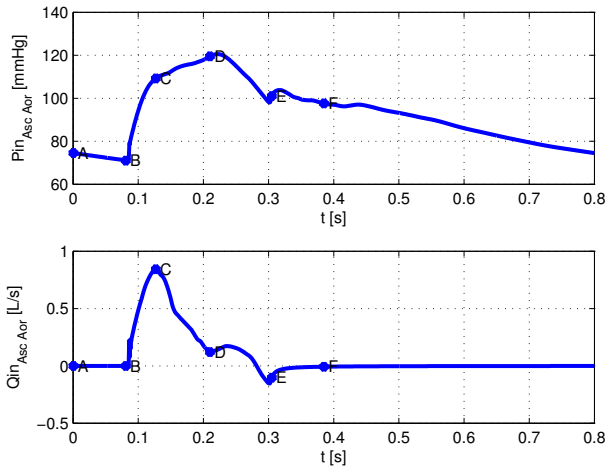

Figure 4.3: Pin_{AscAor} (top) and Qin_{AscAor} (bottom) for $RR = 0.8$ s.

- The flow motion in all arteries is governed by the pressure gradient rather than by the pressure. Important to note that there is always a not negligible difference of phase between a pressure wave and the corresponding pressure gradient wave. As an example, given the sinusoidal pressure wave

$$P = P_0 \cos[\omega(t - x/c)], \tag{4.1}$$

its pressure gradient along x is

$$-\partial P/\partial x = -\frac{\omega P_0}{c} \sin[\omega(t - x/c)]. \tag{4.2}$$

So, the pressure gradient wave continues to be sinusoidal and has the same frequency of the pressure wave but there is a phase angle difference of $\pi/2$ between the signals.

- The amplitude and phase of each flow signal are influenced by α (Eq. 3.4), which depends on the viscosity as well as on the frequency. In fact, it is not possible to reproduce the correct shape of a flow signal when neglecting viscosity or referring to the simple linear wave theory. According to this, we should find that the pressure and flow waves, at a general site, are equal, as concern both waveform and phase.

Getting back to the image 4.3, we have measured that, at C, the difference between P_{LV} and Pin_{AscAor} is positive and maximal. Point E is clearly visible on the Qin_{AscAor} record. Indeed, at the closure of the aortic valve, there is a small suck of Qin_{AscAor}, i.e the flow leaps slightly down to negative values at the end of the left ventricle. Now systole gets to end. Once the closure of the aortic valve is over, Qin_{AscAor} practically returns to be zero value, while Pin_{AscAor} continues to decrease. Another important instant of a classical cardiac cycle is indicated with the letter D. It is the time when the difference between P_{LV} and Pin_{AscAor} gets to its negative and minimal value within the range B-E.

The values of P_{LV}, V_{LV}, Pin_{AscAor} and Qin_{AscAor}, obtained at the characteristic points (Table 4.4), are summarized in the Table 4.5.

Table 4.5: P_{LV}, V_{LV}, Pin_{AscAor} and Qin_{AscAor} at the characteristic points indicated in the Table 4.4 for $RR = 0.8$ s.

Point	Time [s]	P_{LV} [mmHg]	V_{LV} [ml]	Pin_{AscAor} [mmHg]	Qin_{AscAor} [L/s]
A	0	8.35	120.20	74.53	0
B	0.0810	69.96	120.30	71.01	0
C	0.127	112.20	96.64	109.20	0.84
D	0.210	119.00	60.38	120.54	0.12
E	0.305	94.90	53.41	101.00	-0.10
F	0.385	8.34	55.12	97.59	0

In view of the above, one can see that systole takes 0.305 s and diastole 0.495 s.

First stretch of the Ascending Aorta

As a result of the present work, Figure 4.4 shows how pressure and flow records change when we move from the beginning to the end of the ascending aorta. First of all, we notice that both pressure and flow signals at the end of the vessel are behind those at the entrance to the aorta. This agrees

with the theoretical considerations [37], [50]. Indeed, pulses generated by the heart travel down the aorta and the major conduit arteries as waves and at a finite speed. This is the wave speed, just introduced in section 2.1. Secondly, it is possible to seize a certain difference in the shape of both the pressure and flow waves, as we go from the entry to the end of the vessel. This is mainly due to the way in which the forward and backward waves combine together. Indeed, in section 2.3, we have seen that the total pressure and flow waves are given by the combination of their backward and forward waves. Note that the factors managing this combination are different and varied; the most important ones are: the wave speed, the distance between the site of interest and the reflection sites but also the way in which the waves are affected at the reflection sites. For example, when, at a reflection site, the waves are reflected out of phase, an apparent distance has to be added. Therefore, the fact that we find a certain shape difference in the pressure and flow waves, as we pass the beginning of the aorta, is in good agreement with what is declared in the literature [37], [50].

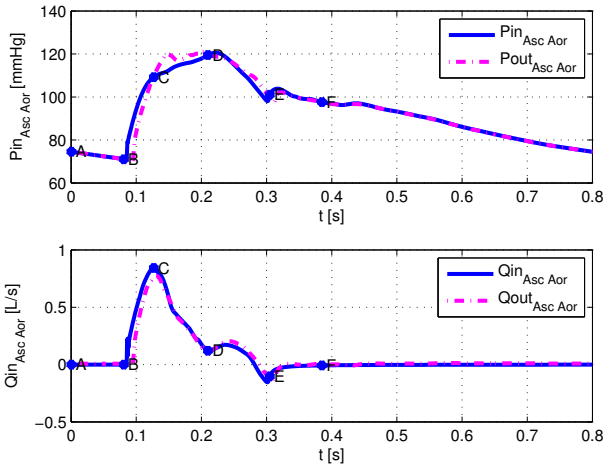

Figure 4.4: Pressure (top) and flow (bottom) at the two ends of the ascending aorta for $RR = 0.8$ s.

Increasing distance from the heart

As output of the simulation, we indicate how pressure and flow signals evolve, backing away from the heart (Figure 4.5). One can see that the pressure waves are progressively delayed and also steepen, increasing their

amplitude. As a consequence, diastolic pressures tend to reduce while systolic pressures usually grow with the distance from the heart. All these considerations are in accordance with fluid dynamics studies [6], [37]. Note that the way in which the pressure waves propagate along the arterial is almost completely explained by the linear wave theory. According to this, the tapering of the vessels and the wave reflections at the bifurcations are the main responsible for the increasing in the pressure wave amplitude, moving from the heart to major conduit arteries. Indeed, if vessels experiment gradual changes in their elastic and geometric properties along the aorta, the pressure wave amplitude, during this transfer, will be expected to grow, proportionally to the square-root of the local Z_c. In this work, we have not analysed how the pressure signals vary at extremely distal region, but certainly, there is a significant reduction of the pressure wave amplitude there.

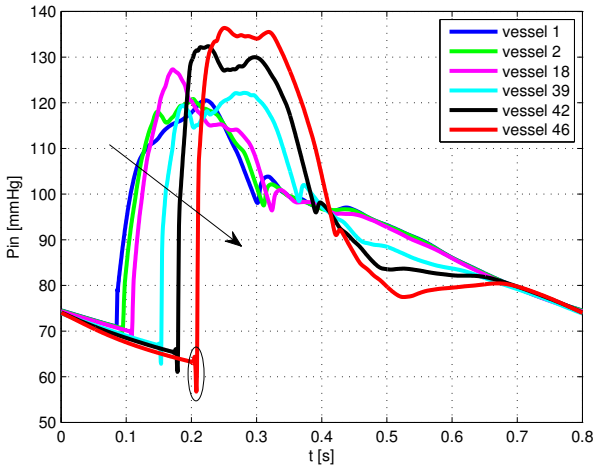

Figure 4.5: Pressures at the entrance to different sites along the aorta for $RR = 0.8$ s. The arrow indicates the increasing distance from the heart. The ellipse marks the numerical error.

Surely, the linear wave theory enables us to predict important features about the mechanism of pressure pulse propagation, however, it does not justify the characteristic steepening of the pressure wave, moving away from the heart. It has been demonstrated that it is due to both the elastic and fluid dynamic non linearities, neglected in the simple theory [6].

Paying again one's attention to the Figure 4.5, the positive jump marking

the aortic valve closure tends to disappear as we travel down the aorta.

Looking at the same image, one may point out that, at more distal arteries, the diastolic pressure seems to decrease sharply. For sake of clarity, it is better to say that it is not what really happens. The stressed drop through the ellipse (Figure 4.5) is probably due to a numerical error. It appears only at more distant large vessels, since, there, the pressure signal steepens much faster than at more central sites.

Even if systolic pressure becomes grater with the distance from the heart, we find that the mean level of arterial pressure decreases as moving away from the heart. This is visible in the Figure 4.6.

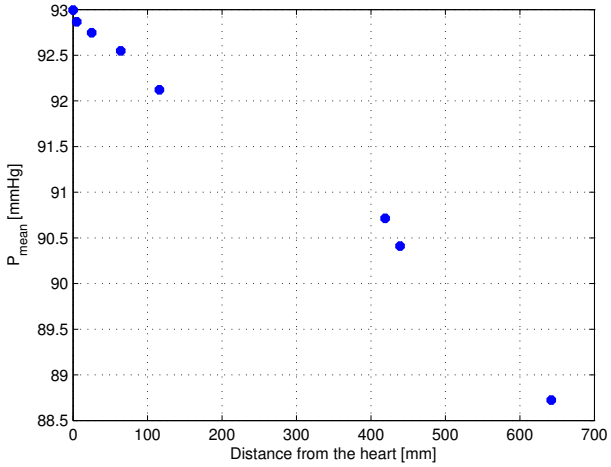

Figure 4.6: Mean pressures along the aorta for $RR = 0.8$ s.

Between the latest piece of the thoracic aorta (vessel 27) and the first section of the abdominal aorta (vessel 28), the previous trends of the pressure signals undergo some modifications. In this portion of the arterial tree, there is a significant reduction in the pressure amplitude. Along the subsequent vessels of the abdominal aorta (vessel 35, 37, 39, 41), the amplitude of the pressure wave begins to rise again, but, at the beginning of the vessel 41, the latest section of the abdominal aorta, it doesn't still succeed to go beyond the maximal pressure at the entrance to the vessel 27. This issue is represented in the Figure 4.7. Along the abdominal aorta, it is verified that the medium pressure grows, in opposition to the trend observed for the other large vessels along the arterial tree (Figure 4.8).

These "anomalies" in the pressure wave evolution along the abdominal

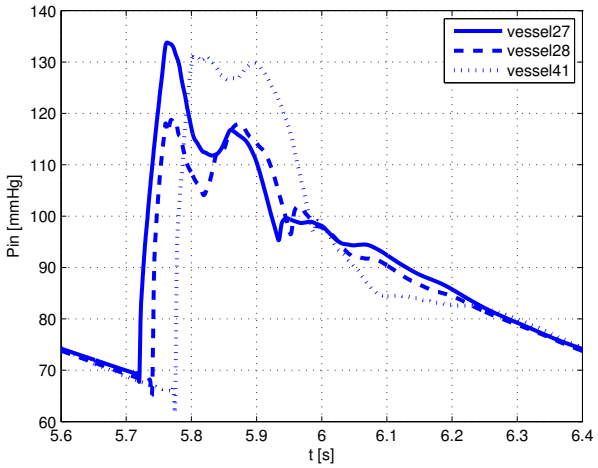

Figure 4.7: Pressure signals at the entrance to the vessels 27, 28 and 41 for $RR = 0.8$ s.

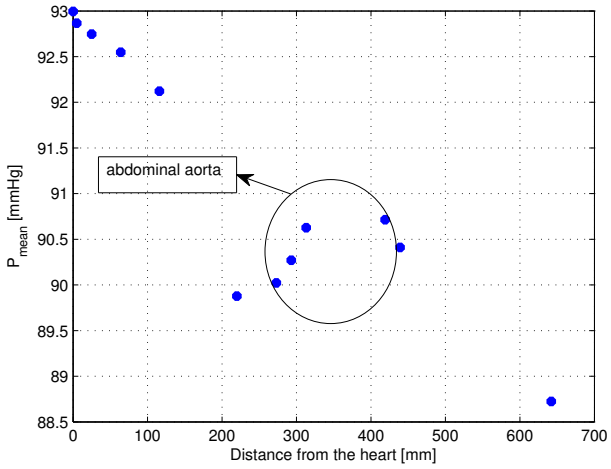

Figure 4.8: Mean pressure along the abdominal aorta for $RR = 0.8$ s.

aorta could have different explanations. For example, they could be due to the influence of the mesenteric, coeliac and renal group of arteries, placed exactly where the expected behaviour of the pressure records breaks down. Note that, in this portion of the aorta, different experiments done on dogs, whose anatomy is similar to ours here, show other types of "irregualarities",

concerning velocity profiles [6], [37]. In this region, they appear particularly rounded (viscosity is very important), in opposition with the classical shape of the other arterial velocity profiles, but also skewed, in relation to the presence of the closest branches (Figure 4.9). As a consequence, it would not be surprisingly the fact that, along the abdominal aorta, the pressure signals do not match the standard evolutions recorded in other areas of the systemic circulation. Moreover, the validity of the linear wave theory about the fact that the pressure wave amplitude increases, from the heart and along the large arteries, have some limitations, when taking into account viscosity and viscoelasticity, both present in the model. However, since we have not studied in detail the above "anomalies" about abdominal aorta, always present in all the subsequent chapters, we take them with a grain of salt and postpone their justification in future.

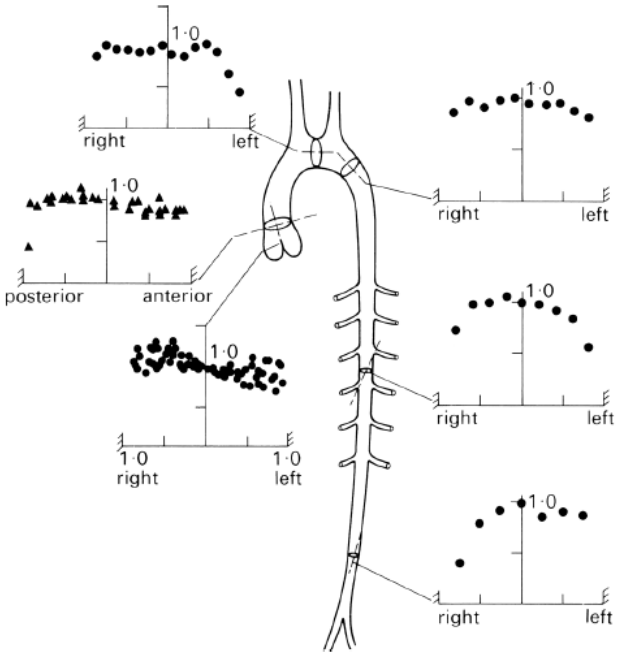

Figure 4.9: Velocity profiles along the aorta of the dog [6].

Concerning the flow signal, Figure 4.10 represents the evolution of the flow waves, according to the results of this study. It respects the known theoretical results [6], [37], [50]. We find that the flow wave amplitudes always reduce and the typical mark of the aortic valve closure is gradually

lost, as we move along arterial tree. The amplitude reduction of the flow wave along the aorta is typically due to the compliances of the arteries, accommodating flow during the systole phase, the inertial forces, which slow the blood motion, and the bifurcations, which force the flow to separate between the arterial branches [38].

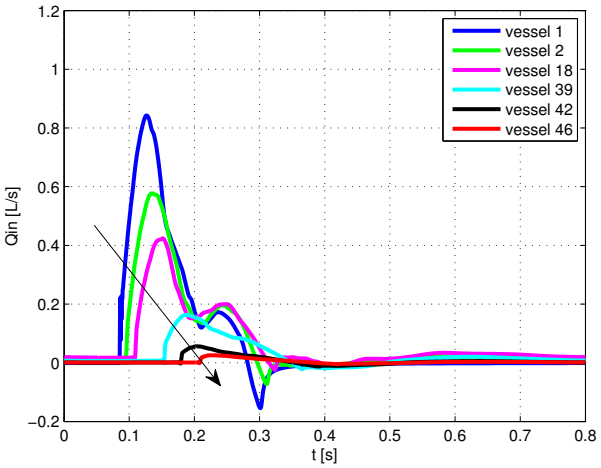

Figure 4.10: Flows at the entrance to different sites along the arterial tree for $RR = 0.8$ s. The arrow indicates the increasing distance from the heart.

4.2.2 Phase velocities for a standard beat

Phase velocities of Figure 4.11 derive from the three methods in section 2.1, applied to the model results. For the first technique, we adopt the (2.1). From Figure 4.11 and 4.12, one can see that, at each site, the phase velocities related to the second and the third approach are exactly the same but are pretty lower than those evaluated through the first method. We can explain such a difference taking into account what we have just written in section 2.1. Indeed, the phase velocities we have derived from the first technique here use values of distensibility, at each site, referred to a pressure of 100 mmHg. Looking at the Table 4.2, we see that the pressure corresponding to the foot of the pressure wave is always lower than 100 mmHg, this at all the chosen sites. Therefore, it is confirmed that, when we do not use the value of distensibility relative to the foot of the wave, Eq. (2.1) does not furnish the correct local phase velocity. Moreover, since distensibility decreases as

pressure rises and c is inversely proportional to the distensibility, the speed velocities from the first method are greater than the effective ones.

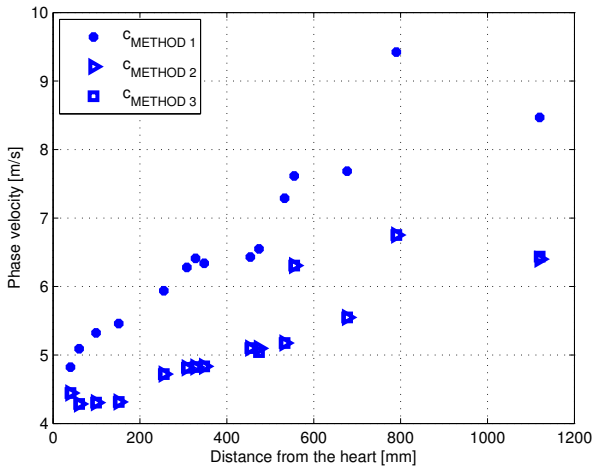

Figure 4.11: Phase velocity with the distance from the heart for $RR = 0.8$ s. The three methods adopted are presented in the section 2.1.

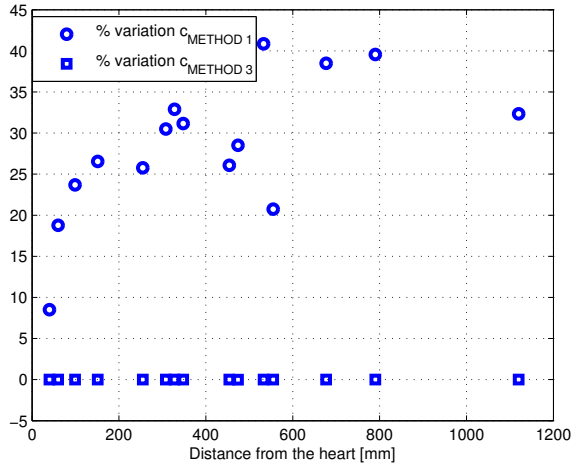

Figure 4.12: Percentage variations of the phase velocities evaluated through the first and the second method in reference to the values of c given by the first method. $RR = 0.8$ s.

We assume that the correct phase velocities at the different sites are those calculated through the second method. The numeric values are indicated in the Table 4.6. We can see that c becomes greater as we move towards distal vessels. It is in accordance with theory [20].

Table 4.6: Phase velocities at the end of the indicated vessels for $RR = 0.8$ s.

Vessel	1	2	14	18	27	28	35	37	39	41	42	44	46
c [m/s]	4.44	4.29	4.30	4.31	4.72	4.81	4.82	4.83	5.10	5.10	5.17	5.55	6.40

4.2.3 Characteristic impedances for a standard beat

Using phase velocities in the Table 4.6 and adopting the (2.5), we find that, as it should be, the characteristic impedances rise with distance from the heart (Table 4.7). This is not surprisingly, since c grows and vessel lumen area (Table 3.1) declines, when moving to more peripheral regions.

Table 4.7: Characteristics impedances at the end of the indicated vessels for $RR = 0.8$ s.

Vessel	1	2	14	18	27	28	35	37	39	41	42	44	46
$Z * 10^3$ [mmHgs/L]	0.054	0.075	0.10	0.12	0.28	0.32	0.38	0.39	0.42	0.47	1.06	1.50	4.44

4.2.4 Reflections for a standard beat

To evaluate the magnitude of reflections at different location of domain, we determine the quantities RM and RI at the exit of some vessels (Table 4.8). We adopt the formulas indicated in section 2.3 and use the pressure and flow signals provided by the model for $RR = 0.8$ s. One can see that the amplitude of the backward wave is not negligible between the end of the thoracic aorta and the beginning of the abdominal one (vessels 27 and 28, respectively).

As it has already been said previously, the shapes of the total pressure and flows waves are influenced by the way the reflected waves are created at the bifurcation sites. Useful information can be gained thanks to the quantities R and T, as well as the reflection and transmission coefficients, calculated at the junctions along the aorta (Table 4.9). These parameters have been presented in section 2.4 and derive from the characteristic

Table 4.8: RM and RI at the end of the indicated vessels for $RR = 0.8$ s.

Vessel	1	2	14	18	27	28	35	37	39	41	42	44	46
RM	0.56	0.46	0.39	0.36	0.46	0.49	0.47	0.42	0.44	0.43	0.41	0.42	0.31
RI	0.36	0.31	0.28	0.27	0.32	0.33	0.32	0.30	0.30	0.30	0.29	0.29	0.24

impedances in the Table 4.7. Firstly, we note that the reflections at the principal bifurcations along the arterial tree are always negative; it follows what we have previously said in section 2.4. Moreover, the most powerful bifurcation to the generation of reflected waves is the $XXIV$, best known as iliac bifurcation. Here, a great deal of energy (if compared with that at the other junctions) returns towards the heart through the backward waves. Other important junctions in the reflected waves generation are those at the entrance to the aortic arch A (I) and along the first portion of the abdominal aorta (XIV).

Table 4.9: R, T, R^2 and $\frac{{Z_1}^{-1}+{Z_2}^{-1}}{{Z_0}^{-1}}T^2$ at the indicated junctions for $RR = 0.8$ s.

Junction	R	T	R^2	$\frac{{Z_1}^{-1}+{Z_2}^{-1}}{{Z_0}^{-1}}T^2$
I	-0.18	0.82	0.0342	0.9658
II	-0.12	0.88	0.0137	0.9863
$VIII$	-0.12	0.88	0.0151	0.9849
X	-0.18	0.82	0.0331	0.9669
XIV	-0.15	0.85	0.0239	0.9761
XV	-0.17	0.83	0.0300	0.9700
$XVIII$	-0.09	0.91	0.0076	0.9924
XIX	-0.09	0.91	0.0078	0.9922
XX	-0.08	0.92	0.0070	0.9930
$XXIV$	-0.33	0.67	0.1111	0.8889
XXI	-0.14	0.86	0.0197	0.9803
$XXII$	-0.18	0.82	0.0313	0.9687

Chapter 5

Sequence of constant short and long beats

Before analysing what happens for an atrial fibrillated heartbeat, we see how beats simply shorter and longer than the standard one ($RR = 0.8$ s) influence the PV loop, the pressure and flow signals, but also the phase velocities and the magnitude of reflections, at different sites along the arterial tree. We see the results of interest for a short beat of period 0.5 s and for a long beat whose period is 1.1 s.

Important to stress is the fact that the model, calibrated to give average corrected results for a regular beat, is not equipped with either long-term or short-term autoregulation systems, certainly present in a real circular system. This means that we do not consider the influence of any internal adaptive mechanism able to adjust the arterial system response to the left ventricle stimuli, according to the beat duration. This lack would present a problem, if we wanted to compare two individuals that, systematically, have different beat frequencies. To this purpose we should modify the model, introducing something similar to a baroreceptors system and taking into account probable plastic variations for the vessels. However, in this work, we are interested in studying what happens, along the arterial tree, when we introduce a time limited sequence of irregular beats (either a series of constant anomalous beats either a combination of two or more successions of constant non standard beats or a chain of random unusual beats). To achieve this goal, the model is expected to give acceptable results, obviously, within the limits of a model. Actually, a potential autoregulation system would take a certain time before influencing the real arterial system response.

5.1 PV loop

Varying constantly the beat period, we have an immediate impact on the functioning of the left ventricle. It is clear looking at the elastance function, already introduced in paragraph 3.2.2. Indeed, the left ventricle elastance depends on RR. As the beat is shorter than the normal one, the left ventricle has a greater elastance; this means that is much more contractile. The opposite happens for $RR > 0.8$ s. Through Figure 5.1, one can see that both the maximal P_{LV} and the minimal V_{LV} grow as the beat is shorter than usual. On the other hand, the same quantities reduce for a beat longer than the standard one. Table 5.1 indicates that the beat period reduction makes the left ventricle work more while the beat period extension operates in reverse. The area delimited by the PV loop curve defines the stroke work, SW.

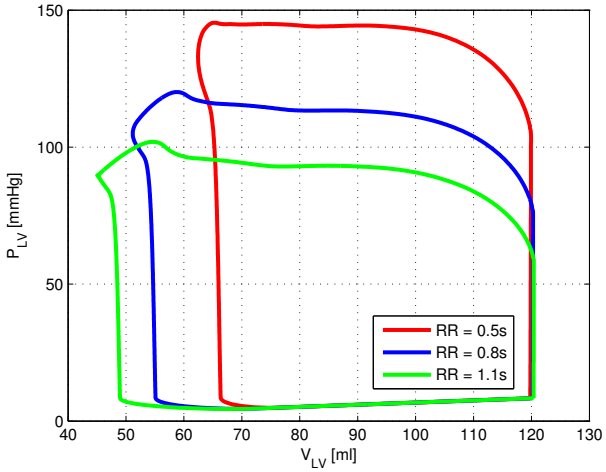

Figure 5.1: PV loop for $RR = 0.5$ s, $RR = 0.8$ s and $RR = 1.1$ s.

Table 5.1: Stroke work for $RR = 0.5$ s, $RR = 0.8$ s and $RR = 1.1$ s.

RR [s]	SW [J]
0.5	0.95
0.8	0.92
1.1	0.88

5.2 Pressures and flows

We have the pressure and flow records along the aorta for constant sequences of short beats, with $RR = 0.5$ s, and long beats, with $RR = 1.1$ s. The beat period does not change for each sequence, so the corresponding numerical solution from the model is constant, as numerical convergence is reached. In light of this, for $RR = 0.5$ s and $RR = 1.1$ s, we have just one representative pressure record and one symbolic flow record, at each site.

Looking at Figure 5.2, we have that, at the entrance to the ascending aorta, pressure values always rise for a short beat and decrease for a long beat, if compared with the reference pressure ($RR = 0.8$ s) at the same site.

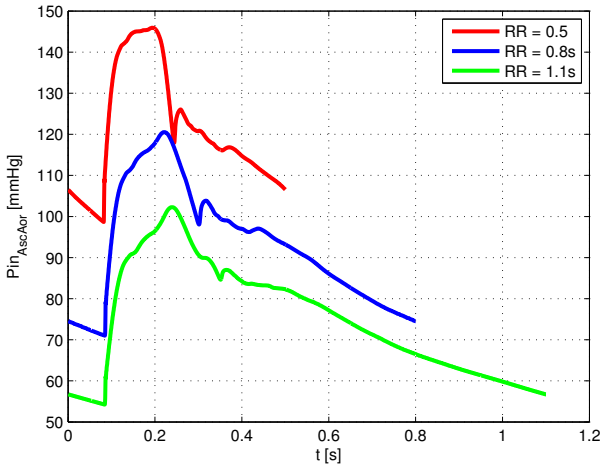

Figure 5.2: Pin_{AscAor} for $RR = 0.5$ s, $RR = 0.8$ s and $RR = 1.1$ s.

Figures 5.3 and 5.4 show the evolutions of the pressure signals, as we move from the heart, in the cases of $RR = 0.5$ s and $RR = 1.1$ s, respectively. Looking at these, one can see that the beat duration has a strong effect on the minimal and maximal pressure values at each site, but does not modify the typical evolution of the pressures, going towards more distal regions (Figure 4.5). In other words, despite the RR variations, it is still true that the diastolic pressures fall and the systolic ones rise, almost everywhere, when leaving the heart.

Important to stress is that, with $RR \neq 0.8$ s, between the vessel 27 and the vessel 41, systolic pressures follow the same evolution presented for $RR = 0.8$ s (Figure 4.7), although the numerical values change.

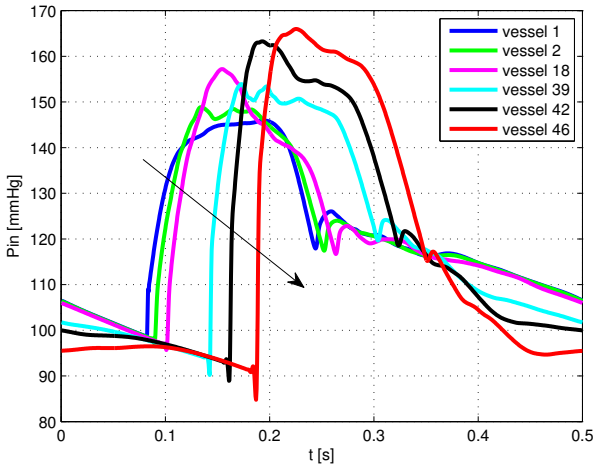

Figure 5.3: Pressures at the entrance to different sites along the aorta for $RR = 0.5$ s. The arrow indicates the increasing distance from the heart.

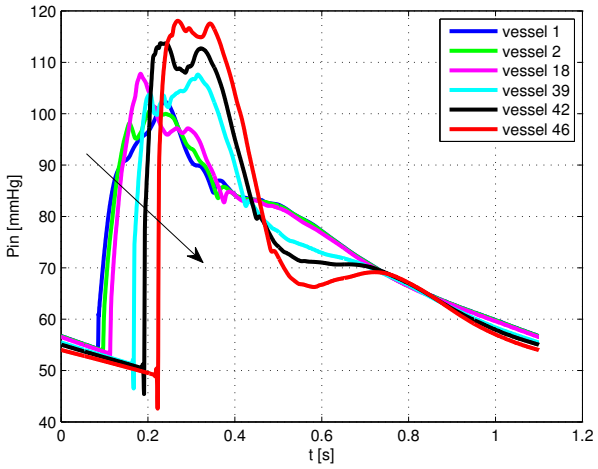

Figure 5.4: Pressures at the entrance to different sites along the aorta for $RR = 1.1$ s. The arrow indicates the increasing distance from the heart.

Figures 5.5 and 5.6 indicate the systolic, diastolic and mean pressures, leaving the heart, for $RR = 0.5$ s and $RR = 1.1$ s, together with the same quantities when $RR = 0.8$ s. Through these, it is quite clear that, it does not matter what the distance from the heart is, a beat shorter than the

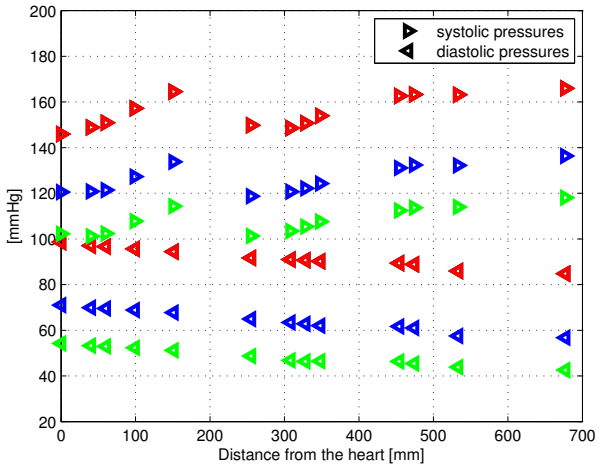

Figure 5.5: Systolic and diastolic pressures with the distance from the heart for $RR = 0.5$ s (red), $RR = 0.8$ s (blue) and $RR = 1.1$ s (green).

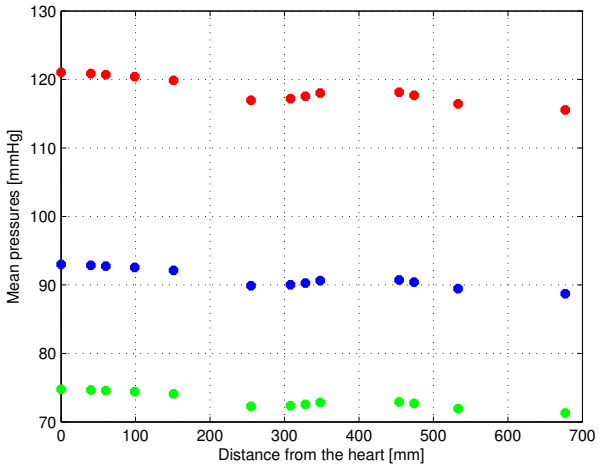

Figure 5.6: Mean pressures with the distance from the heart for $RR = 0.5$ s (red), $RR = 0.8$ s (blue) and $RR = 1.1$ s (green).

normal one brings on a general gain of pressure while a beat longer than the standard one causes an overall pressure reduction. However, we have to remember that the introduction of an adequate baroreceptor system would tend, in the long term, to eliminate pressure differences in the cases of

beats systematically long or short. Looking at the Figure 5.6, we find that, altering the beat period, the mean pressures decrease with the distance from the heart, except between the vessel 27 and the vessel 41. Therefore mean pressure trend is similar, even if numerical values are different, to that referred to $RR = 0.8$ s (Figure 4.8).

Figure 5.7 shows that the percentage variations of the diastolic pressures are greater, in modulus, than those of the systolic pressures. It is quite evident that there is no symmetry in the pressure results, for $RR = 0.5$ s and $RR = 1.1$ s, despite the short beat and the long one are in symmetric positions relatively to the standard beat.

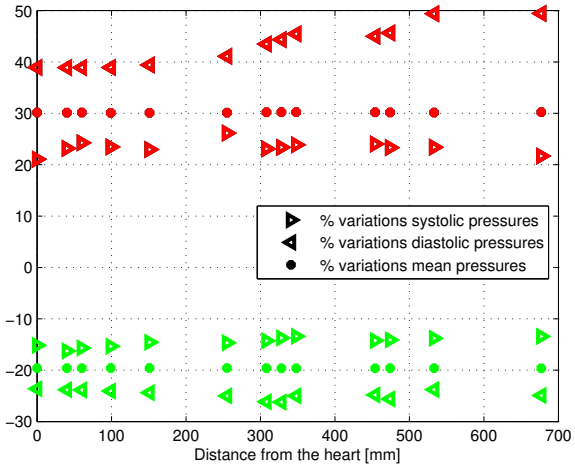

Figure 5.7: Percentage variations of the systolic, diastolic and mean pressures with the distance from the heart for $RR = 0.5$ s (red) and $RR = 1.1$ s (green). Reference values are determined for $RR = 0.8$ s.

Figure 5.8 displays that, at the beginning of the ascending aorta, the maximal flow rises and the minimal one decreases (becomes more negative) when reducing the beat duration. On the other hand, at the same point, for a beat longer than the standard one, the maximal flow decreases and the minimal one increases (becomes less negative).

Figures 5.9 and 5.10 give the evolution of the flows with the distance from the heart, for $RR = 0.5$ s and $RR = 1.1$ s, respectively. We have noted that, as RR reduces, while maximal flows always grow, independently from the distance from the heart, minimal flows rise, far away from the heart. This is in opposition to the classical trend at the entrance to the aorta when

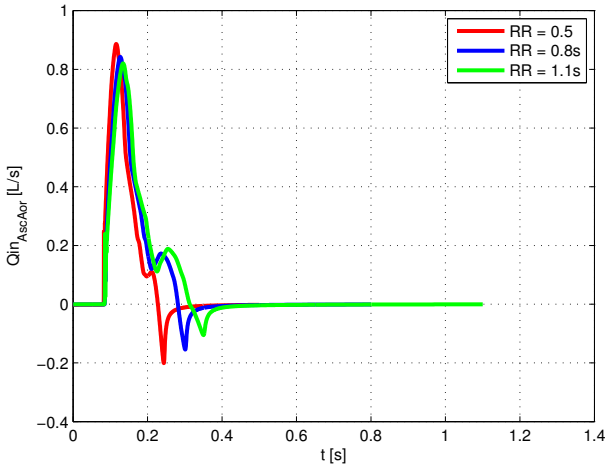

Figure 5.8: Qin_{AscAor} for $RR = 0.5$ s, $RR = 0.8$ s and $RR = 1.1$ s.

varying RR.

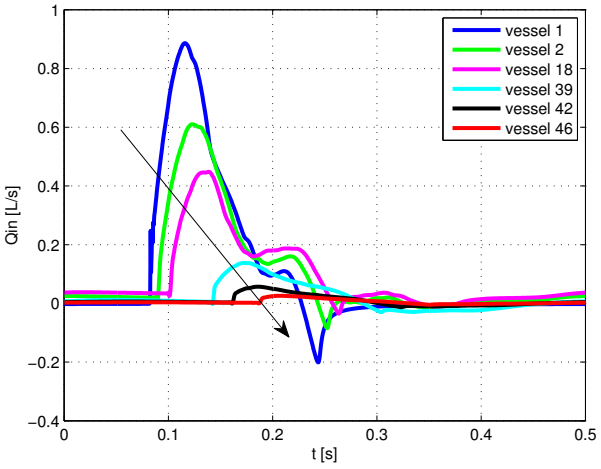

Figure 5.9: Flows at the entrance to different sites along the aorta for $RR = 0.5$ s. The arrow indicates the increasing distance from the heart.

From Figure 5.11, one can appreciate that the variations of the maximal and minimal flows with RR tend to disappear as one is distant from the heart.

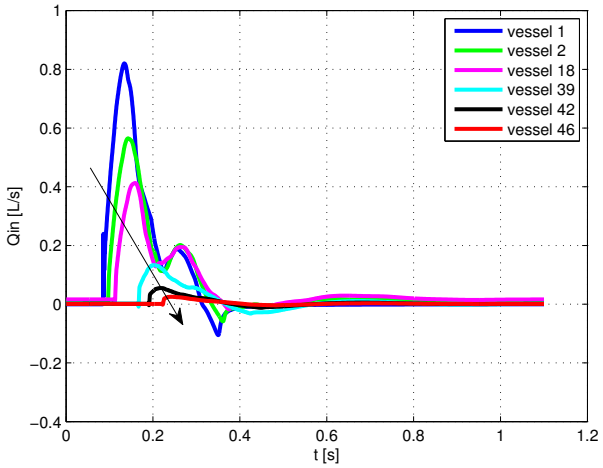

Figure 5.10: Flows at the entrance to different sites along the aorta for $RR = 1.1$ s. The arrow indicates the increasing distance from the heart.

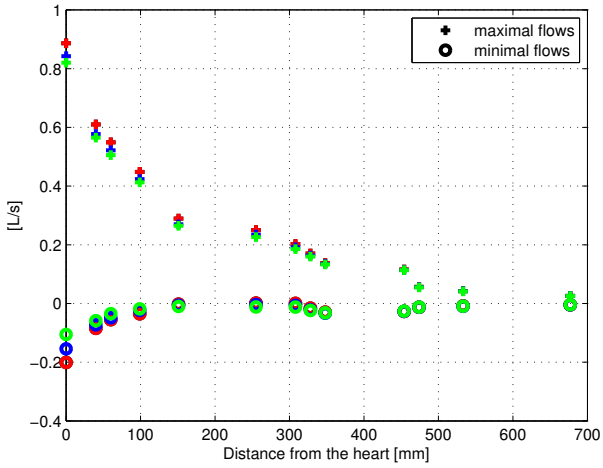

Figure 5.11: Maximal and minimal flows with the distance from the heart for $RR = 0.5$ s (red), $RR = 0.8$ s (blue) and $RR = 1.1$ s (green).

It is useful to analyse how the mean flows are affected by the beat duration along the aorta. To this purpose, Figure 5.12 gives the mean flows for $RR = 0.5$ s, $RR = 0.8$ s and $RR = 1.1$ s, at different sites of domain. Figure 5.13, instead, shows the percentage variations of the mean flows, for

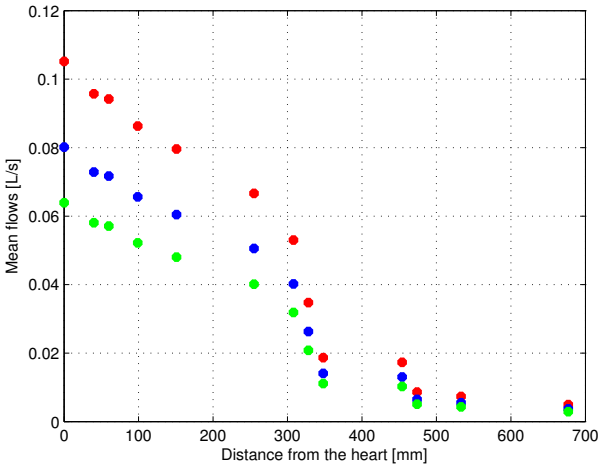

Figure 5.12: Mean flows with the distance from the heart for $RR = 0.5$ s (red), $RR = 0.8$ s (blue) and $RR = 1.1$ s (green).

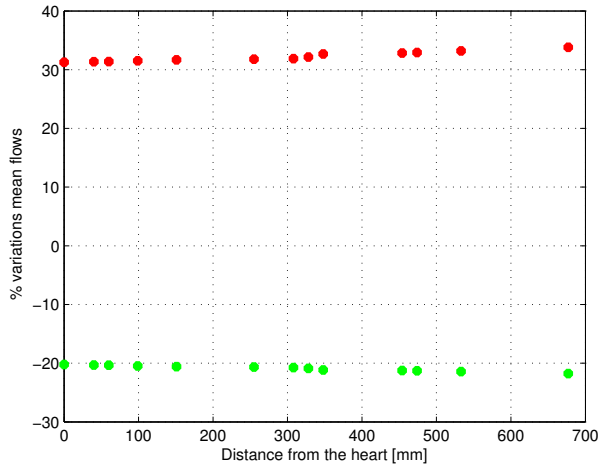

Figure 5.13: Percentage variations of the mean flows with the distance from the heart for $RR = 0.5$ s (red) and $RR = 1.1$ s (green). Reference values are determined for $RR = 0.8$ s.

$RR = 0.5$ s and $RR = 1.1$ s, in reference to the corresponding values for a normal beat. At each site, mean flows rise as RR reduces and decrease with the distance from the heart. The effect of the beat duration does not

tend to disappear when we are at more distal regions. It is apparent in the Figure 5.13. The changes of the mean flows, due to the chosen values of RR, are not symmetric, even if short and long beats are in symmetric positions in reference to the standard beat. Anyway, the above changes, because of the different values of RR, would tend to be eliminated, in the long term, by an appropriate baroreceptors system.

5.3 Phase velocities

We consider the phase velocities along the aorta, for $RR = 0.5$ s and $RR = 1.1$ s, by adopting the second method explained in section 2.1. Figure 5.14 shows these, but also the phase velocities, at corresponding sites, for $RR = 0.8$ s. It is evident that, decreasing the beat duration, the phase velocity becomes greater everywhere. The opposite happens when RR is higher.

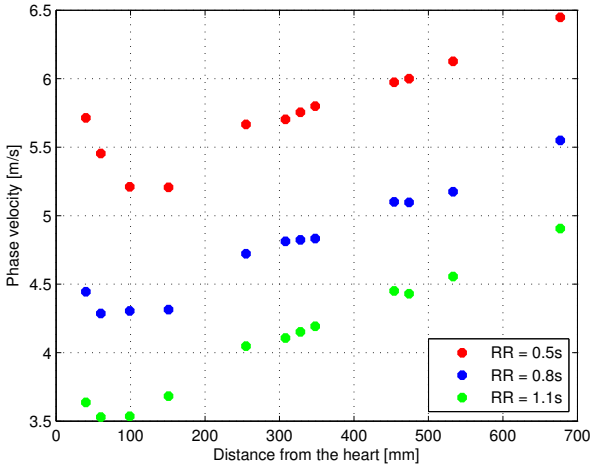

Figure 5.14: Phase velocities with distance form the heart for $RR = 0.5$ s, $RR = 0.8$ s and $RR = 1.1$ s.

Figure 5.15 demonstrates that, as we have just seen concerning pressures and mean flows, the variations of c, due to the alterations to RR, are not symmetric for the two cases $RR = 0.5$ s and $RR = 1.1$ s too.

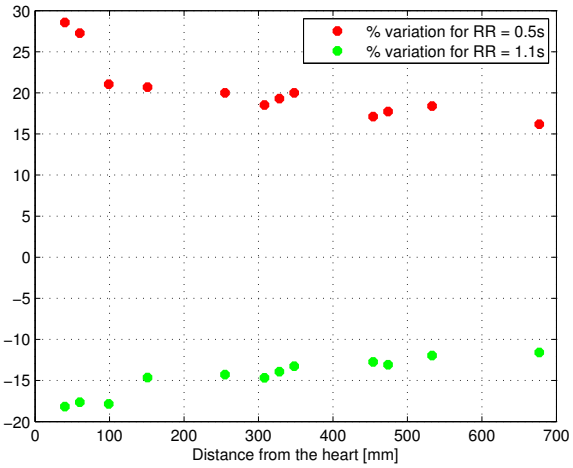

Figure 5.15: Percentage variations of the phase velocities with distance form the heart for $RR = 0.5$ s and $RR = 1.1$ s. Reference value are determined for $RR = 0.8$ s.

5.4 RI and RM

We have the parameters RM and RI, for $RR = 0.5$ s and $RR = 1.1$ s. Figure 5.16 shows their percentage variations, at different distances from the heart, in reference to the standard RM and RI (those calculated when $RR = 0.8$ s).

These results are very interesting. We find that, before the end of abdominal aorta, RM and RI grow for $RR > 0.8$ s and are almost equal to those for a standard beat as $RR < 0.8$ s. However, at regions more distant from the heart than the abdominal aorta, RM and RI reduce for the short beat and are nearly those for $RR = 0.8$ s as RR is higher than 0.8 s. It means that, long beats produce significant alterations in the magnitude of reflection at more central regions while short beats tend to vary more the reflection conditions at distal zones.

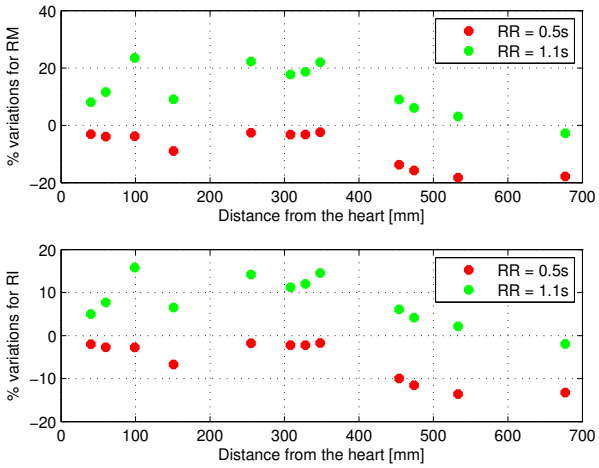

Figure 5.16: Percentage variations of RM and RI with distance form the heart for $RR = 0.5$ s and $RR = 1.1$ s. Reference value are determined for $RR = 0.8$ s.

5.5 Conclusions

The beat duration has a strong impact on the pressure signals but also on the flow records, along the arterial tree.

The modelling provides pressures and flows at each point of domain, according to RR. For $RR < 0.8$ s, we have a general gain of pressure and a grater mean flow, at each site and during the completed beat time. When $RR > 0.8$ s, instead, pressures and mean flows reduce everywhere within the beat time. As a result of a minimal viscoelasticity in the model, pressures influence some elastic characteristics of the vessels, such as distensibility, depending on RR. Therefore, phase velocities adapt to the model pressures, i.e are related to RR. In particular, c reduces as RR grows. Since phase velocities and input waves depend on RR, the reflection plays and the modalities under which forward and backward waves combine at each site are dependant on the beat period. Important to note that, as concern the magnitude of reflections, it is not possible to identify a specific trend in reference to the only beat period. This because we can have different evolutions, chosen RR, according to the distance from the heart.

Arterial system exhibits asymmetric behaviours for constant sequences of heartbeat periods that are in symmetric position relatively to $RR =$

0.8 s. In particular, we have that a beat longer than the standard one introduces minor variations in the values of pressure, flow and phase velocity, in reference to the case $RR = 0.8$ s. By contrast, concerning the magnitude of reflection, it seems that long and short beats can introduce almost the same percentage variations in both RI and RM, even if at different arterial regions.

In light of all this, we recognise different specific and steady behaviours for the simulated circulatory system, when imposing a constant RR, according to its value. Fixed RR, this behaviour can be given in terms of pressure and flow signals, phase velocities and parameters to estimate the magnitude of reflections, at different sites of domain.

Results of this chapter are expected to be acceptable, within the limits of the model and under the considerations presented at the beginning of this chapter.

Chapter 6

Abrupt changes of the beat duration

In the previous chapter, we have studied the effects of RR on the systemic circulation behaviour. Now we want to study how it changes when RR goes from a constant value to one another. We analyse what happens when going from $RR_1 = 0.8$ s to $RR_2 = 0.5$ s (case a) as well as from $RR_1 = 0.8$ s to $RR_2 = 1.1$ s (case b). Tables 6.1 indicates the sequences of the beat periods corresponding to the solutions, at each site, in the figures below.

Table 6.1: Sequence of the represented beat periods going from $RR_1 = 0.8$ s to $RR_2 = 0.5$ s (case a) and from $RR_1 = 0.8$ s to $RR_2 = 1.1$ s (case b).

	Beat	1	2	3	4	5	6	7	8	9	10
case a	Period [s]	0.8	0.5	0.5	0.5	0.5	0.5	0.5	0.5	0.5	0.5
case b	Period [s]	0.8	1.1	1.1	1.1	1.1	1.1	1.1	1.1	1.1	1.1

We analyse the characteristics of the transition phase, in terms of pressures and flows, for the cases a and b and at different distances from the heart. We are also interested in estimating the time it takes to establish a steady solution, when RR suddenly changes. We define it as recovery time. To this purpose, we record, during the transition phase, the systolic, diastolic and mean pressure values, as well as the mean flow values. We assume that the transition phase is over when all the previous pressure and flow quantities differ for not more than 1% from the corresponding values related to RR_2. Therefore, chosen a site, the recovery time is the temporal interval required to conclude there the transition phase, clearly, from when RR is altered. This theme has been dealt with, at various sites, for both

the cases a and b.

6.1 Pressures

We want to study the modifications in the pressure signals, at different distances from the heart, having a beat whose period goes from RR_1 to RR_2. In order to quantify these alterations, we focus, at each site, on specific pressure values: the systolic, the diastolic and the mean value.

Looking at Figure 6.1, we see that both systolic and diastolic pressures rise everywhere for $RR_1 > RR_2$. The opposite happens for $RR_1 < RR_2$. As the transition phase is evolving, each point tends to establish the local value for RR_2. We observe that the ways for which pressures vary with the distance from the heart are not altered by the beat period, as we have just verified in section 5.2. In fact, systolic and diastolic pressures, respectively, grow and decrease with the distance from the heart, less than a few exceptions along the abdominal aorta.

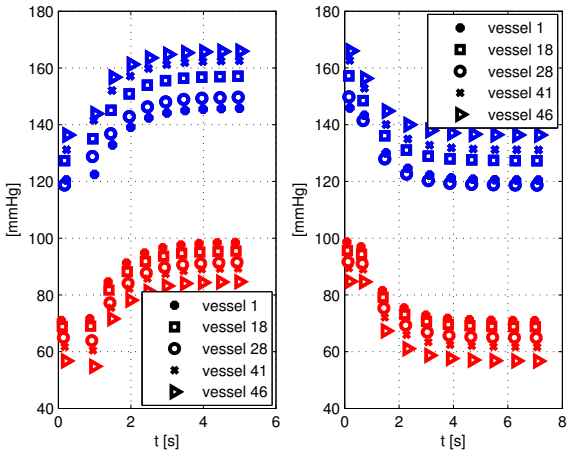

Figure 6.1: Systolic (blue) and diastolic (red) pressures at the entrance to the indicated vessels, from $RR_1 = 0.8$ s to $RR_2 = 0.5$ s (left) and from $RR_1 = 0.5$ s to $RR_2 = 0.8$ s (right).

One of the most staggering aspect of Figure 6.2 is that, during the passage from RR_1 to RR_2, each site exhibits different percentage variations in terms of pressure. As the evolutionary time is getting to its end, these differences become negligible or completely disappear.

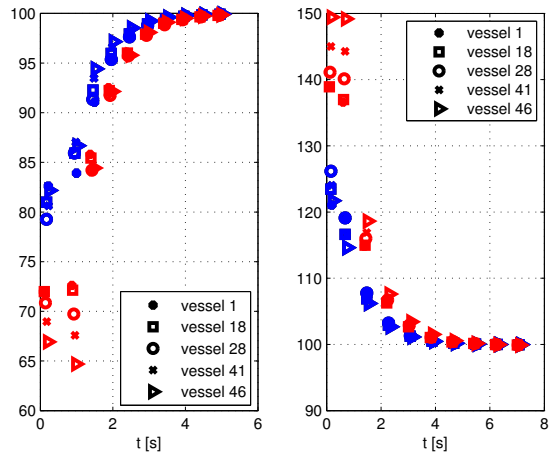

Figure 6.2: Percentage variations of the systolic (blue) and diastolic (red) pressures at the entrance to the indicated vessels, from $RR_1 = 0.8$ s to $RR_2 = 0.5$ s (left) and from $RR_1 = 0.5$ s to $RR_2 = 0.8$ s (right). Reference values are those calculated for RR_2.

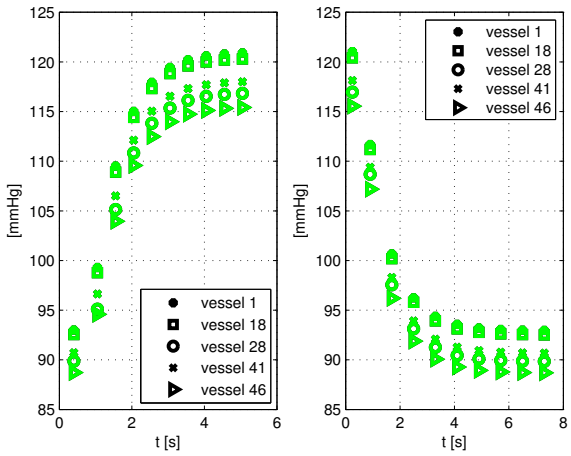

Figure 6.3: Mean pressures at the entrance to the indicated vessels, from $RR_1 = 0.8$ s to $RR_2 = 0.5$ s (left) and from $RR_1 = 0.5$ s to $RR_2 = 0.8$ s (right).

Figure 6.3 describes the behaviour of the mean pressures with the distance from the heart. Figure 6.4, instead, gives the percentage variations of

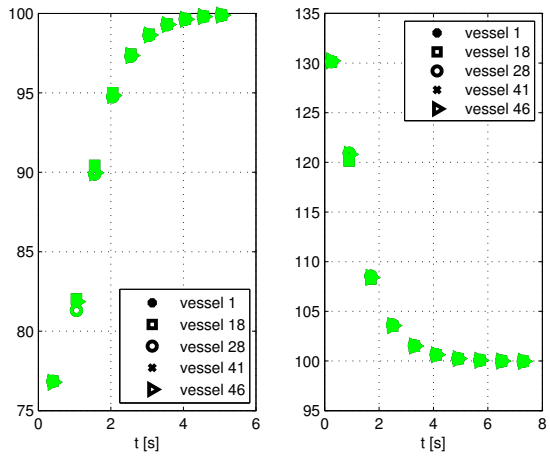

Figure 6.4: Percentage variations of the mean pressures at the entrance to the indicated vessels, from $RR_1 = 0.8$ s to $RR_2 = 0.5$ s (left) and from $RR_1 = 0.5$ s to $RR_2 = 0.8$ s (right). Reference values are those calculated for RR_2.

the same quantities, in reference to the corresponding steady mean pressures for RR_2. One can see that the mean pressures, as well as the systolic and diastolic ones, become higher for $RR_1 > RR_2$ and reduce for $RR_1 < RR_2$. Percentage variations tend to assume the same values, moving away from the heart, as the transition time is reaching the end. With a few exceptions along the abdominal aorta, mean pressures decline moving away from the heart. This happens independently from the value of RR.

Having $RR_1 = 0.8$ s and $RR_2 = 1.1$ s, and vice versa, but also $RR_1 = 0.5$ s and $RR_2 = 1.1$ s, and vice versa, we have observed trends similar to the previous ones.

6.2 Flows

Concerning flows, we study how their mean values vary for the two cases a and b. We do not consider the evolution of the maximal and minimal flows when altering the beat period. Minimal flows evolution, at each site, as varying RR, is strongly affected by the distance from the heart and is extremely sensitive to very little pressure modifications, surely present during the terminal transition phase.

Figure 6.5 tells us that, during the transition phase, mean flows grow

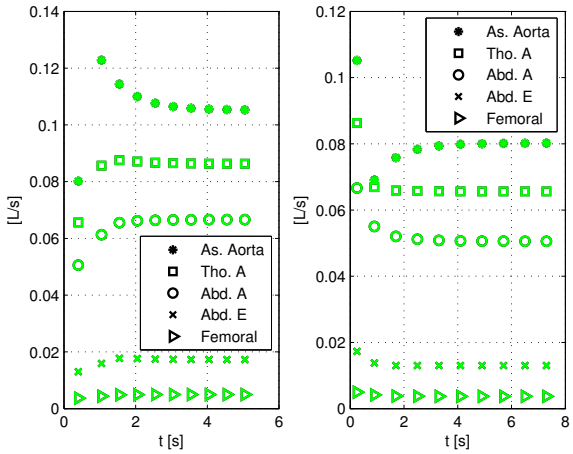

Figure 6.5: Mean flows at the entrance to the indicated vessels, from $RR_1 = 0.8$ s to $RR_2 = 0.5$ s (left) and from $RR_1 = 0.5$ s to $RR_2 = 0.8$ s (right).

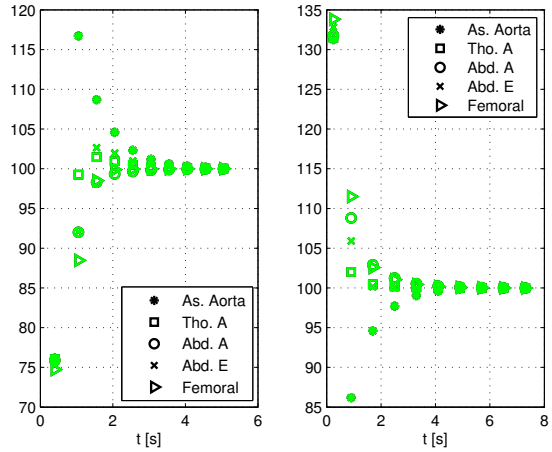

Figure 6.6: Percentage variations of the mean flows at the entrance to the indicated vessels, from $RR_1 = 0.8$ s to $RR_2 = 0.5$ s (left) and from $RR_1 = 0.5$ s to $RR_2 = 0.8$ s (right). Reference values are those calculated for RR_2.

everywhere, for $RR_1 > RR_2$, and reduce at each site, for $RR_1 < RR_2$. One can observe that the growth/reduction level becomes less significant with the distance from the heart. Certainly, mean flows are smaller, moving from the heart, independently from the beat period. Figure 6.6, instead, shows

that at the end of the transition phase, mean flows are everywhere equal to those evaluated as RR_2. At the beginning of the adjustment period, from RR_1 to RR_2, the percentage variations of the mean flow quantities differ site by site.

Similar trends have been found moving from $RR_1 = 0.8$ s to $RR_2 = 1.1$ s, and vice versa, as well as from $RR_1 = 0.5$ s to $RR_2 = 1.1$ s, and vice versa.

6.3 Recovery time intervals

With the data available, we calculate the recovery time. However, we think it is better to express it in the form of number of beats required to the recovery rather than in the form of time. So, we assume as recovery time the number of beats necessary to conclude the transition phase, from when RR is modified. Table 6.2 indicates, for different RR_1 and RR_2, the number of beats it takes, at different sites, to recover, as concern systolic, diastolic and mean pressures, but also mean flows.

From these results we can draw the following conclusions.

- Given RR_1 and RR_2, at each site, diastolic pressure requires a beat number grater than or equal to that necessary to the other quantities (systolic pressure, mean pressure and mean flow) to recover. One can derive that, everywhere, it is diastolic pressure to define the beat number to conclude the transition phase. For this reason, we have indicated diastolic pressures of the Table 6.2 in bold.

- Chosen one of the transition phase among those in the Table 6.2 (for example $RR_1 = 0.8$ s and $RR_2 = 0.5$ s), one can look at the beat number to the complete recovery, at all the indicated sites. Please, do the same thing for the complementary case, where RR_1 and RR_2 are inverted (for the previous example, $RR_1 = 0.5$ s and $RR_2 = 0.8$ s). One can easily see that, going from a longer beat to a shorter one, the beat number to recover is greater than or equal to that expected to accomplish the inverse passage. This is true at all sites.

- Defined RR_1 and RR_2, there is not any clear and identifiable correlation between the beat number to recover and the distance from the heart. This is probably due to the fact that the number of beats to conclude the transition phase depends on how the forward and backward signals combine at each point. Indeed, this combination varies site by site and is subjectively affected by the beat alterations.

Table 6.2: Number of beats to recover characteristic pressure and flow values, at different distances from the heart, for the indicated RR_1 and RR_2.

Distance from the heart [mm]	0	40	99	151	255	328	454	533	677
From $RR_1 = 0.8$ s to $RR_2 = 0.5$ s									
Beats to recover the systolic pressure	5	5	5	4	5	5	4	4	4
Beats to recover the mean pressure	5	5	5	5	5	5	5	5	5
Beats to recover the diastolic pressure	**6**	**5**	**5**	**6**	**6**	**6**	**5**	**6**	**5**
Beats to recover the mean flow	5	4	2	1	2	1	3	1	2
From $RR_1 = 0.5$ s to $RR_2 = 0.8$ s									
Beats to recover the systolic pressure	4	4	4	3	4	4	4	3	4
Beats to recover the mean pressure	4	4	4	4	4	4	4	4	4
Beats to recover the diastolic pressure	**5**	**4**	**4**	**4**	**4**	**4**	**5**	**4**	**5**
Beats to recover the mean flow	3	2	1	2	3	2	1	2	3
From $RR_1 = 0.8$ s to $RR_2 = 1.1$ s									
Beats to recover the systolic pressure	3	7	3	3	3	3	3	3	3
Beats to recover the mean pressure	3	3	3	3	3	3	3	3	3
Beats to recover the diastolic pressure	**4**	**4**	**4**	**4**	**4**	**4**	**4**	**6**	**4**
Beats to recover the mean flow	3	2	1	2	2	2	1	0	2
From $RR_1 = 1.1$ s to $RR_2 = 0.8$ s									
Beats to recover the systolic pressure	4	4	4	3	4	4	4	3	3
Beats to recover the mean pressure	5	5	5	5	5	5	5	4	5
Beats to recover the diastolic pressure	**5**	**5**	**5**	**5**	**5**	**5**	**5**	**4**	**5**
Beats to recover the mean flow	3	2	0	2	3	0	1	1	2
From $RR_1 = 0.5$ s to $RR_2 = 1.1$ s									
Beats to recover the systolic pressure	4	4	4	3	4	4	4	4	4
Beats to recover the mean pressure	4	4	4	4	4	4	4	4	4
Beats to recover the diastolic pressure	**5**	**5**	**5**	**5**	**5**	**5**	**5**	**3**	**5**
Beats to recover the mean flow	4	2	2	3	3	3	1	2	3
From $RR_1 = 1.1$ s to $RR_2 = 0.5$ s									
Beats to recover the systolic pressure	6	6	5	5	6	5	5	5	5
Beats to recover the mean pressure	6	6	6	6	6	6	6	6	6
Beats to recover the diastolic pressure	**6**	**6**	**6**	**7**	**7**	**7**	**6**	**8**	**6**
Beats to recover the mean flow	6	5	3	2	3	3	4	1	2

6.4 Conclusions

We change the beat duration, going from a constant sequence of regular beats to one another. We can record and study the transitional solutions. At each site, during this period, pressures and flows gradually evolve, until it is reproduced the final solution: that corresponding to the terminal value of RR. In general, going from a longer to a shorter beat, pressures and mean flows rise. Opposite results are found as passing from a shorter to a longer beat. Each point takes a certain number of beats to recover the solution correlated to the latest beat period, there. This number of beats depends on the final beat period but also on the distance from the heart.

Chapter 7

Single irregular beat within sequences of standard beats

We have a look at what happens when a single anomalous beat is introduced within a sequence of standard beats. We examine two cases. The first one (case c) uses an irregular beat of period $RR = 0.5$ s, while the second one (case d) adopts a non standard beat with $RR = 1.1$ s. Table 7.1 shows the sequences of beat periods for the solutions of the images below in the case c and d.

Table 7.1: Sequence of the represented beat periods with $RR = 0.5$ s in second position (case c) and with $RR = 1.1$ s in second position (case d).

	Beat	1	2	3	4	5	6	7	8	9	10
case c	Period [s]	0.8	0.5	0.8	0.8	0.8	0.8	0.8	0.8	0.8	0.8
case d	Period [s]	0.8	1.1	0.8	0.8	0.8	0.8	0.8	0.8	0.8	0.8

As in the previous chapter, we are interested in the pressure and flow variations, as a consequence of a discontinuous beat period among the simulated heartbeats. Also, we want to define how many beats are necessary, after the introduction of the irregular beat, because a steady solution can be restored. These themes are solved for both the cases c and d and at different distances from the heart.

7.1 Pressures

For the cases c and d, we look at the systolic, diastolic and mean pressure values. From Figure 7.1, one can easily see that the irregular beat introduc-

tion alters the systolic and diastolic pressures at all the considered sites.

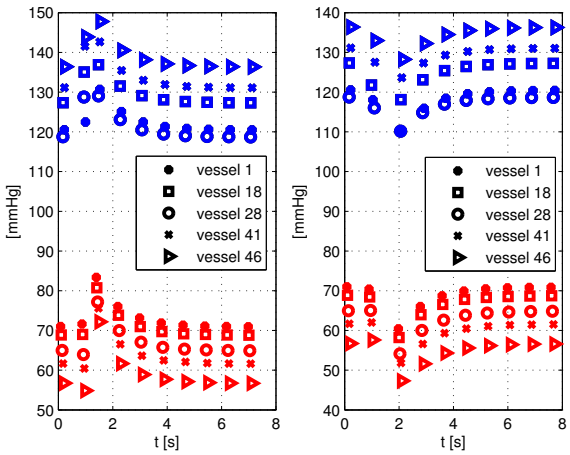

Figure 7.1: Systolic (blue) and diastolic (red) pressures at the entrance to the indicated vessels, for an irregular beat with $RR = 0.5$ s in second position (left) and for an irregular beat with $RR = 1.1$ s in second position (right).

In particular, these pressures rise in the case c and reduce in the case d. Interesting to note that, despite the irregular beat is in second position, the maximal pressure variations are associated to the third beat, which follows the irregular one. After this, at all sites, there is a progressive return to the pressures expected there for a normal beat. As one has just seen in the previous sections, the beat period alteration does not manage to vary the classical evolution of the pressures along the arterial tree: systolic pressures grow while diastolic ones decrease, with the distance from the heart, except along the abdominal aorta.

From Figure 7.2, it is clear that, when introducing an irregular beat, the percentage variations of the pressure values are quite different according to the distance from the heart. This, especially on the irregular beat and on the subsequent one. As time goes by, these differences between the various sites tend to disappear.

Through the Figure 7.3, we can demonstrate that an irregular beat also leads to an increase or reduction of the mean pressure, according to its period. It rises in the case c and reduces in the case d. It is still true that, even after the abnormal beat introduction, mean pressures reduce as we move away from the heart, less than a few exceptions along the abdominal aorta. Like the systolic and diastolic pressures variations, the mean pressure

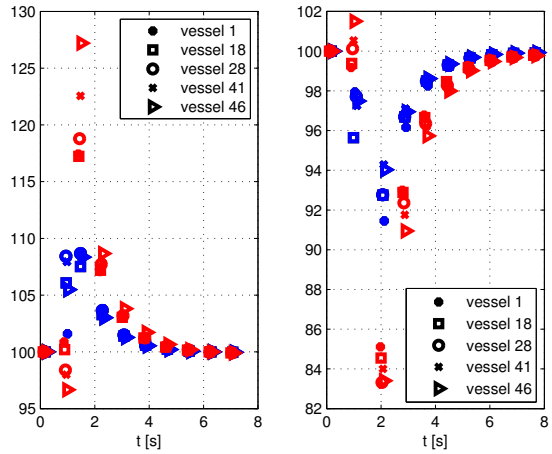

Figure 7.2: Percentage variations of the systolic (blue) and diastolic (red) pressures at the entrance to the indicated vessels, for an irregular beat with $RR = 0.5$ s in second position (left) and for an irregular beat with $RR = 1.1$ s in second position (right). Reference values are those calculated for $RR = 0.8$ s.

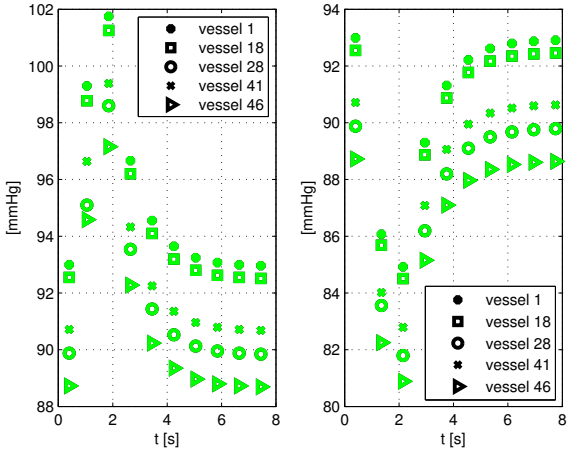

Figure 7.3: Mean pressures at the entrance to the indicated vessels, for an irregular beat with $RR = 0.5$ s in second position (left) and for an irregular beat with $RR = 1.1$ s in second position (right).

alterations are greater on the beat following the non standard one.

Figure 7.4 confirms all the previous considerations about mean pressures.

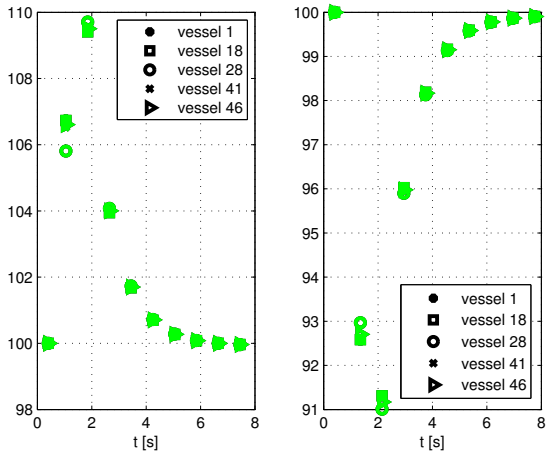

Figure 7.4: Percentage variations of the mean pressures at the entrance to the indicated vessels, for an irregular beat with $RR = 0.5$ s in second position (left) and for an irregular beat with $RR = 1.1$ s in second position (right). Reference values are those calculated for $RR = 0.8$ s.

7.2 Flows

As just done in the previous chapter, concerning flows, we turn our attention to the mean flows only. Thanks to the Figure 7.5, we appreciate that the mean flows become larger for an anomalous beat shorter than the standard one whereas reduce as the irregular RR rises. Moreover, as expected, mean flows reduce travelling down the arterial tree. Mean flow variations are significant where we have varied the beat duration and on the subsequent position but vanish quickly, especially further away from the heart. This is apparent in the Figure 7.6.

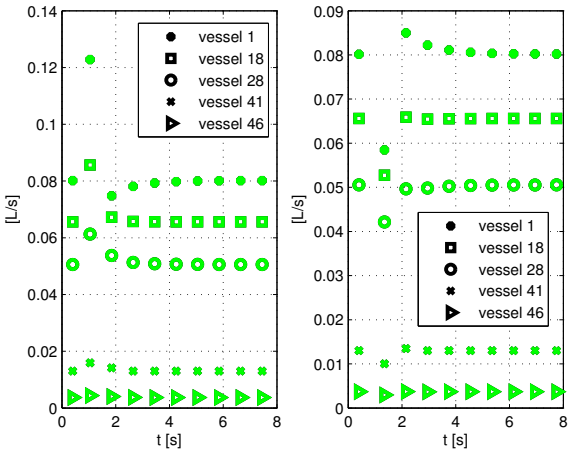

Figure 7.5: Mean flows at the entrance to the indicated vessels, for an irregular beat with $RR = 0.5$ s in second position (left) and for an irregular beat with $RR = 1.1$ s in second position (right).

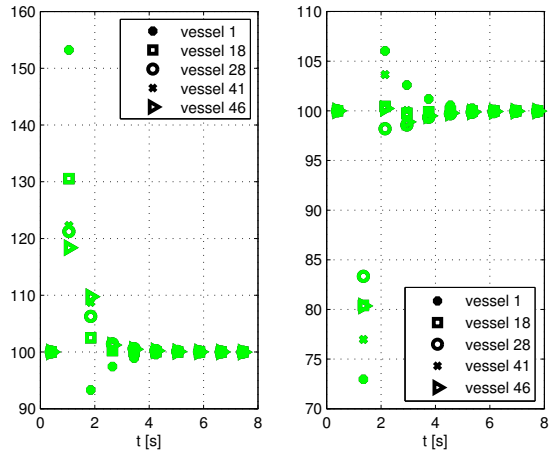

Figure 7.6: Percentage variations of the mean flows at the entrance to the indicated vessels, for an irregular beat with $RR = 0.5$ s in second position (left) and for an irregular beat with $RR = 1.1$ s in second position (right). Reference values are those calculated for $RR = 0.8$ s.

7.3 Recovery intervals

Table 7.2: Number of beats to recover characteristic pressure and flow values, at different distances from the heart, for an irregular beat in second position (its period is indicated).

Distance from the heart [mm]	0	40	99	151	255	328	454	533	677
Irregular beat with $RR = 0.5$ s.									
Beats to recover the systolic pressure	3	3	3	3	3	3	3	3	3
Beats to recover the mean pressure	3	3	3	3	3	3	3	3	3
Beats to recover the diastolic pressure	**4**	**4**	**4**	**4**	**4**	**3**	**4**	**3**	**4**
Beats to recover the mean flow	3	2	1	1	2	1	1	1	2
Irregular beat with $RR = 0.6$ s.									
Beats to recover the systolic pressure	4	4	3	3	3	4	3	3	3
Beats to recover the mean pressure	3	3	3	3	3	3	3	3	3
Beats to recover the diastolic pressure	**4**	**4**	**4**	**4**	**4**	**4**	**4**	**4**	**5**
Beats to recover the mean flow	2	1	1	1	1	1	1	1	1
Irregular beat with $RR = 0.7$ s.									
Beats to recover the systolic pressure	3	3	3	2	3	3	3	2	2
Beats to recover the mean pressure	2	2	2	2	2	2	2	2	2
Beats to recover the diastolic pressure	**3**	**3**	**3**	**3**	**3**	**3**	**3**	**3**	**4**
Beats to recover the mean flow	1	1	0	0	0	0	0	0	1
Irregular beat with $RR = 0.9$ s.									
Beats to recover the systolic pressure	3	3	3	2	3	3	3	3	3
Beats to recover the mean pressure	2	2	2	2	2	2	2	2	2
Beats to recover the diastolic pressure	**4**	**4**	**4**	**4**	**4**	**4**	**4**	**3**	**4**
Beats to recover the mean flow	1	1	0	0	0	0	1	1	0
Irregular beat with $RR = 1.0$ s.									
Beats to recover the systolic pressure	4	4	3	3	4	4	3	3	3
Beats to recover the mean pressure	3	3	3	3	3	3	3	3	3
Beats to recover the diastolic pressure	**5**	**5**	**5**	**5**	**5**	**5**	**5**	**4**	**5**
Beats to recover the mean flow	2	1	0	0	0	0	1	1	0
Irregular beat with $RR = 1.1$ s.									
Beats to recover the systolic pressure	3	3	3	3	3	3	3	3	3
Beats to recover the mean pressure	3	3	3	3	3	3	3	3	3
Beats to recover the diastolic pressure	**4**	**4**	**4**	**4**	**4**	**4**	**4**	**4**	**4**
Beats to recover the mean flow	3	2	0	0	2	1	1	1	2

Following the scheme presented in the Table 7.1, we introduce an irregular beat with $RR \neq 0.8$ s in second position. We estimate, at different sites, how many beats are needed before restoring the calculated systolic,

diastolic and mean pressure values, as well as mean flows, for $RR = 0.8$ s, with a difference always less than $\pm 1\%$. These results are available in the Table 7.2. From these data we can conclude what follows.

- As we have just observed for the abrupt changes of the beat duration, at each site, it is diastolic pressure (indicated in bold) to define the number of beats to restore the expected values of pressure and flow.
- Chosen a point, the beat number to conclude the transition phase is not always equal for simulations whose irregular beats have symmetric periods in reference to the value 0.8 s. If irregular beats are symmetric in reference to the standard beat, at each site, the beat number to recover from the longer beat will be greater or equal to that required with a non standard shorter beat. This is in good agreement with what found in the previous chapter. In fact, introducing an irregular longer beat within a chain of traditional beats means that, to end the transition time, we have to wait for a passage from a longer to a shorter beat. This operation, at all sites, is typically slower or takes the same time than the opposite one.
- There is not a precise relationship between the distance from the heart and time required to recover.

7.4 Conclusions

When introducing only one non standard beat among chains of traditional beats, it determines everywhere not negligible alterations of pressure and flow values. In particular, for a beat shorter than the standard one, we measure a general gain of pressure and a growth in the mean flow, at all sites. The opposite trend can be observed for a longer irregular beat. After the anomalous beat, since RR returns to be normal, all pressure and flow values go back, with a certain inertia, to the starting ones. The transition phases take different times, according to the irregular beat period but also the position of the considered site. Interesting is the fact that the greatest pressure variations are always associated to the beat following the irregular one while the highest flow alterations are correlated to the previous beat.

Chapter 8

Sequences of fibrillated heartbeats

Until now, we have demonstrated that the beat duration has a strong impact on the values of the pressures and flows along the arterial tree. Moreover, any beat period change not only leads to some variations in the heart workload but also produces significant alterations to the conditions of the reflected and transmitted signals due to the pumping activity of the heart.

At this stage, we study what happens, within domain, during an episode of atrial fibrillation (AF) lasting about half an hour (2000 heartbeats), with a mean heartbeat frequency of 75 bpm. To this purpose, we continue adopting the numerical model by Guala [16]. In section 1.2, we said that, in case of AF, the main problem is related to the generation of the electrical impulses causing the beats. However, in the model, the mechanism of beat generation is not automatised: we have to impose the chain of the beat periods we want to simulate as input data. This means that first we have to identify the typical distribution of RR in AF. The first part of this chapter aims at briefly explaining how we can construct a general sequence of fibrillated heartbeats. After this, we are going to describe some results, at various distances from the heart and for all the 2000 simulated heartbeats. Concerning heart performances, results consist in the pressure and volume of the left ventricle, at the end of both systole and diastole, the stroke volume (SV), the ejection fraction (EF), the cardiac output (CO) and the stroke work (SW). As regards blood vessels, instead, we concentrate on systolic and diastolic pressures, mean flows, phase velocities and coefficients of reflection, for a certain number of sites.

8.1 Distribution of RR in case of atrial fibrillation

Until now, we have indicated as normal a beat period of 0.8 s. This is not absolutely true. Indeed, if the heart is regularly beating (the heart has a normal sinus rhythm (NSR)), the beat period will show small oscillations around a mean value almost always around 0.8 s. This means that, even if one is not affected by any type of arrhythmia, the value of RR will not be perfectly constant. It has been checked that the distribution of RR for a normal sinus rhythm is Gaussian, with a coefficient of variation $cv = \sigma/\mu$ between 0.05 and 0.013 [23], [44]. In this formula, σ and μ are the standard deviation and the mean value of the RR distribution, respectively. Moreover, for a normal beat, the RR intervals produce an approximately $1/f$ power spectrum, named $S(f)$, where f is the beat frequency. Therefore, a normal heartbeat is an example of pink noise, for which we have a temporary correlation.

Something different happens in reference to a beat during AF. In fact, for this, $S(f)$ is composed by two different contributions. While the first one ($S_1(f)$) is the same as the normal beat and varies as $1/f$, the second one ($S_2(f)$) has the characteristics of the white noise, uncorrelated in time. When a signal is temporary uncorrelated, its power spectral density will remain constant with frequency. Important to say is that $S_1(f)$ covers the small frequency range while $S_2(f)$ involves the high frequency domain. In general, a sequence of RR in AF can be calculated as $RR = \tau + \eta$, where τ derives from a pink Gaussian distribution, with typical parameters μ_G and σ_G, whereas η depends on an uncorrelated exponential distribution through γ. To conclude, the complete RR distribution for a case of AF has mean value $\mu = \mu_G + \gamma^{-1}$ and standard deviation $\sigma = \sqrt{\sigma_G^2 + \gamma^{-2}}$, with cv approximately equal to 0.24 [22], [23], [44].

In the run simulation, the RR sequence has $\mu = 0.8$ s and $\sigma = 0.19$ s; its PDF is shown in Figure 8.1. Since the mean value of the RR distribution is equal to that is usually measured in NSR, the calculations in AF will refer to the same heartbeat frequency typically associated to a normal beat: 75 bpm. This means that this study of AF is limited to look into the global effect of only same characteristic aspects of AF: the absence of temporary correlation within the high frequency range (long beats) and the greater dispersion of data around the mean value of the simulated RR sequence, in reference to the case of NSR (fixed μ, the value cv for RR is certainly higher during AF). As showed in the first chapter, AF often causes a growth in the mean frequency of the beat; this study, to facilitate the comparison, does

not consider this feature.

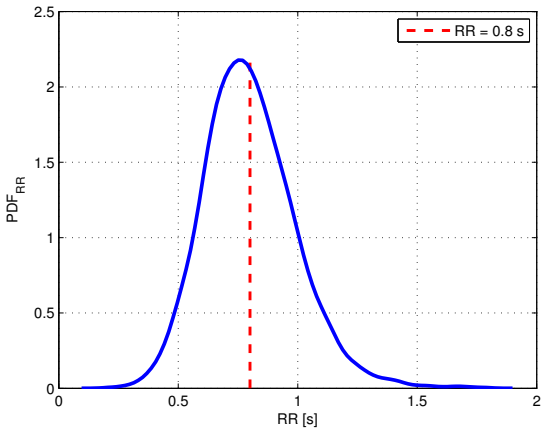

Figure 8.1: PDF of the RR distribution adopted in this study in case of AF.

8.2 Results in case of atrial fibrillation

Fibrillated simulation provides us, beat by beat, the complete signals of pressure and flow at each site, as well as the total values of pressure and volume for the left ventricle. Figure 8.2 shows a piece of both pressure and flow time series, at the entrance to the aorta, for all the 2000 heartbeats. Maximal and minimal values of systolic and diastolic pressures are in the range of possible pressure values during the simulated time. Furthermore, we do not observe strange and enormous oscillations in the solutions, unless small numerical fluctuations everywhere as aortic valve opens and closes at each beat. However, these are not significant in the subsequent analysis, since we want to analyse more general changes in pressure and flow results when the beat is fibrillated.

From Figure 8.2, one clearly understands that, chosen a quantity of interest, for example systolic pressure, we find for it as many values as the simulated heartbeats (2000) at each site. Thus, in order to draw some useful conclusions from the huge amount of available data, we calculate, for each arterial section, the probability density function (PDF) of all the quantities we are interested in. The information related to each PDF are summarized again in terms of mean value, μ, standard deviation, σ, coefficient of variation, cv, and some higher order moments, such as skewness S and kurtosis

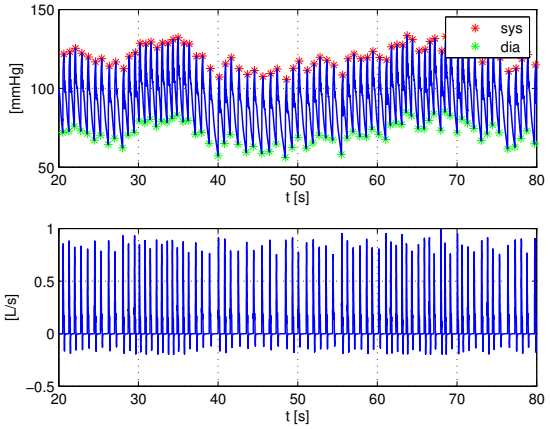

Figure 8.2: Examples of pressure time series (top) and flow time series (bottom) at the entrance to the aorta during AF (mean heartbeat frequency: 75 bpm). Red and green marks indicate systolic and diastolic pressures, respectively.

K. S is a measure of lack of symmetry of the local distribution of the quantity under exam (for example systolic or diastolic pressure) about its mean value. Note that, for a Gaussian distribution, S = 0. Otherwise, if S > 0, positive fluctuations are more probable than negative ones, if S < 0, it is more likely to have negative fluctuations (Figure 8.3).

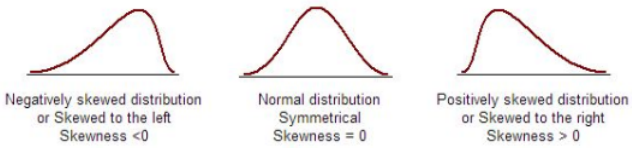

Figure 8.3: Examples of negative, zero and positive skewed distributions.

As concern K, it provides information about how extensive the tails of the distribution are (is a measure of intermittency in the recorded quantity). For a Gaussian distribution, K = 3. Therefore, when K > 3, tails of the distribution concerned cover an interval wider than that for a normal distribution, the opposite is true as K < 3 (Figure 8.4).

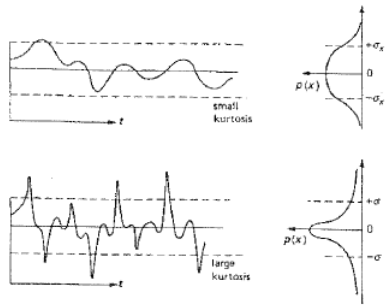

Figure 8.4: Examples of large and small kurtosis.

8.2.1 Response of the heart in case of atrial fibrillation

In case of AF, Figure 8.5 and 8.6 show the PDFs for some of the quantities describing the performances of the heart, while Table 8.1 summarizes the principal features of these PDFs.

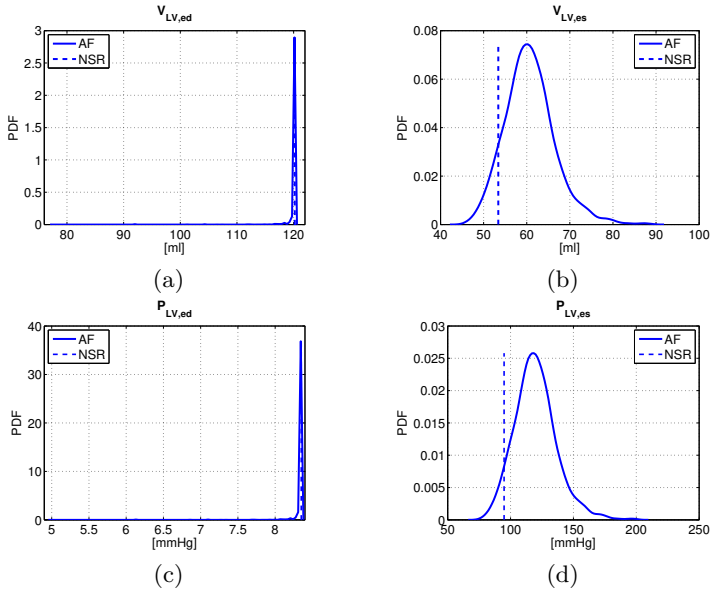

Figure 8.5: PDFs of some of the heart parameters during AF (mean heartbeat frequency: 75 bpm). Dotted lines indicate the same corresponding quantities in NSR (mean heartbeat frequency: 75 bpm). $V_{LV,ed}$ and $V_{LV,es}$: left ventricle volume end diastole and end systole, respectively. $P_{LV,ed}$ and $P_{LV,es}$: left ventricle pressure end diastole and end systole, respectively.

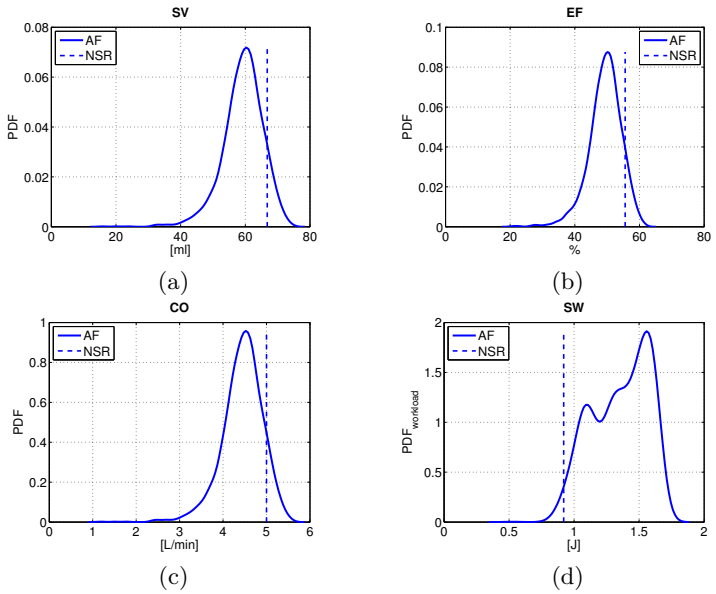

Figure 8.6: PDFs of some of the heart parameters during AF (mean heartbeat frequency: 75 bpm). Dotted lines indicate the same corresponding quantities in NSR (mean heartbeat frequency: 75 bpm). SV: stroke volume, CO: cardiac output, EF: ejection fraction, SW: stroke work.

Table 8.1: Principal properties of the PDFs of the heart parameters during AF (mean heartbeat frequency: 75 bpm).

Quantity	μ	σ	cv	S	K
$V_{LV,ed}$	119.95 ml	1.49 ml	0.012	−18.01	431.34
$V_{LV,es}$	60.74 ml	5.85 ml	0.10	0.64	4.23
$P_{LV,ed}$	8.33 mmHg	0.12 mmHg	0.014	−18.01	431.34
$P_{LV,es}$	119.95 mmHg	16.88 mmHg	0.14	0.64	4.23
SV	59.20 ml	6.32 ml	0.11	−0.99	6.18
EF	49.34%	5.11%	0.10	−0.85	5.20
CO	4.44 L/min	0.47 L/min	0.11	−0.99	6.18
SW	1.35 J	0.21 J	0.16	−0.38	2.01

One of the most important consideration is that, in AF, the stroke work, SW, left ventricle has to do in order to properly accomplish its functions grows, on average, of about 50%, going from 0.92 J to 1.35 J (as the mean heart frequency is fixed). Moreover, negative fluctuations are usually more probable than positive ones, having S<0, apart from pressure and volume

of the left ventricle at the end of diastole. As concern K, it is almost always greater than 3. We find that, as diastole concludes, the level of intermittency in pressure and volume of the left ventricle is much more evident than that evaluated in case of Gaussian distributions.

8.2.2 Response of the arterial tree in case of atrial fibrillation

Systolic and diastolic pressures

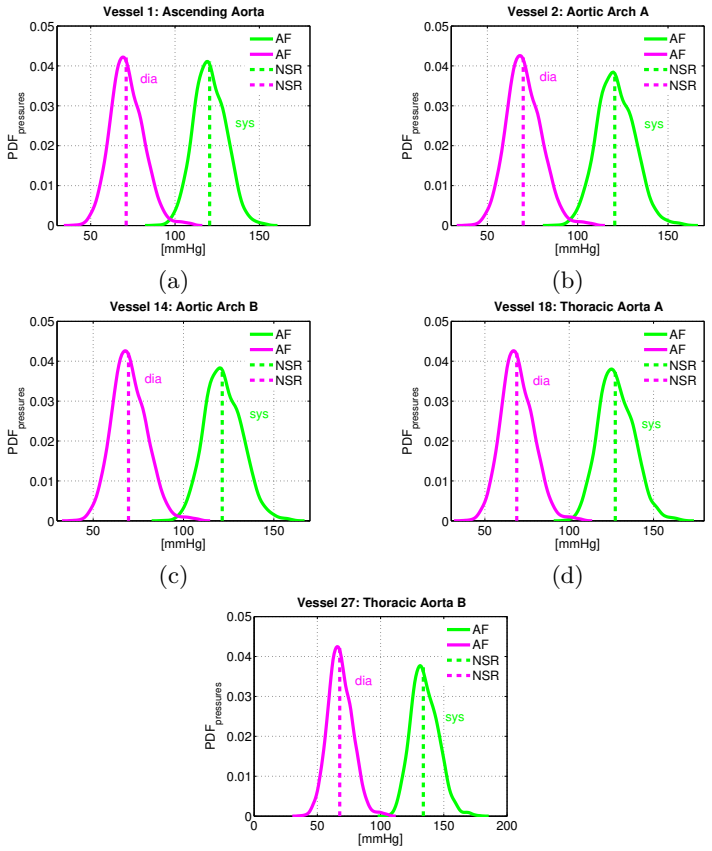

Figure 8.7: PDFs of some systolic and diastolic pressures along the arterial tree (vessels: 1, 2, 14, 18, 27) during AF (mean heartbeat frequency: 75 bpm). Dotted lines indicate the same pressure values in NSR (mean heartbeat frequency: 75 bpm).

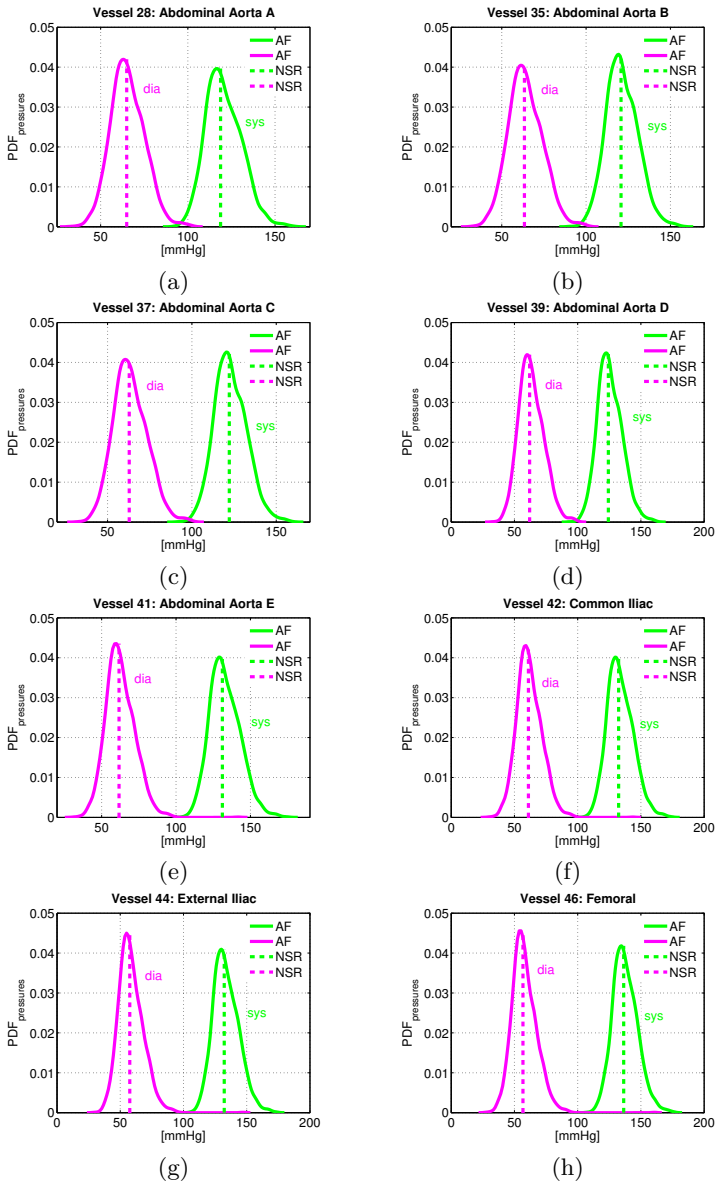

Figure 8.8: PDFs of some systolic and diastolic pressures along the arterial tree (vessels: 28, 35, 37, 39, 41, 42, 44, 46) during AF (mean heartbeat frequency: 75 bpm). Dotted lines indicate the same pressure values in NSR (mean heartbeat frequency: 75 bpm).

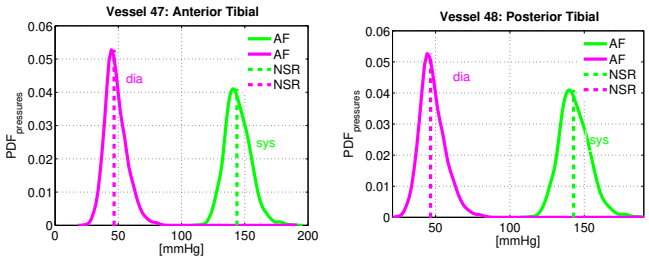

(a) (b)

Figure 8.9: PDFs of some systolic and diastolic pressures along the arterial tree (vessels: 47, 48) during AF (mean heartbeat frequency: 75 bpm). Dotted lines indicate the same pressure values in NSR (mean heartbeat frequency: 75 bpm).

The figures above display the PDFs of the systolic and diastolic pressures during AF, at the beginning of all the indicated vessels along the arterial tree. We give also, for each vessel, the reference systolic and diastolic pressures in NSR, at the same mean frequency (75 bpm).

From Figure 8.10, one can see that the typical trends of the maximal and minimal values of pressure, on average, are not varied in AF and are similar to those expected in NSR. Indeed, while diastolic pressures always reduce, leaving the heart, systolic pressures grow, moving away from the heart, except at the region between the end of the thoracic aorta and the beginning of the abdominal one, marked in the figure. The same figure indicates the evolution of the pulse pressure (PP), difference between systolic and diastolic pressure, with the distance from the heart. This quantity is particularly interesting under a medical point of view, being a measure of the heart efficiency (the smaller is PP, the lower is the heart efficiency).

Standard deviations in AF are about between 9 and 10 mmHg for both systolic and diastolic pressures. However, we want to know how much mean systolic and diastolic pressure fluctuations are considerable in reference to their mean values at each arterial point. To this purpose, we calculate the coefficients of variation cv for both systolic and diastolic pressures at all the sites of interest. These results are summarized in the Figure 8.11. From this, one can see that cv values for diastolic pressures almost double those for systolic ones everywhere. Moreover, as we move away from the heart, cv grows for diastolic pressure while reduces for systolic one. This means that, in AF, arterial system tends to amplify diastolic pressure oscillations whereas reduces systolic pressure variations. From the values of cv for the pulse

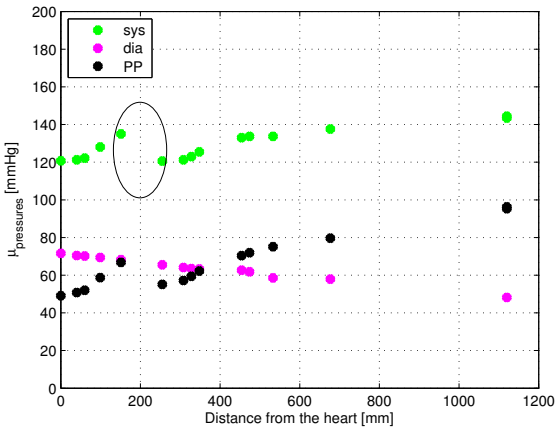

Figure 8.10: Mean values of the systolic, diastolic and pulse pressures along the arterial tree during AF (mean heartbeat frequency: 75 bpm). The points in the ellipse indicate the end of thoracic aorta and the beginning of abdominal aorta.

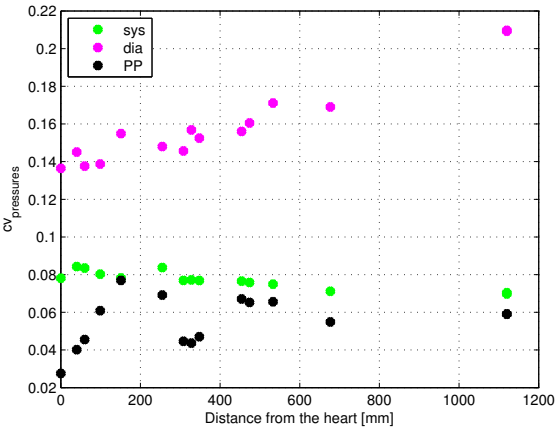

Figure 8.11: Coefficients of variation for systolic, diastolic and pulse pressures along the arterial tree during AF (mean heartbeat frequency: 75 bpm).

pressure, we can see that it fluctuates less than both systolic and diastolic pressure leaving the heart. However, arterial system tends to amplify PP oscillations at some special regions.

In AF, mean systolic and diastolic pressures are slightly higher than the

Table 8.2: Percentage variations of the mean systolic and diastolic pressures along the arterial tree during AF, in reference to the corresponding pressures in NSR. Skewness and kurtosis of the same pressures during AF. For both AF and NSR simulations, mean heartbeat frequency is 75 bpm.

Vessel	% var sys	% var dia	S sys	K sys	S dia	K dia
1	0.16	0.89	0.18	2.98	0.44	3.54
2	0.33	0.80	0.26	3.13	0.43	3.54
14	0.62	0.83	0.31	3.10	0.43	3.54
18	0.57	0.73	0.35	3.09	0.40	3.50
27	0.90	0.73	0.43	3.22	0.37	3.45
28	1.58	0.81	0.45	3.16	0.32	3.32
35	0.80	0.83	0.33	3.20	0.31	3.33
37	1.13	0.72	0.35	3.23	0.37	3.22
39	0.46	1	0.42	3.30	0.44	3.26
41	0.62	1.05	0.49	3.29	0.62	5.19
42	0.98	2.04	0.47	3.26	0.61	5.34
44	1.43	1.53	0.48	3.28	0.85	6.45
46	1	1.24	0.44	3.37	1.00	9.04
47	1.13	1.78	0.51	3.67	2.25	28.18
48	0.87	2.09	0.51	3.67	2.21	27.40

corresponding in NSR. Evidence of this is given in Table 8.2. It indicates also S and K of the PDFs for the systolic and diastolic pressures during AF. From these data, we can draw a certain number of conclusions. First of all, we see that all the diastolic and systolic pressure distributions are asymmetric in reference to their mean values, indeed, S is always different from zero. Moreover, positive pressure fluctuations are more likely than negative ones since S$>$ 0. We note that the tails of the distribution cover intervals wider than those in case of normal distribution (almost always K$>$ 3). The most persistent pressure fluctuations are located between the latest portion of the abdominal aorta and the anterior/posterior tibial arteries. In fact, in this region, K assumes values quite high, especially as concern diastolic pressures.

Mean flows

Figures below are the PDFs of the mean flows along aorta during AF, with reference mean flows in NSR at the same mean frequency of 75 bpm.

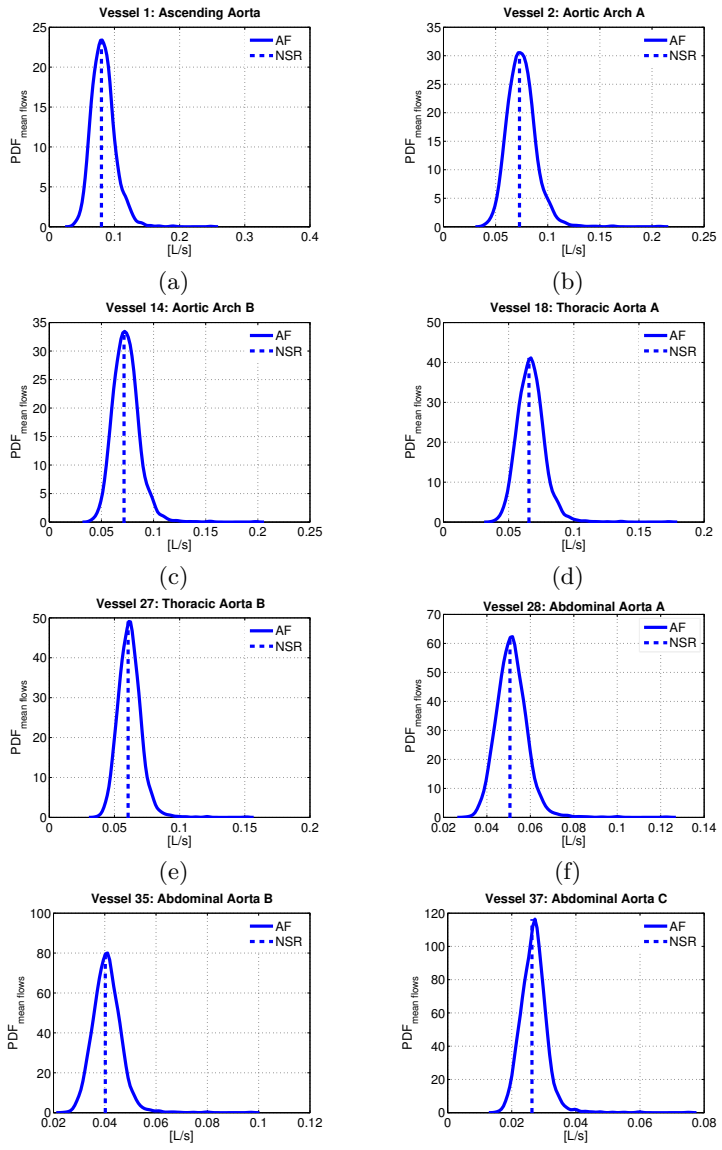

Figure 8.12: PDFs of some mean flows along the arterial tree (vessels: 1, 2, 14, 18, 27, 28, 35, 37) during AF (mean heartbeat frequency: 75 bpm). Dotted lines indicate mean flow values in NSR (mean heartbeat frequency: 75 bpm).

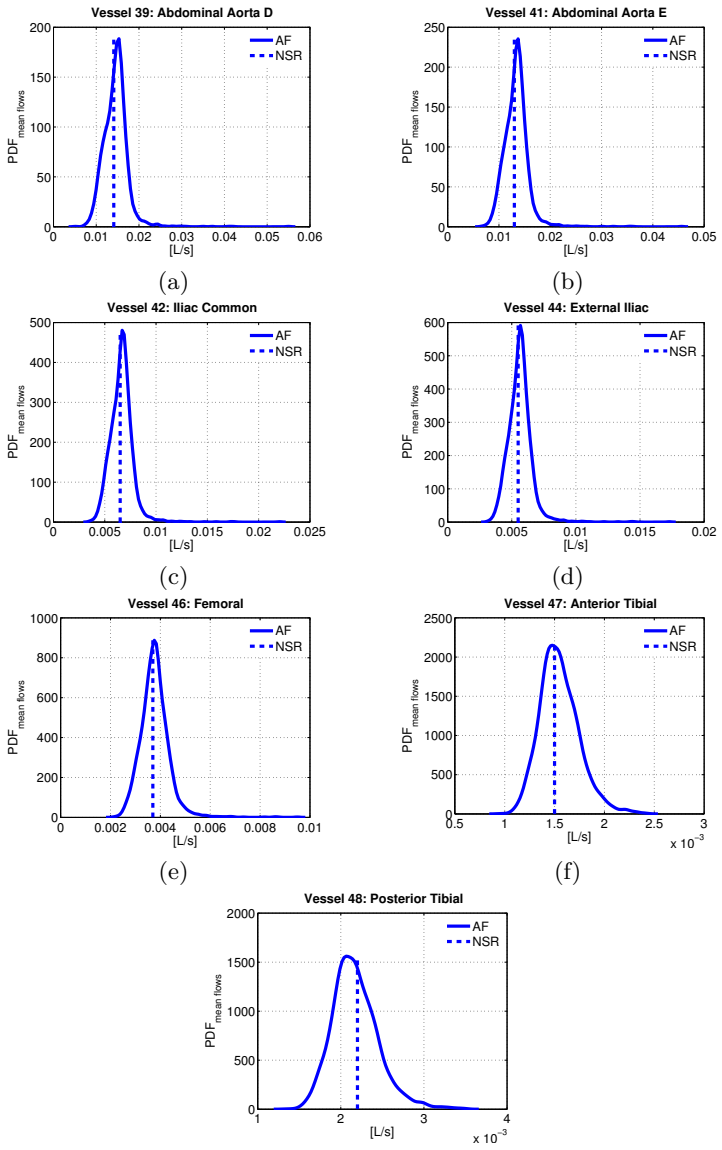

Figure 8.13: PDFs of some mean flows along the arterial tree (vessels: 39, 41, 42, 44, 46, 47, 48) during AF (mean heartbeat frequency: 75 bpm). Dotted lines indicate mean flow values in NSR (mean heartbeat frequency: 75 bpm).

From Figure 8.14, one can see that, on average, the mean flows reduces

leaving the heart in AF, as happens for NSR.

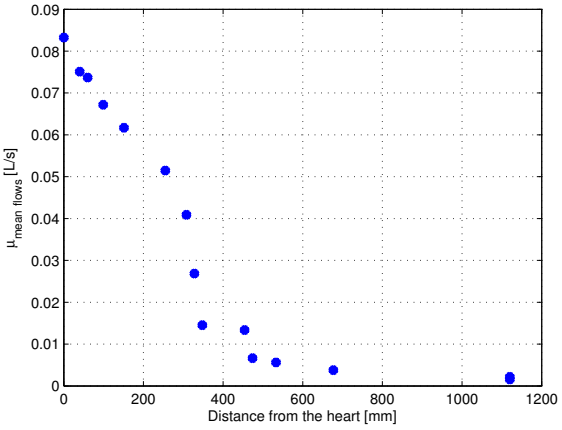

Figure 8.14: Mean values of the mean flows along the arterial tree during AF (mean heartbeat frequency: 75 bpm).

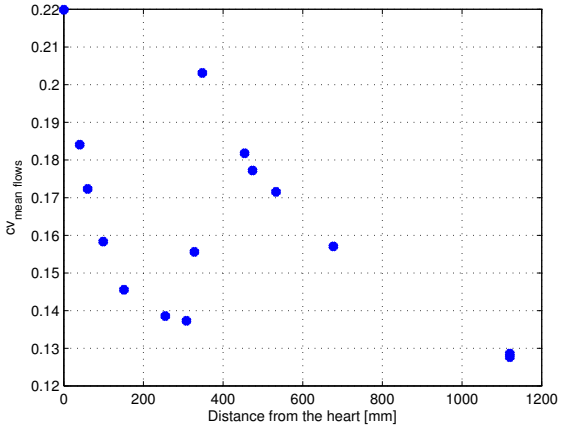

Figure 8.15: Coefficients of variation for mean flows along the arterial tree during AF (mean heartbeat frequency: 75 bpm).

Concerning the coefficients of variations for the mean flows in AF, these diminish with the distance from the heart, except along the central portions of the abdominal aorta (Figure 8.15).

A fibrillated heartbeat brings on a general growth in the mean flows

almost everywhere, as visible in Table 8.3. This shows percentage variations higher that those observed for the mean systolic and diastolic pressures. The only site in which we have a decrease in the mean level of the mean flow is the posterior tibial (vessel 48). Regarding the PDFs of the mean flows, through the skewness and kurtosis values (Table 8.3), we verify that there are significant positive oscillations (S$>$ 0) and that these take up intervals decisively larger than those relative to a Gaussian distribution (K$>$ 3). It is especially true between the end of the abdominal aorta and the beginning of the femoral artery. The frequency of large fluctuations in mean flows, around mean values, during atrial fibrillation, is much more evident than for systolic and diastolic pressures.

Table 8.3: Percentage variations of the mean flows along the arterial tree during AF, in reference to the same corresponding quantities in NSR. Skewness and kurtosis of the mean flows during AF. For both AF and NSR simulations, mean heartbeat frequency is 75 bpm.

Vessel	% var	S	K
1	3.91	1.12	7.88
2	3.01	1.21	9.31
14	2.76	1.23	9.84
18	2.41	1.27	10.42
27	1.96	1.28	10.74
28	1.72	1.31	11.07
35	1.70	1.34	11.38
37	2.08	1.89	17.80
39	2.95	2.88	31.43
41	2.68	2.85	29.82
42	2.07	2.80	28.83
44	2.31	2.61	24.75
46	2.11	1.89	15.16
47	3.39	0.67	3.99
48	-1.06	0.80	4.54

Phase velocities

From Figure 8.16, we can see that mean phase velocities will continue rising, moving away from the heart, if we have a fibrillated heartbeat, as for a NSR.

About coefficients of variations in AF (Figure 8.17), these fall along the arterial tree, until the end of the abdominal aorta is reached. At this point,

cv values tend to stabilize around 0.075, moving again towards more distal regions.

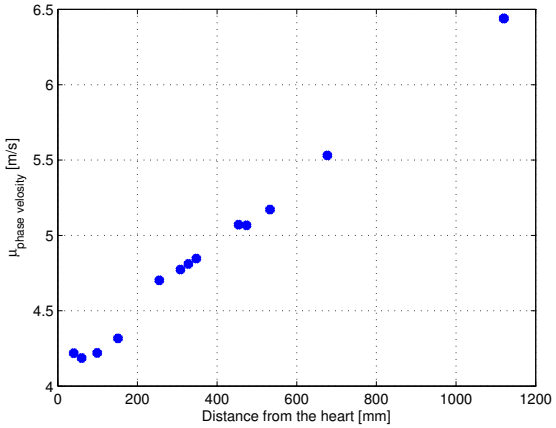

Figure 8.16: Mean phase velocities along aorta during AF (mean heartbeat frequency: 75 bpm).

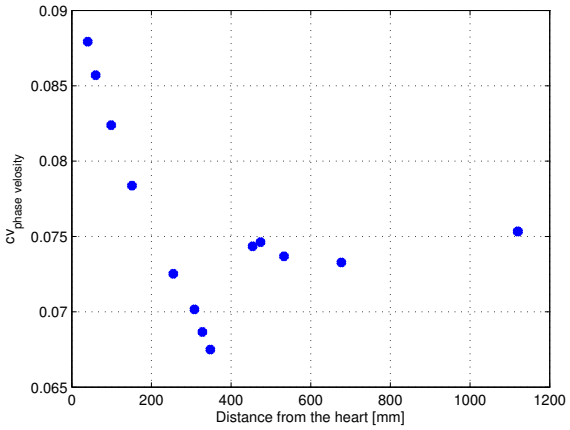

Figure 8.17: Coefficients of variation for mean phase velocities along aorta during AF (mean heartbeat frequency: 75 bpm).

Table 8.4 supports the following considerations. Mean phase velocity values slightly grow in AF, in reference to the case of NSR. From the calculations of skewness and kurtosis at the various arterial sections we find

interesting informations. Firstly, the phase velocity distributions are never symmetric anywhere (S$\neq$ 0). However, while some regions are more likely to experience positive fluctuations, other regions have an higher probability to feel negative oscillations. Moreover, the level of asymmetry where we have more probable negative alterations (from the terminal abdominal aorta to the tibial arteries) is definitely much more evident than where the alterations are typically positive. Looking at kurtosis measures, we have that the extension of phase velocity tails is pretty similar to the Gaussian one almost everywhere (even if a little higher), apart from the same regions in which negative fluctuations are more frequent.

Table 8.4: Percentage variations of the mean phase velocities along aorta in AF, in reference to the same corresponding quantities in NSR. Skewness and kurtosis of the phase velocities during AF. For both AF and NSR simulations, mean heartbeat frequency is 75 bpm.

Vessel	% var	S	K
2	0.20	0.27	3.30
14	1.17	0.25	3.34
18	0.17	0.27	3.30
27	1.49	0.30	3.25
28	0.50	0.36	3.29
35	0.74	0.40	3.33
37	1.21	0.41	3.33
39	0.97	0.41	3.32
41	0.53	-5.93	145.68
42	0.48	-6.21	154.51
44	0.90	-7.40	192.33
46	0.50	-9.73	271.71
47	0.62	-16.03	518.05
48	0.62	-16.04	518.27

RI and RM

As we have already seen having $RR = 0.8$ s, in AF, there is not a clear relationship between the magnitude of reflections and the distance from the heart too. This is due to the fact that, during AF, reflection conditions continue depending on a variety of factors, which change site by site. For the sake of completeness, we report in Figure 8.18 the evolution of the mean RI and RM with the distance from the heart, when we have a fibrillated

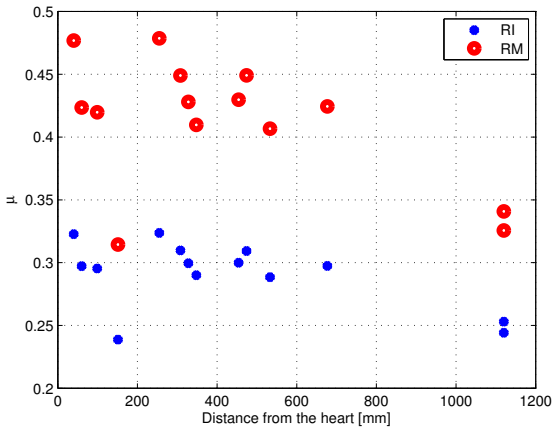

Figure 8.18: Mean RI and RM along aorta during AF (mean heartbeat frequency: 75 bpm).

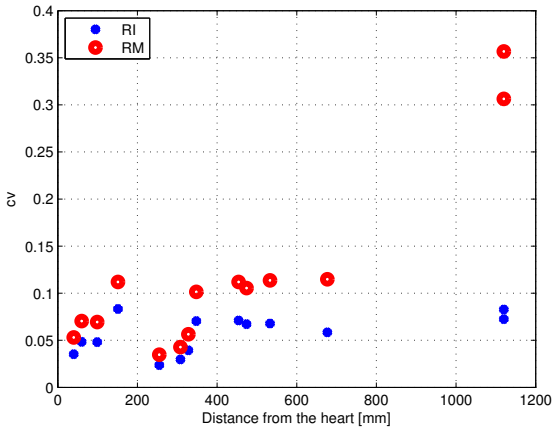

Figure 8.19: Coefficients of variation for *RI* and *RM* along aorta during AF (mean heartbeat frequency: 75 bpm).

heartbeat. In case of both AF and NSR, it is certainly true that the area in which the amplitudes of the reflected waves contribute greatly to the amplitudes of the total waves is located between the end of the thoracic aorta and the beginning of the abdominal one. As regards coefficients of variations, these rise or reduce specifically according to the position we take into account. It is apparent that the greatest values of *cv* for both *RM* and

RI take place between thoracic and abdominal aorta, as well as at posterior and anterior tibial arteries. The evolution of *cv* values leaving the heart is given in Figure 8.19.

Table 8.5: Percentage variations of the mean RI and RM along the aorta during AF, in reference to the same corresponding quantities in NSR. Skewness and kurtosis of RI and RM during AF. For both AF and NSR simulations, mean heartbeat frequency is 75 bpm.

Vessel	% var *RI*	% var *RM*	S *RI*	K *RI*	S *RM*	K *RM*
2	1.80	2.76	1.12	5.12	1.27	5.70
14	1.51	2.33	1.04	4.82	1.22	5.60
18	1.64	2.49	0.72	3.77	0.86	4.30
27	0.24	0.65	0.79	6.23	1.18	7.60
28	−1.03	−1.02	−0.79	5.68	−0.66	4.40
35	−1	−1.39	−0.53	4.79	−0.39	4.50
37	−0.95	−1.24	0.21	5.38	0.44	5.70
39	0.46	0.94	0.69	4.53	0.97	5.30
41	−1.12	−1.27	1.57	23.40	5.86	126.5
42	−1.26	−1.53	1.31	20.84	4.91	100.80
44	−1.54	−1.87	2.69	51.58	11.54	325.20
46	−1.13	−1.35	5.37	119.32	20.74	713.80
47	−0.99	−0.67	15.41	495.45	41.39	1804.40
48	19.29	24.32	12.65	391.12	41.31	1799.80

From Table 8.5, we obtain significant information. First of all, we have that, on average, the mean values of RI increase or reduce in reference to the case of NSR, during AF. This means that, in AF, the mean contribution of the reflection waves to the total waves can grow or diminish in terms of amplitude, at each site. Theses changes are described by the percentage variations in RI. About *RM*, expression of the reflected wave amplitude over the forward wave amplitude, on average, it can rise or decrease according to the site. However, unless a few exception, mean *RM*, like mean *RI*, becomes littler in AF than in NSR, at almost all the arterial points. For both *RI* and *RM*, positive fluctuations are more likely than negative ones almost everywhere. Incredible intermittency levels in *RI* and *RM* are observed between femoral and tibial arteries.

8.2.3 Response of the arms in case of atrial fibrillation

As we have just done to study what happens along aorta, we can now analyse pressures, flows, phase velocities and reflection conditions for the two arms.

Systolic and diastolic pressures

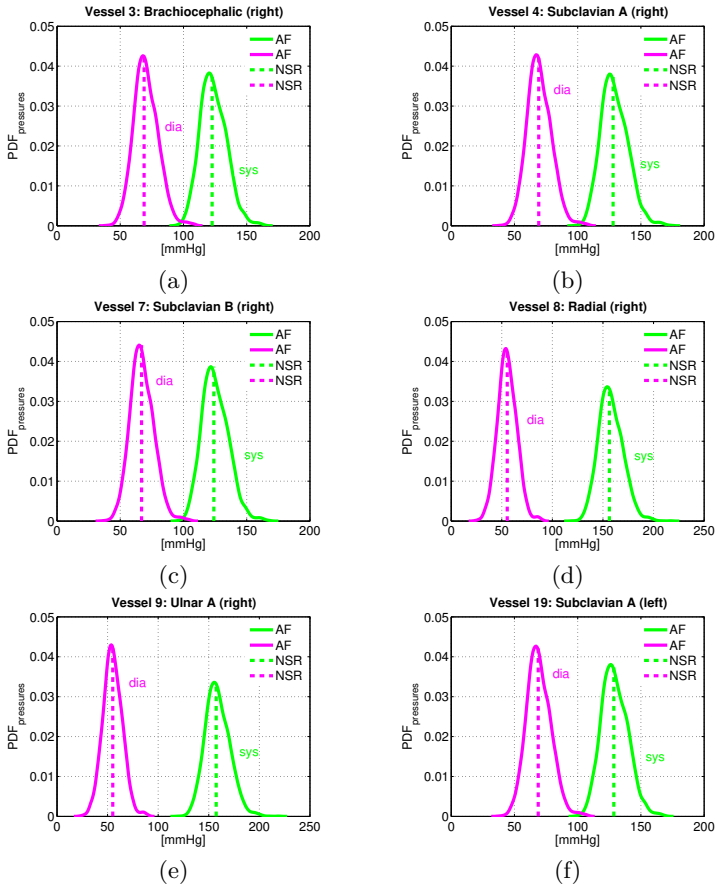

Figure 8.20: PDFs of some systolic and diastolic pressures along the two arms (vessels: 3, 4, 7, 8, 9, 19) during AF (mean heartbeat frequency: 75 bpm). Dotted lines indicate the same pressure values in NSR (mean heartbeat frequency: 75 bpm).

Figure 8.20 and 8.21 represent the PDFs of the systolic and diastolic pressures for the arm vessels during AF, with an indication of the same pressures in NSR at the same mean frequency (75 bpm).

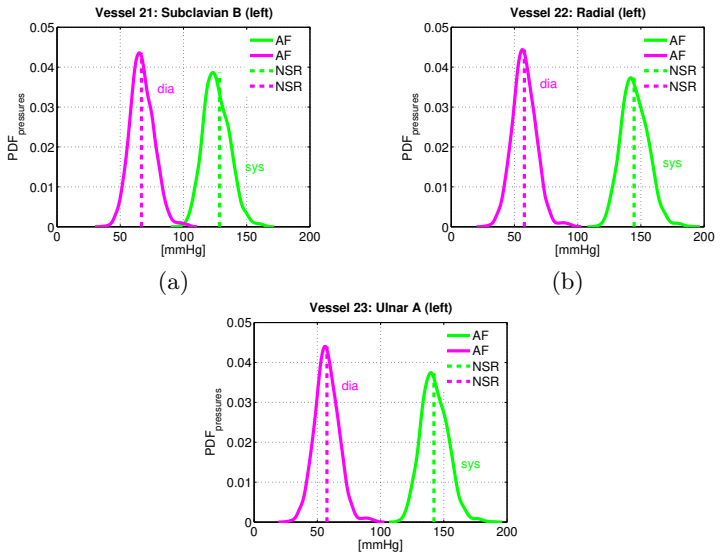

Figure 8.21: PDFs of some systolic and diastolic pressures along the two arms (vessels: 21, 22, 23) during AF (mean heartbeat frequency: 75 bpm). Dotted lines indicate the same pressure values in NSR (mean heartbeat frequency: 75 bpm).

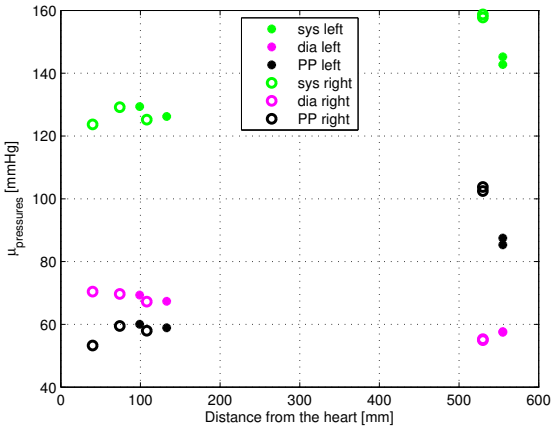

Figure 8.22: Mean values of the systolic, diastolic and pulse pressures along the left and right arm during AF (mean heartbeat frequency: 75 bpm).

As one can observe from Figure 8.22, mean diastolic pressures reduce along the two arms while systolic and pulse pressures grow, on average, following the same path. However, at the ulnar A, all the previous evolutions are reversed.

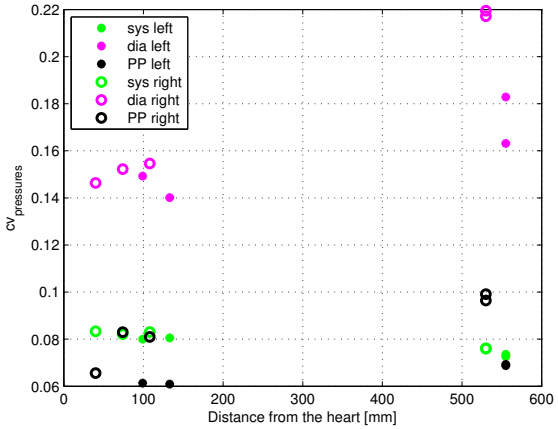

Figure 8.23: Coefficients of variation for systolic, diastolic and pulse pressures along the left and right arm during AF (mean heartbeat frequency: 75 bpm).

Table 8.6: Percentage variations of the mean systolic and diastolic pressures along the arm vessels during AF, in reference to the corresponding pressures in NSR. Skewness and kurtosis of the same pressures during AF. For both AF and NSR simulations, mean heartbeat frequency is 75 bpm.

Vessel	% var sys	% var dia	S sys	K sys	S dia	K dia
3	0.86	2.27	0.41	3.23	0.43	3.54
4	0.91	0.70	0.48	3.37	0.42	3.54
7	0.94	0.58	0.48	3.36	0.40	3.56
8	0.91	−0.18	0.45	3.52	0.21	3.33
9	0.90	−0.21	0.45	3.54	0.20	3.33
19	0.60	0.73	0.38	3.15	0.40	3.50
21	0.57	0.74	0.37	3.15	0.39	3.52
22	0.40	−0.24	0.38	3.26	0.34	3.77
23	0.42	−0.30	0.40	3.33	0.33	3.77

Regarding coefficients of variation (Figure 8.23), these rise for diastolic pressures along the previous vessels (except at the ulnar A), reduce for

systolic pressures with the distance from the heart and fluctuate a bit for the pulse pressures at the same vessels.

Looking at the Table 8.6, we have that, in AF, mean systolic pressures are a bit higher than those evaluated in NSR, even if there is no symmetry between left and right arm. This asymmetry is also clearly visible as concern mean diastolic pressures, which decrease at both left/right radial and ulnar A arteries. The PDFs for the systolic and diastolic pressures have $S > 0$ and $K > 3$, along both the arms, with different numerical values.

Mean flows

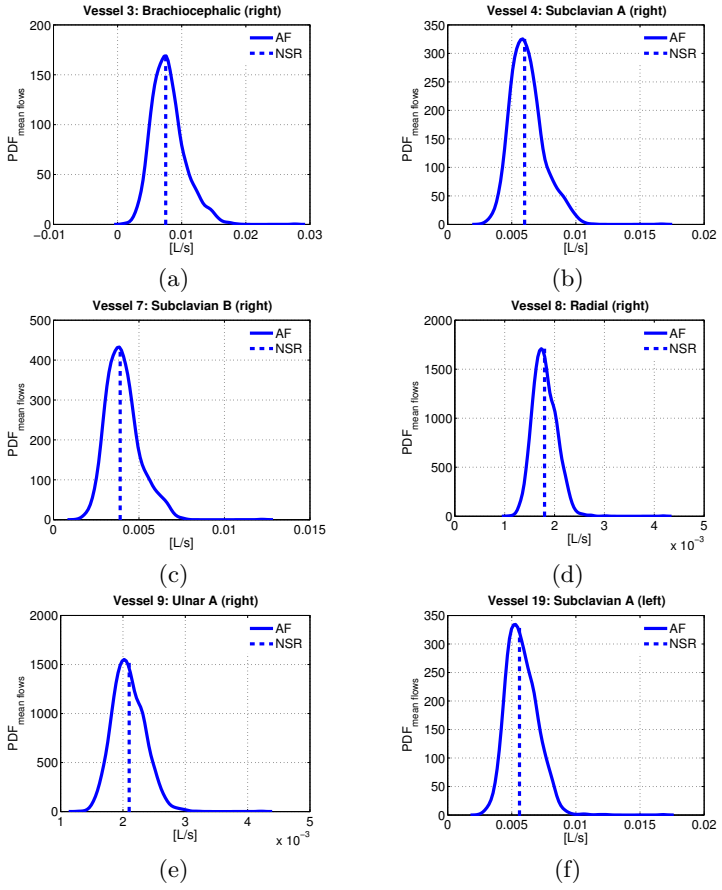

Figure 8.24: PDFs of some mean flows during AF along the two arms (vessels: 3, 4, 7, 8, 9, 19) (mean heartbeat frequency: 75 bpm). Dotted lines indicate mean flow values in NSR (mean heartbeat frequency: 75 bpm).

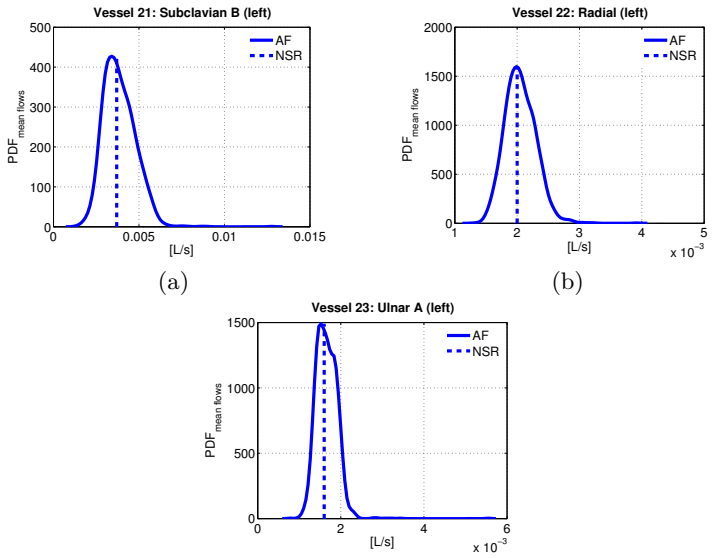

Figure 8.25: PDFs of some mean flows during AF along the two arms (vessels: 21, 22, 23) (mean heartbeat frequency: 75 bpm). Dotted lines indicate mean flow values in NSR (mean heartbeat frequency: 75 bpm).

The images of the Figure 8.24 and 8.25 show the PDFs of the mean flows along the arms during AF, with the same quantities in NSR.

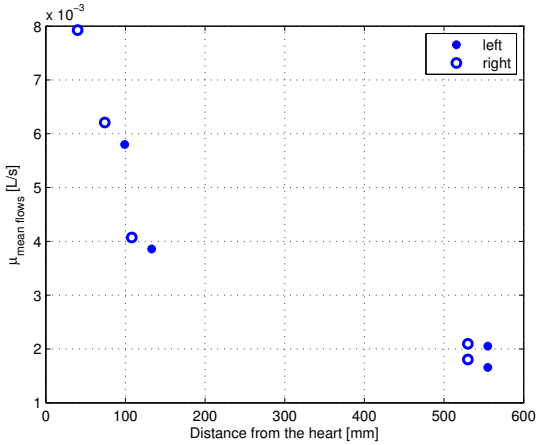

Figure 8.26: Mean values of the mean flows along the arms (vessels: 3, 4, 7, 8, 9, 19) during AF (mean heartbeat frequency: 75 bpm).

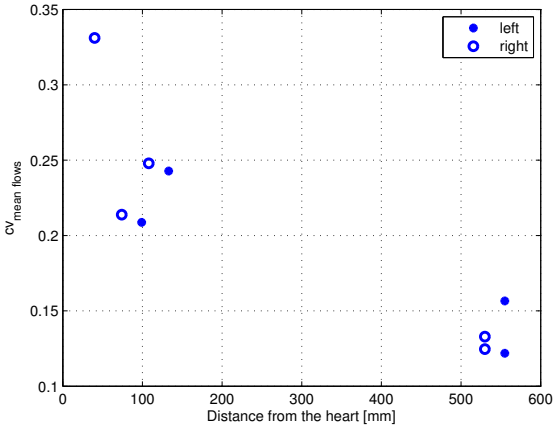

Figure 8.27: Coefficients variations of the mean flows along the arms (vessels: 21, 22, 23) during AF (mean heartbeat frequency: 75 bpm).

From Figure 8.26 and 8.27, one finds that the mean values and the coefficients of variation of the mean flows dwindle proceeding towards the terminal regions of the arms, on the left as well as on the right. However, we can note that, on the right, the previous quantities are almost always slightly higher than on the left.

Table 8.7: Percentage variations of the mean flows along the arms during AF, in reference to the same corresponding quantities in NSR. Skewness and kurtosis of the mean flows during AF. For both AF and NSR simulations, mean heartbeat frequency is 75 bpm.

Vessel	% var	S	K
3	5.69	0.90	5.03
4	3.49	0.85	5.08
7	4.40	0.89	5.27
8	0.33	0.89	7.89
9	0.22	0.62	5.14
19	3.57	0.90	6.81
21	4.27	0.94	7.41
22	2.63	0.62	4.94
23	3.62	2.23	29.71

Table 8.7 enables us to describe completely how mean flows behave in AF at the arm vessels. Like along the arterial tree, we have that, on average,

the mean flow values are greater than those in NSR, with $S > 0$ and $K > 3$. Furthermore, the extensions of the tails of the mean flow distributions at the left arteries are wider than those on the right.

Phase velocities

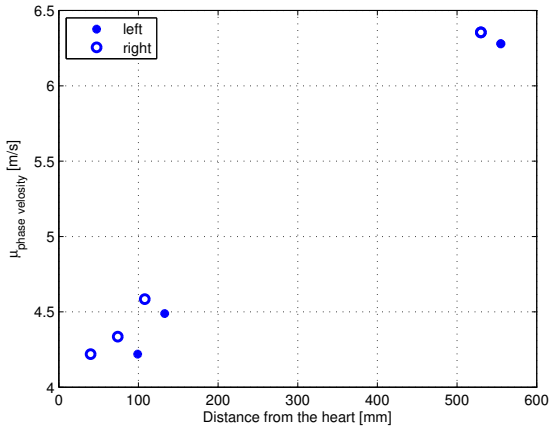

Figure 8.28: Mean values of the phase velocities along the arms during AF (mean heartbeat frequency: 75 bpm).

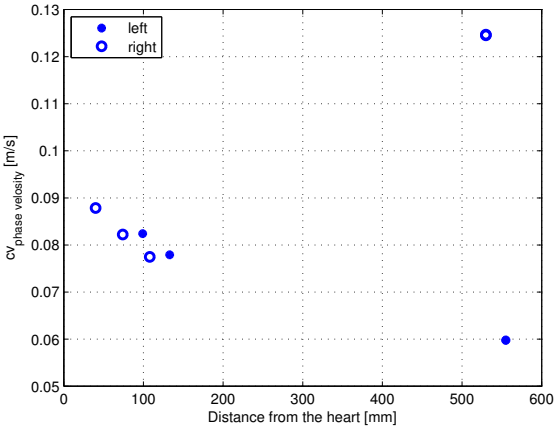

Figure 8.29: Coefficients of variation for the phase velocities along the arms during AF (mean heartbeat frequency: 75 bpm).

Figures 8.28 and 8.29 give the evolutions of the mean values and the coefficients of variation of the phase velocities, respectively.

Concerning the first image, one can see that, as it should be, mean phase velocities grow moving towards the terminal arteries of the two arms. In particular, on the right, mean phase velocities are a bit greater than on the left. About coefficients of variations for the phase velocity, instead, we observe similar trends at the left and right arteries along the arms, except at the ulnar A arteries. In fact, here, the cv values on the right are more than twice those on the left.

Table 8.8: Percentage variations of the phase velocities along the arms during AF, in reference to the same corresponding quantities in NSR. Skewness and kurtosis of the phase velocities during AF. For both AF and NSR simulations, mean heartbeat frequency is 75 bpm.

Vessel	% var	S	K
3	0.22	0.27	3.30
4	2.52	0.23	3.26
7	1.88	0.22	3.24
8	0.13	−14.97	303.86
9	0.11	−14.95	303.45
19	0.17	0.27	3.30
21	1.25	0.27	3.30
22	0.70	0.31	3.34
23	0.69	0.31	3.34

From Table 8.8, one can observe that phase velocities certainly become larger during AF, on average. As we have already seen, concerning the previous quantities, there is no symmetry in the phase velocities for the arms too. However, in this case, not only numerical values are different but also we find opposite trends at the terminal areas of the two arms. Indeed, at the left radial and ulnar A arteries, positive fluctuations are more likely than negative ones, with K very close to 3. By contrast, the same arteries on the right experience more probable negative fluctuations, with tails decisively longer.

RI and RM

From Figure 8.30, we notice that the magnitude of reflections reduces along the arms, as the distance from the heart grows. There are not significant differences between the left and the right arm. Figure 8.31, instead, indicates

the evolution of the coefficients of variations of RI and RM for the arms. We can see that these vary minimally at arteries more proximal to the heart, on the left as well as on the right, but become decisively larger at the final arteries of the two arms. This is not too surprisingly since the number of bifurcations per unit of length upsurges when we are more distant from the heart.

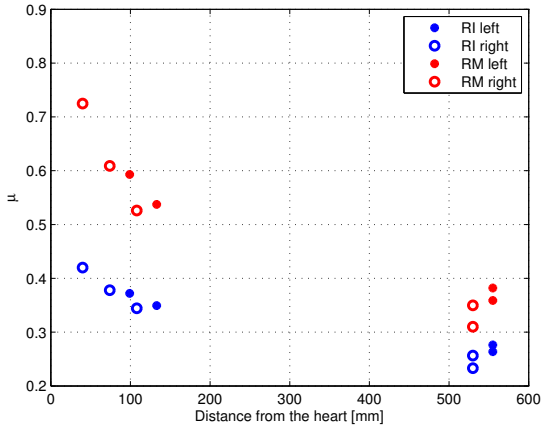

Figure 8.30: Mean values of RI and RM along the arms during AF (mean heartbeat frequency: 75 bpm).

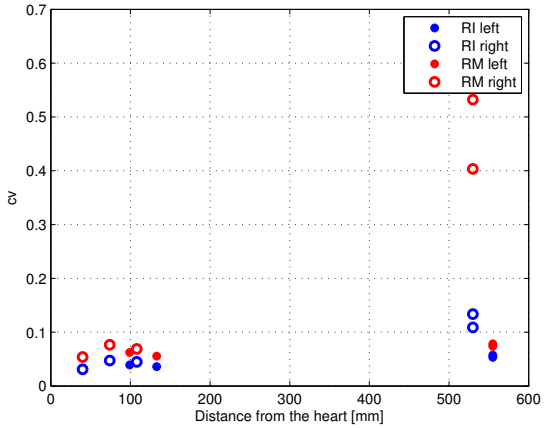

Figure 8.31: Coefficients of variation for RI and RM along the arms during AF (mean heartbeat frequency: 75 bpm).

Looking at the Table 8.9, we recognise, at some regions, dramatic reductions in the mean magnitude of reflection during AF, with percentage variations in the mean values of RI (in reference to the the same quantities in NSR) varying between about -2% to just below -50%, according to the site. We have also that it is more likely to have positive fluctuations, with some probable weak negative fluctuations. In general, the greatest levels of intermittency are located on the right.

Table 8.9: Percentage variations of RI and RM along the arms during AF, in reference to the same corresponding quantities in NSR. Skewness and kurtosis of RI and RM during AF. For both AF and NSR simulations, mean heartbeat frequency is 75 bpm.

Vessel	% var RI	% var RM	S RI	K RI	S RM	K RM
3	-14.63	-25.12	0.29	3.87	0.48	4.10
4	-15.77	-25.18	0.10	4.27	0.38	4.40
7	-2.29	-3.32	0.18	6.13	0.54	6.50
8	-16.60	-20.09	12.30	212.68	22.99	605.10
9	-47.51	-63.39	13.36	238.03	21.67	517.20
19	-11.65	-18.42	-0.092	4.97	0.18	4.90
21	-18.45	-28.29	0.079	5.05	0.31	5.20
22	-37.72	-52.03	-0.044	4.33	0.16	4.50
23	-46.29	-62.82	0.14	5.18	0.41	5.80

8.2.4 Conclusions in case of atrial fibrillation

We here summarize the principal results of this chapter. Note that mean heartbeat period in AF is equal to that typically assumed in NSR. Therefore, all the previous results derive from the irregularity of the beat periods produced in AF.

We discover that atrial fibrillation puts an enormous strain on heart. In fact, when the beat is fibrillated, the mean stroke work will double that done for a perfect rhythmical heartbeat. Negative fluctuations are more likely than positive ones and vary over an interval smaller than that we would have for a perfectly Gaussian distribution.

AF introduces minimal growths in the mean systolic and diastolic pressures everywhere, in reference to the case of NSR. This is not true for diastolic pressures at the radial and ulnar A arteries of both the arms. Positive pressure alterations are more probable than negative ones and produce coefficients of variations greater for diastolic pressures than for systolic ones.

Moreover, arterial system contributes to amplify diastolic pressure fluctuations with the distance from the heart, doing the opposite as regards systolic ones. Mean pulse pressure increases with the distance from the heart during AF, while the coefficients of variation for the same quantity behave differently according to site.

Concerning mean flows, like diastolic and systolic pressures, we have again an increase in the mean values, in reference to those found for NSR, and more probable positive fluctuations. However, percentage changes in the flow records during AF seem to be more evident than in the pressure ones. Coefficients of variation for the mean values typically reduce with the distance from the heart, along the aorta as well as for the two arms, except at the central area of the abdominal aorta.

Mean phase velocities slightly swell in AF, if compared with those in NSR. For this quantities, according to the chosen site, we can have either more probable positive fluctuations or more probable negative ones. It is important to note that where it is more likely to find negative alterations, fluctuations range within intervals much more wider than those related to sites more keen on positive alterations. Coefficients of variations for phase velocities have different attitudes moving away from the heart; along aorta, it reduces until the end of abdominal aorta then grows again and levels off, along the arms, it diminishes as going to distal vessels but can upsurge at the terminal arteries.

The mean magnitude of reflection vary in case of AF, almost everywhere, in reference to the classical rhythmical beat. This is visible by comparing the mean coefficients RI in AF with those in NSR. Coefficients of reflections exhibit more frequent positive fluctuations and cover larger or littler intervals depending on the site. About the coefficients of variations for RI and RM, these change with the position from heart.

One of the most sensible zone to the fluctuations brought by AF is that between the latest section of the abdominal aorta and the tibial arteries. Here, the extension of intervals within fluctuations vary is decisively wider than that in other arterial regions.

Interesting to note is that atrial fibrillation affects differently the final arteries of the left and right arm. To some extent, it is not surprising, since there is no symmetry in the pressure measures for both the arms in NSR too. Indeed, for a normal beat, we have a difference of 10% in the pressure measures between right and left arm.

As last consideration, we can say that AF, on average, does not alter the typical trends of all the analysed quantities with the distance from the heart.

Chapter 9

Analysis of the results during an episode of atrial fibrillation

In the previous chapter, we have described in detail the behaviour of the systemic circulation during an episode of atrial fibrillation. We remember that the RR distribution we have simulated is a combination of short and long heartbeats, producing a mean heartbeat frequency equal to that expected in NSR (75 bpm). As a consequence, the presented results do not take into account any frequency variation, typically observed during AF, but represent the other two effects of atrial fibrillation on arterial system response: the RR distribution is temporary uncorrelated within the high frequency domain and the coefficient of variation for the same RR sequence is greater than that we would measure in NSR. These two elements, globally, contribute to create a chain of RR intervals which lacks the typical rhythm regularity we have for a normal beat.

Here, we are going to achieve a double purpose. On the one hand, we want to give a justification to the little variations in the mean values of all the quantities useful to represent the functioning of both heart and arterial tree, for the event of AF concerned, even if the mean heartbeat frequency is equal to that without AF. On the other hand, we will compare the obtained results with those available in literature, in order to verify the acceptability of this work. Clearly this comparison has some limitations. Indeed, the greatest portion of literature data derive from experiments conducted on real patients. These have profiles ranging within extremely wide scenarios, according to age, sex and contemporary pathologies in addition to AF.

9.1 Results for the heart

Numerical data

Table 9.1 enables us to compare the mean quantities concerning the heart and provided by the numerical model in NSR with the corresponding ones relative to the AF simulation. Mean frequency (75 bpm) for the two cases is the same. One can see that, on average, all the AF results we are considering grow or reduce in reference to the case of NSR. If the succession of short and long heartbeats we simulate does not produce, on average, the results given in NSR (even if the mean heart beat frequency is maintained constant for AF as well as NSR), it will mean that short and long beats affect differently the arterial system response. In other words, the percentage variations of all the considered quantities in AF, in reference to those in NSR, are different in modulus, when due to RR values in symmetric positions, in respect to $RR = 0.8$ s. This is not surprisingly if we look at what done in Chapter 4. The images of Figure 9.1 and 9.2 give evidence of this.

Table 9.1: Comparison between the mean quantities describing the heart performances in NSR and AF, for equal mean heartbeat frequency (75 bpm). At the last row, we indicate + or − as the quantity under exam grows or reduces in AF in reference to what happens in NSR. $V_{LV,ed}$ and $P_{LV,ed}$: left ventricle volume and pressure -end diastole-. $V_{LV,es}$ and $P_{LV,es}$: left ventricle volume and pressure -end systole-. SW: stroke work, SV: stroke volume, CO: cardiac output, EF: ejection fraction.

	$V_{LV,ed}$ [ml]	$V_{LV,es}$ [ml]	$P_{LV,ed}$ [mmHg]	$P_{LV,es}$ [mmHg]	SW [J]	SV [ml]	CO [L/min]	EF %
NSR	120.21	52.85	8.35	97.31	0.92	67.36	5.05	56.04
AF	119.95	60.74	8.33	119.95	1.35	59.20	4.44	49.34
From NSR to AF	− 0.22%	+ 14.93%	− 0.24%	+ 23.27%	+ 46.74%	− 12.11%	− 11.90%	− 11.96%

As an example, we can look at what happens for the left ventricular volume and at the end of diastole in the cases NSR and AF. We have that, in AF, $V_{LV,ed}$ reduces, on average, in reference to the value for NSR (Table 9.1). Looking at Figure 9.1a, we note that, in NSR, short beats are responsible for a decreasing in the mean value of $V_{LV,ed}$, while the opposite is true for long beats. Moreover the variations of the mean value of $V_{LV,ed}$ induced by short beats are greater in modulus than those due to the long ones. So, the mean value of $V_{LV,ed}$ dwindles in AF, in reference to the case of NSR, for equal

mean heartbeat frequency, since short beats' effect prevails on that of the long ones. In general, we have that, as regard the heart, during AF, short beats play a bigger role on the final results than heartbeats with $RR > 0.8$ s. Concerning the stroke work, SW, we find something interesting. In fact, percentage alterations in the SW, caused by short beats in the AF sequence, are littler in modulus than those provoked by long beats, but it tends to rise dramatically in AF. This can be explained under two different points of view. Firstly, SW becomes stable as RR belongs to the interval 0.5 s and 0.6 s (Figure 9.2a). Secondly, even if mean SV reduces for a fibrillated sequence, mean $P_{LV,es}$ is decisively higher in AF, leading, on average, to a growth in the total stroke work.

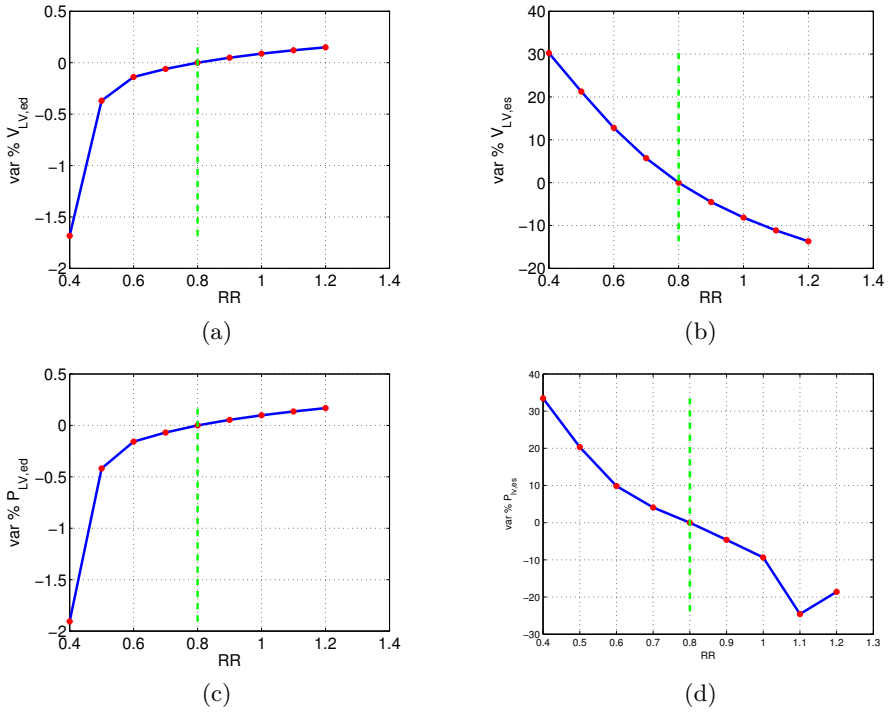

Figure 9.1: Evolutions of the percentage variations in some mean quantities relative to the heart when varying the value of RR in NSR. Reference values are those obtained for $RR = 0.8$ s, in case of NSR. Red marks indicate results from simulations while dotted green lines show the reference values. $V_{LV,ed}$ and $P_{LV,ed}$: left ventricle volume and pressure -end diastole-. $V_{LV,es}$ and $P_{LV,es}$: left ventricle volume and pressure -end systole-.

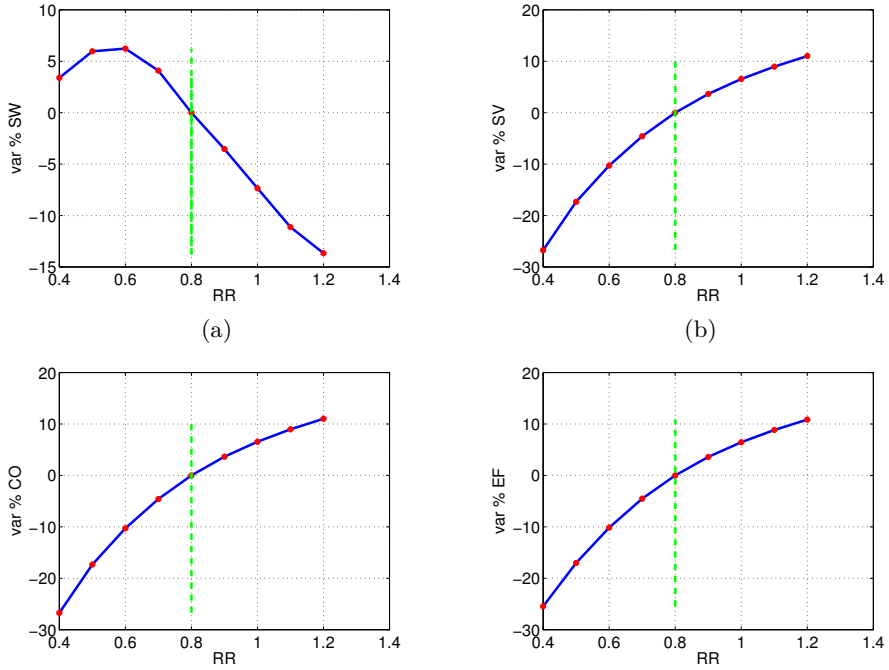

Figure 9.2: Evolutions of the percentage variations in some mean quantities relative to the heart when varying the value of RR in NSR. Reference values are those obtained for $RR = 0.8$ s, in case of NSR. Red marks indicate results from simulations while dotted green lines show the reference values. SW: stroke work, SV: stroke volume, CO: cardiac output, EF: ejection fraction.

Literature data

As concern left ventricular volumes at the end of both systole and diastole, Braunwald [5] indicates possible reductions in $V_{LV,ed}$, after a short episode of atrial fibrillation, while Orlando [35] finds that there are not significant differences in $V_{LV,ed}$ and $V_{LV,es}$, as cardioversion [1] is completed. [47] and [3] indicate, instead, a progressive decreasing in the left ventricular dimen-

[1] Cardioversion is a medical procedure useful to convert cardiac arrhthmias to a normal rhythm. If it is not spontaneous, it can be achieved by using a therapeutic dose of electric current (synchronized electrical cardioversion) or drugs (chemical cardioversion).

sions, as diastole and systole conclude, after cardioversion and ablation [2], respectively. Therefore, literature data do not report clear evolution of the mean $V_{LV,ed}$ and $V_{LV,es}$ values during events of AF limited in time. These should be useful for the validation of our results, covering only 30 minutes of simulation. However, some measures demonstrate that, on average, $V_{LV,ed}$ can slightly diminish whereas $V_{LV,es}$ can rise during a brief episode of AF. About $P_{LV,es}$, there are no data in literature while, concerning $P_{LV,ed}$, we have found a result only [1], showing that left ventricular pressure at the end of systole tends to dwindle during AF. This is accordance to our result in Table 9.1. Concerning the stroke work or the work left ventricle has to do in order to accomplish its function, literature data [26], [35] say that it grows after cardioversion, that means that stroke work is expected to reduce in case of AF. This is in opposition to our results. However we have to consider the fact that, experimentally, it is not possible to calculate the previous quantity exactly. For example, [26] extracts the stroke work as the product between the stroke volume and the mean arterial pressure during ejection. In our calculations, instead, we obtain the stroke work as the area of the PV loop. Thus, it could be normal that our observation for the stroke work in AF are in opposition to those presented in the articles. Furthermore, various literature data gives the mean stroke work in AF, for a mean beat frequency higher than in this study. Some data [52], [27] reveal that there are not significant alterations in the mean value of stroke volume in AF. However, a good number a articles ([1], [11], [14], [21], [43]) publish that stroke volume diminishes in AF; this is in agreement with what is indicated in Table 9.1. Different studies ([10], [11], [12], [21], [26], [33], [35], [43], [48]) prove a reduction in the cardiac output in atrial fibrillation; this is in accordance with this work results. Furthermore, some articles point out that CO decreases more during AF when there are other pathologies active [27] or as the subject is under stress [39], [45] or when we refer to patients for which an important decrease in the ventricular frequency has been observed [15]. Regarding EF of the left ventricle, almost every research investigation ([3], [8], [13], [46], [47], [51]) has found that this quantity is subjected to a certain decrease in presence of AF.

Overall, apart from some quantities, like the stroke work, the mathematical model is proved to provide satisfactory solutions about the heart (or more specifically the left ventricle) performances when AF is active. As we have already explained at the beginning of this chapter, our simulation in

[2] Ablation is a method adopted to treat atrial fibrillation. It aims at eliminating the cardiac tissue responsible for the onset and the maintenance of atrial fibrillation.

atrial fibrillation does not consider frequency alteration. However, in light of above, we can conclude that the only effect of an AF arrhythmical beat is sufficient to produce the typical responses during AF, maintaining the mean heartbeat frequency of the NSR (75 bpm).

Table 9.2 represents a quick overview of the comparison between our results and the available literature data.

Table 9.2: Mean results for heart (II column) and corresponding literature data (III column): '+' increase during AF, '-' decrease during AF, '=' no significant variations during AF, '/' no data available.

Variable	Mean results	Literature data
$V_{LV,ed}$	−	=[35], +[3][47]
$V_{LV,es}$	+	=[35], +[3][47]
$P_{LV,ed}$	−	−[1]
$P_{LV,es}$	+	/
SW	+	−[26][35]
SV	−	−[1][11][14][21][43], =[27][52]
CO	−	−[10][11][12][21][26][33][35][43][48], =[39][45]
EF	−	−[3][8][13][46][47][51]

9.2 Results for the arterial tree

Numerical data

As done in previous section, we report now some quantities (Table 9.3) relative to the ascending aorta and obtained from the simulations in NSR and AF, with the same mean heartbeat frequency of 75 bpm.

It is true the same reasoning offered for the heart. Fixed the mean beat frequency, the minimal alterations in the mean quantities of Table 9.3, passing from NSR to AF, derive from a different influence of short and long beats of the RR chain to the arterial system response. Figures 9.3 and 9.4 demonstrate this point. For example, if we consider the pulse pressure (PP) at the entrance to the aorta, we will find that it diminishes, on average, in presence of AF (Table 9.3). Indeed, from Figure 9.4a, everyone can understand the reason: negative percentage variations in PP, in NSR, have an higher modulus than the positive ones. Regarding the beginning of aorta, we can see that short beats are more powerful than long ones only for certain quantities, such as systolic and diastolic pressure, mean flow, phase velocity, that is in accordance with what is presented in Chapter 4. Turning

Table 9.3: Comparison between some mean quantities referred to the ascending aorta in NSR and AF, for equal mean heartbeat frequency (75 bpm). c, RI and RM are calculated at the end of the vessel while the other at the beginning of the same vessel. At the last row, we indicate + or − as the quantity under exam grows or reduces in AF in reference to what happens in NSR.

	P_{sys} [mmHg]	P_{dia} [mmHg]	PP [mmHg]	Q_{mean} [L/s]	c [m/s]	RI	RM
NSR	120.54	71.01	51.16	0.080	4.21	0.31	0.46
AF	120.74	71.64	49.10	0.083	4.22	0.32	0.48
From NSR to AF	+ 0.16%	+ 0.89%	− 4.03%	+ 3.91%	+ 0.20%	+ 3.23%	+ 4.35%

to PP and RM and RI, instead, it is true the opposite. We have also verified that the roles, during AF, of short and long beats, on the quantities reported in Table 9.3, do not change with the distance from the heart, apart from the values of RI and RM. For these, the play between short and long beats within the AF sequence have to be redefined site by site.

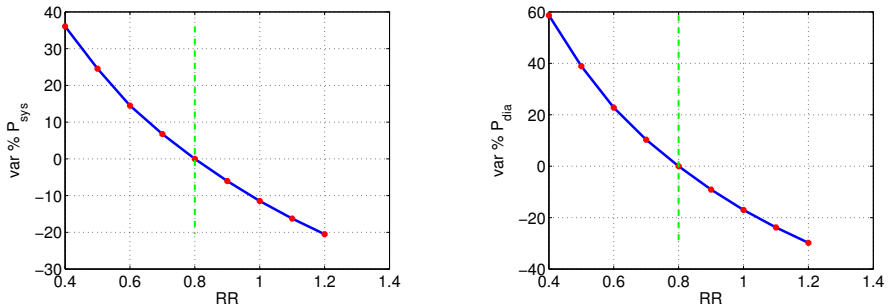

(a) (b)

Figure 9.3: Evolutions of the percentage variations in some mean quantities relative to the ascending aorta when varying the value of RR in NSR. Reference values are those obtained for $RR = 0.8$ s, in case of NSR. Red marks indicate results from simulations while dotted green lines show the reference values. Trends calculated at the beginning of the ascending aorta.

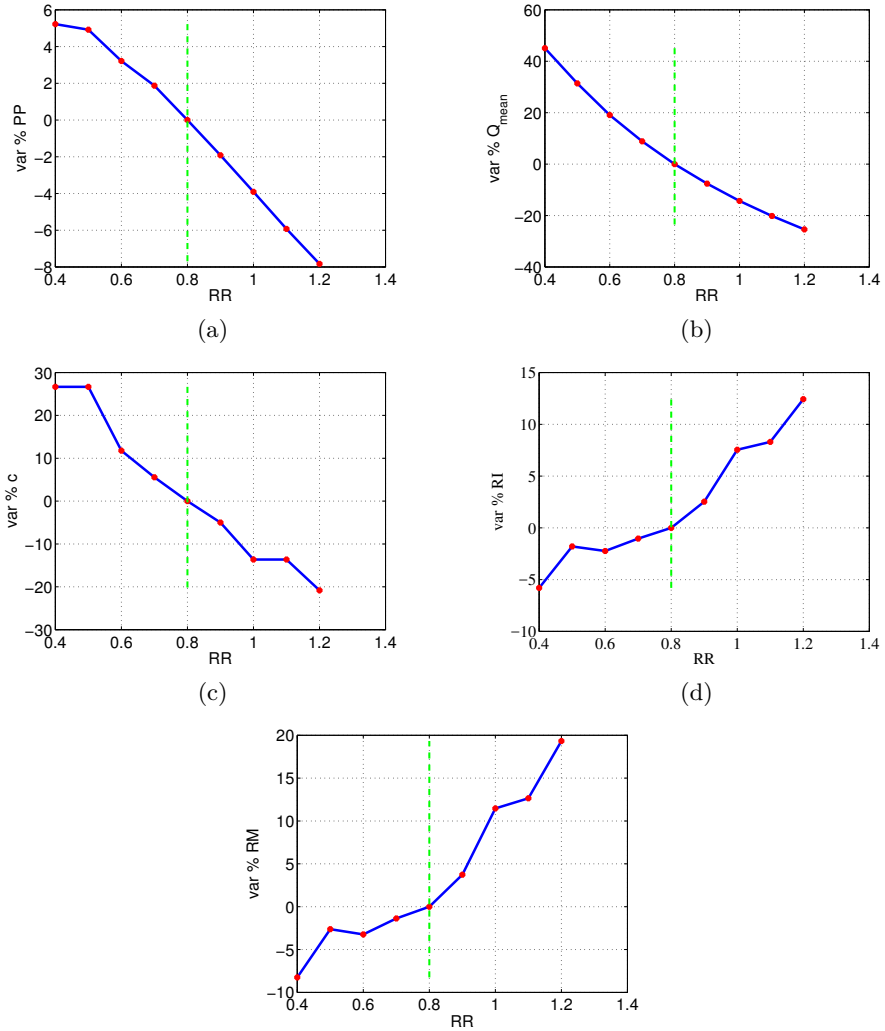

Figure 9.4: Evolutions of the percentage variations in some mean quantities relative to the ascending aorta when varying the value of RR in NSR. Reference values are those obtained for $RR = 0.8$ s, in case of NSR. Red marks indicate results from simulations while dotted green lines show the reference values. The trends of c, RI and RM are calculated at the end of the vessel while the other at the beginning of the same vessel.

Literature data

To the best of our knowledge, the only data available in literature as an instrument of comparison regards systolic, diastolic and pulse pressure at the beginning of the aorta. Concerning systolic and diastolic pressure, different works ([1], [14], [24]), confirm that they grow or remain almost constant during AF. This is in good agreement with our results. About pulse pressure, instead, we have found an article only [24], declaring that it dwindles during AF, as in this study.

Thus, this brief section leads to the following conclusions. First, frequency alterations in AF are not necessary to generate the typical behaviour of arterial system in AF. Second, the numerical method is able to reproduce the expected response of arterial vessels to a fibrillated heartbeat. Unfortunately, at the moment, we lack literature information describing other parameters in AF along arterial tree (for example the coefficients of reflection). As a consequence, the process of validation for the mathematical model, associated to the global functioning of the largest arteries in AF, is not complete. On the other hand, the ability of the model to calculate everywhere total pressure and flow records, and to inquire into phenomena such as the magnitude of the reflections site by site, represents its highest highlight.

Table 9.4 represents a quick overview of the comparison between our results and the available literature data.

Table 9.4: Mean results for the ascending aorta (II column) and corresponding literature data (III column): '+' increase during AF, '-' decrease during AF, '=' no significant variations during AF, '/' no data available.

Variable	Mean results	Literature data
P_{sys}	+	+[1][14][24]
P_{dia}	+	+[1][14][24]
PP	−	−[24]
Q_{mean}	+	/
c	+	/
RI	+	/
RM	+	/

Conclusions

In the present work, a multi-scale mathematical model has been adopted to have an insight into the effects of abnormal heartbeats on our heart and large-to-medium arteries. The model has proved to have a lot of benefits. First of all, imposing the sequence of the heartbeat periods we want to simulate, it gives, as output, the complete pressure and flow time series, at all the arterial sites of domain. This huge amount of data, properly treated, allows us to draw global conclusions about how systemic arteries function under the imposed heartbeat period chain. This approach has also the advantage to isolate the beat duration role on the blood flow dynamics along the arterial tree. In fact, geometries and properties of domain, as just said, refer to a young and health man, free from any type of other potential pathology connected to the beat period alteration.

This work enables us to identify clear results.

We have that heartbeats simply shorter and longer than the standard one strongly makes arterial system response vary. Pressures and mean flows grow for a short beat and decrease for a long one. The same is true for the phase velocities, while the magnitude of reflections change differently with RR according to the distance from the heart. As concern pressures, we find that diastolic pressure alterations are more significant than systolic ones. Furthermore, there is no symmetry in the results found for symmetric beat periods in reference to the standard one ($RR = 0.8$ s, on average).

When introducing a single change in the simulated sequence of periods (we go from a constant heartbeat period to one another or have an irregular period within a sequence of standard beat durations), arterial system clearly experiments a transition phase and tends to establish a steady solution again with a certain inertia. We have that the number of beats required by the various sites to recover, after the alteration, is always determined by diastolic pressure which, among all the other quantities, is that calling for the longest recovery time. Moreover, the passage from a longer beat to a shorter one is proved to take more time or the same time than the opposite one. It is not

possible to identify a close relationship between the time to recover and the distance from the heart, hence, each site exhibits a personal behaviour.

During an episode of atrial fibrillation, stroke work done by heart increases significantly in its mean value, with minimal fluctuations (the negative ones are more probable). Systolic and diastolic pressures, as well as mean flows, on average, experience a small growth (unless a few exceptions), more evident on mean flows than on pressures. Al these quantities are more likely to fluctuate positively around their mean values. Arterial system tends to damp and amplify, moving from the heart, systolic and diastolic pressure fluctuations, respectively. Concerning mean flows, instead, coefficients of variation, symbols of the magnitude of fluctuations over the mean values, typically reduce with the distance from the heart, with a few exception along the abdominal aorta. Phase velocities experience, on average, a small increase in their mean values, are more keen on positive or negative fluctuations according to the site, with a trend for the coefficients of variation variable according to the arterial position. Mean coefficients of reflection RI grow or reduce depending on the point while RI fluctuations can be more or less positive according to the site, with an evolution not extremely clear as following the distance from the heart. The amplitudes of the intervals within the previous quantities can vary are strongly dependant on the site. The most variable locations are those belonging to the abdominal regions until we reach the leg arteries. We have also that the left and right arm do not exhibit symmetrical behaviours. What is apparent from the study of the episode of atrial fibrillation is that, on average, chosen a quantity and a site, the role of short and long beats of the simulated RR intervals is more or less powerful, on the final result, according to the magnitude of the variations they are able to generate there, in reference to the mean heartbeat period of the simulated RR sequence. On average, left ventricle parameters, diastolic and systolic pressures, mean flows and phase velocities, at any vessel, are more influenced by short beats (beats whose $RR < 0.8$ s).

We note that the general trends of the various quantities with the distance from the heart are not affected by any type of beat period alterations.

We remember that all these conclusions are the results of a mathematical model having some limitations. These derive from both the elements neglected in the modelled circular system (the cerebral circulation, the venous return and the coronary arteries) and the different hypothesis reflecting the equations constituting the total model (axisymmetric geometry, wall impermeability, no longitudinal artery deformation and Newtonian blood behaviour). Some of these limitation could be overcome in future since, for example, it is fairly possible to implement the coronary contribution.

Another factor to take into account is that the model lacks a baroreceptor system able to adapt the output response to the ventricular stimuli. This means that all these results are valid if always referred to the same subject, whose systemic circulation is not accustomed to continuous variations in the heartbeat period. Indeed, in the long term, each system tends to adjust its way of working to its forcings, showing a different behaviour. This aspect could be corrected in future, too.

In conclusion, new efforts could be addressed not only to improve the level of detail of the presented mathematical model, but also to explore, through it, other forms of arrhythmias. For example, it should be interesting to investigate cardiac arrhythmias during spaceflight. These types of arrhythmias can have various causes, among which microgravity. Knowing more about these cardiac events, is necessary to have a clear overview of all the risks astronauts involved in long-duration spaceflights may undergo.

Bibliography

[1] Alboni, P., S. Scarfo, G. Fuca, N. Paparella, P. Yannacopulu. Hodynamics of idopathic paroxismal atrial-fibrillation. *Pacing. Clin. Electrophysiol.*, 18:980-985, 1995.

[2] Alpert, J.S. Atrial fibrillation: a growth industry in the 21st century. *Eur. Heart J.*, 21:1207-1208, 2000.

[3] Anter, E., M. Jessup, D.J. Callans. Atrial fibrillation and heart failure: treatment consideration for a dual epidemic. *Circulation*, 119:2516-2525, 2009.

[4] Blanco, P.J., R.A. Feijòo. A dimensionally-heterogeneous closed-loop model for the cardiovascular system and its application. *Med. Eng. Phys.*, 35(5):652-667, 2013.

[5] Braunwald, E., R. Frye, M. Aygen, J. Gilbert. Studies on Straling's law of the heart. III. Observations in patients with mitral stenosis and atrial fibrillation on the relationship between left ventricular end diastolic segment length, filling pressure, and the characteristics of ventricular contraction. *J. Clin. Invest.*, 39:1874-1884, 1960.

[6] Caro, C.G., T.J. Pedley, R.C. Schroter, W.A. Seed. *The Mechanics of the circulation*, 2th edition. New York, NY: Cambridge University Press, 2012.

[7] Chen, P., A. Quarteroni, G. Gozza. Simulation-based uncertainty quantification of human arterial network hemodynamics. *Int. J. Numer. Methods Biomed. Eng.*, 29(6):698-721, 2013.

[8] Chirillo, F., M.C. Brunazzi, M. Barbiero, D. Giavarina, M. Pasqualini, E. Franceschini-Grisolia et al. Estimating mean pulmonary wedge pressure in patients with chronic atrial fibrillation from transthoracic doppler

indexes of mitral and pulmonary flow velocity. *J. Am. Coll. Cardiol.*, 30:19-26, 1997.

[9] Chugh, S.S., R. Havmoeller, K. Narayanan, D. Singh, M. Rienstra, E.J. Benjamin, R.F. Gillum, Y.H. Kim, J.H. Jr McAnulty, Z.J. Zheng, M.H. Forouzanfar, M. Naghavi, G.A. Mensah, M. Ezzati, C.J. Murray. Worldwide epidemiology of atrial fibrillation: a Global Burden of Disease 2010 Study. *Circulation*, 129(8):837-847, 2014.

[10] Clark, D.M., V.J. Plumb, A.E. Epstein, G.N. Kay. Hemodynamics effects of an irregular sequence of ventricular cycle lengths during atrial fibrillation. *J. Am. Coll. Cardiol.*, 30:1034-1045, 1997.

[11] Corliss, R.J., D.H. McKhenna, C.W. Crumpton, G.G. Rowe. Hemodynamics effects after conversion of arrhythmias. *J. Clin. Invest.*, 47:1774-1786, 1968.

[12] Daoud, E.G., R. Weiss, M. Bahu, P.B. Knight, F. Bogun, R. Goyal et al. Effect of an irregular ventricular rhythm on cardiac output. *AM. J. Cardiol.*, 78:1433-1436, 1996.

[13] Gentlesk, P.J, W.H. Sauer, E.P. Gerstenfeld, D. Lin, S. Dixit, E. Zado et al. Reversal of left ventricular dysfunction following ablation or atrial fibrillation. *J. Cardiovasc. Electr.*, 18:9-14, 2007.

[14] Giglioli, C., M. Nesti, E. Cecchi, D. Landi, M. Chiostri, G.F. Gensini et al. Hemodynamics effect in patients with atrial fibrillation submitted to electrical cardioversion. *Int. J. Cardiol.*, 168:4447-4450, 2013.

[15] Graettinger, J.S., R.A. Carleton, J.J. Muenster. Circulatory consequences of change in cardiac rhythm produced in patients by transthoracic direct-current shock. *J. Clin. Invest.*, 43:2290-2302, 1964.

[16] Guala, A., C. Camporeale, F. Tosello, C. Canuto, L. Ridolfi. Modelling and subject-specific validation of the heart-arterial tree system. *Ann. Biomed. Eng.*, 43(1):222-237, 2014.

[17] Guala, A., C. Camporeale, L. Ridolfi. Compensatory effect between aortic stiffening and remodelling during ageing. *PLOS ONE*, 10(10):e0139211, 2015.

[18] Guala, A., M. Scalseggi, L. Ridolfi. Coronary fluid mechanics in an ageing cardiovascular system. *Meccanica*, 1-12, 2015.

[19] Guala, A. Mathematical modelling of cardiovascular fluid mechanics: physiology, pathology and clinical practice. Ph.D Thesis in Engineering for Natural and Built Environment -XXVII cycle-, 2015.

[20] Guyton, A.C., J.E. Hall. *Textbook of medical physiology*, 11th edition. Philadelphia, PA: Elsevier Sauders, 2006.

[21] Halmos, P.B., C.G. Patterson. Effect of atrial fibrillation on cardiac output. *Brit. Heart J.*, 27:719-723, 1965.

[22] Hayano, J., F. Yamasaki, S. Sakata, A. Okada, S. Mukai, T. Fujinami. Spectral characteristics of ventricular response to atrial fibrillation. *Am. J. Physiol. Heart Circ. Physiol.*, 273:H2811-H2816, 1997.

[23] Hennig, T., P. Maass, J. Hayano, S. Heinrichs. Exponential distribution of long heart beat intervals during atrial fibrillation and and their relevance in white noise behaviour in power spectrum. *J. Biol. Phys.*, 32:383-392, 2006.

[24] Kaliujnaya, V.S, S.I. Kalyuzhny. The assessment of blood pressure in atrial fibrillation. *Comput. Cardiol.*, 32:387-390, 2005.

[25] Kenneth, S.S. *ANATOMIA UMANA*, 3th edition. Padova, IT: PICCIN, 2012.

[26] Khaja, F., J.O. Parker. Hemodynamics effects of cardioversion in chronic atrial fibrillation. *Arch. Intern. Med.*, 129:433-440, 1972.

[27] Killip, T., R.A. Baer. Hemodynamics effects after reversion from atrial fibrillation to sinus rhythm by precordial shock. *J. Clin. Invest.*, 45:658-671, 1966.

[28] Korakianitis, T., Y. Shi. Numerical simulation of cardiovascular dynamics with healthy and diseased heart valves. *J. Biomech.*, 39(11):1964-1982, 2006.

[29] Krahn, D.A., J. Manfreda, R.D. Tate, F.A. Mathewson, T.E. Cuddy. The natural history of atrial fibrillation: incidence, risk factors, and prognosis in the Manitoba follow-up study. *Am. J. Med.*, 98:476-484, 1995.

[30] Ku, D.N. Blood flow in arteries. *Annu. Rev. Fluid. Mech.*, 29:399-434, 1997.

[31] Lighthill, J. *Mathematical Biofluiddynamics*. Philadelphia, PA: Society for Industrial and Applied Mathematics, 1975.

[32] Magnani, J.W., M. Rienstra, H. Lin, M.F. Sinner, S.A. Lubitz, D.D. McManus, J. Dupuis, P.T. Ellinor, E.J. Benjamin. Atrial fibrillation: current knowledge and future directions in epidemiology and genomics. *Circulation*, 124:1982-1993, 2011.

[33] Morris, J.J., M. Entman, W.C. North, Y. Kong, H. McIntosh. The changes in cardiac output with reversion of atrial fibrillation to sinus rhythm. *Circulation*, 31:670-678, 1965.

[34] Olufsen, M.S., C.S. Peskin, W.Y. Kim, E.M. Pedersen, A. Nadim, J. Larsen. Numerical simulation and experimental validation of blood flow in arteries with structured-tree outflow conditions. *Ann. Biomed. Eng.*, 28(11):1281-1299, 2000.

[35] Orlando, J.R., R. Van Herick, W.S. Aronow, H.G. Olson. Hemodynamics and echocardiograms before and after cardioversion of atrial fibrillation to normal sinus rhythm. *Chest.*, 76:521-526, 1979.

[36] Ottesen, J., M.S. Olufsen, J.K. Larsen. *Applied Mathematical Models in Human Physiology*, Vol. 33. Philadelphia, PA: Society for Industrial and Applied Mathematics, 2005.

[37] Pedley, T.J. *The fluid mechanics of large blood vessels*. New York, NY: Cambridge University Press, 1980.

[38] Quarteroni, A. *Cardiovascular Mathematics: Modeling and Simulation of the Circulatory System*. MSA. Milano, IT: Springer-Verlag, 2009.

[39] Resnekov, L., L. McDonald, F. Perren, F. Lazeyras, and N. Stergiopulos. Electroversion of lone atrial fibrillation and flutter including including hemodynamics studies at rest and on exercise. *Brit. Heart J.*, 33:339-350, 1971.

[40] Reymond, P., Y. Bohraus, F. Perren, F. Lazeyras, and N. Stergiopulos. Validation of a patient-specific one-dimensional modelof the systemic arterial tree. *Am. J. Physiol. Heart Circ.*, 297(1):208-222, 2009.

[41] Reymond, P., F. Merenda, F. Perren, D. Rüfenacht, and N. Stergiopulos. Validation of a one-dimensional model of the systemic arterial tree. *Am. J. Physiol. Heart Circ.*, 297(1):208-222, 2009.

[42] Sagawa, K. *Cardiac Contraction and the Pressure-Volume Relationship*. Oxford, UK: Oxford University Press, 1988.

[43] Samet, P. Hemodynamics sequelae of cardiac arrhythmias. *Circulation*, 47:399-407, 1973.

[44] Scarsoglio, S., A. Guala, C. Camporeale, L. Ridolfi. Impact of atrial fibrillation on the cardiovascular system through a lumped-parameter approach. *Med. biol. eng. comp.*, 52(11):905-911, 2014.

[45] Shapiro, W., G. Klein. Alteration in cardiac function immediately following electrical conversion of atrial fibrillation to normal sinus rhythm. *Circulation*, 38:1074-1084, 1968.

[46] Sievers, B., S. Kirchberg, M. Addo, A. Bakan, B. Brandts, H.J. Trappe. Assessment of left atrial volumes in sinus rhythm and atrial fibrillation using biplane area length method and cardiovascular magnetic resonance imaging with trueFISP. *J. Cardiov. Magn. Reson.*, 6:855-863, 1968.

[47] Therkelsen, S.K., B.A. Groenning, J.H. Svendsen, G.B. Jensen. Atrial and ventricular volume and function evaluated by magnetic resonance imaging in patients with persistent atrial fibrillation before and after cardioversion. *Am. J. Cardiol.*, 97:1213-1219, 2006.

[48] Upshaw, C.B. Hemodynamic changes after cardioversion of chronic atrial fibrillation. *Arch. Inter. Med.*, 157:1070-1076, 1997.

[49] van de Vosse, F.N., N. Stergiopulos. Pulse wave propagation in the arterial tree. *Annu. Rev. Fluid. Mech.*, 43(1):467-499, 2011.

[50] Westerhof, N., N. Stergiopulos, M.I.M. Noble. *Snapshots of hemodynamics*, 2th edition. New York, NY: Springer, 2010.

[51] Wozakowska-Kaplon, B. Changes in left atrial size in patients with persistent atrial fibrillation: a prospective echocardiographic study with a 5-year follow-up period. *Int. J. Cardiol.*, 101:47-52, 2005.

[52] Wylie, J.V., D.C. Peters, V. Essebag, W.J. Manning, M.E. Josephson, T.H. Hauser. Left atrial function and scar after catheter ablation of atrial fibrillation. *Hearth Rhythm*, 5:656-662, 2008.

Glossary

CO Cardiac output

EF Ejection fraction

P_{LA} Left atrium pressure

P_{LV} Left ventricular pressure

$P_{LV,ed}$ Diastolic left ventricular pressure

$P_{LV,es}$ Sistolic left ventricular pressure

$P_{LV,max}$ Max left ventricular pressure

$P_{LV,min}$ Min left ventricular pressure

$Pdin_{AbdAorA}$ Diastolic pressure at the beginning of the abdominal aorta A

$Pdin_{AbdAorB}$ Diastolic pressure at the beginning of the abdominal aorta B

$Pdin_{AbdAorC}$ Diastolic pressure at the beginning of the abdominal aorta C

$Pdin_{AbdAorD}$ Diastolic pressure at the beginning of the abdominal aorta D

$Pdin_{AbdAorE}$ Diastolic pressure at the beginning of the abdominal aorta E

$Pdin_{AorArcA}$ Diastolic pressure at the beginning of the aortic arch A

$Pdin_{AorArcB}$ Diastolic pressure at the beginning of the aortic arch B

$Pdin_{AscAor}$ Diastolic pressure at the beginning of the ascending aorta

$Pdin_{ComIli}$ Diastolic pressure at the beginning of the common iliac

$Pdin_{ExtIli}$ Diastolic pressure at the beginning of the external iliac

$Pdin_{Fem}$ Diastolic pressure at the beginning of the femoral

$Pdin_{ThoAorA}$ Diastolic pressure at the beginning of the thoracic aorta A

$Pdin_{ThoAorB}$ Diastolic pressure at the beginning of the thoracic aorta B

$Pdin_{lRad}$ Diastolic pressure at the beginning of the left radial

$Pdin_{lSubB}$ Diastolic pressure at the beginning of the left subclavian B

$Pdin_{rRad}$ Diastolic pressure at the beginning of the right radial

$Pdin_{rSubB}$ Diastolic pressure at the beginning of the right subclavian B

Pin_{AscAor} Pressure at the begging of the ascending aorta

$Psin_{AbdAorA}$ Systolic pressure at the beginning of the abdominal aorta A

$Psin_{AbdAorB}$ Systolic pressure at the beginning of the abdominal aorta B

$Psin_{AbdAorC}$ Systolic pressure at the beginning of the abdominal aorta C

$Psin_{AbdAorD}$ Systolic pressure at the beginning of the abdominal aorta D

$Psin_{AbdAorE}$ Systolic pressure at the beginning of the abdominal aorta E

$Psin_{AorArcA}$ Systolic pressure at the beginning of the aortic arch A

$Psin_{AorArcB}$ Systolic pressure at the beginning of the aortic arch B

$Psin_{AscAor}$ Systolic pressure at the beginning of the ascending aorta

$Psin_{ComIli}$ Systolic pressure at the beginning of the common iliac

$Psin_{ExtIli}$ Systolic pressure at the beginning of the external iliac

$Psin_{Fem}$ Systolic pressure at the beginning of the femoral

$Psin_{ThoAorA}$ Systolic pressure at the beginning of the thoracic aorta A

$Psin_{ThoAorB}$ Systolic pressure at the beginning of the thoracic aorta B

$Psin_{lRad}$ Systolic pressure at the beginning of the left radial

$Psin_{lSubB}$ Systolic pressure at the beginning of the left subclavian B

$Psin_{rRad}$ Systolic pressure at the beginning of the right radial

$Psin_{rSubB}$ Systolic pressure at the beginning of the right subclavian B

Qin_{AscAor} Flow at the begging of the ascending aorta

SV Stroke volume

SW Stroke Work

V_{LV} Left ventricular volume

$V_{LV,ed}$ Diastolic left ventricular volume

$V_{LV,es}$ Sistolic left ventricular volume

$V_{LV,max}$ Max left ventricular volume

$V_{LV,min}$ Min left ventricular volume